A STUDY OF COLLOIDAL HYDROCRACKING CATALYSTS PREPARED IN REVERSE MICELLES

by

ANDREW GRAHAM HALL

B.Sc. The University of Cape Town, 1993

A THESIS SUBMITTED IN PARTIAL FULFILLMENT OF

THE REQUIREMENTS FOR THE DEGREE OF

MASTER OF APPLIED SCIENCE

in

THE FACULTY OF GRADUATE STUDIES

DEPARTMENT OF CHEMICAL ENGINEERING

We accept this thesis as conforming

to the required standard

THE UNIVERSITY OF BRITISH COLUMBIA

May, 1996

In presenting this thesis in partial fulfilment of the requirements for an advanced degree at the University of British Columbia, I agree that the Library shall make it freely available for reference and study. I further agree that permission for extensive copying of this thesis for scholarly purposes may be granted by the head of my department or by his or her representatives. It is understood that copying or publication of this thesis for financial gain shall not be allowed without my written permission.

Department of Chemical Engineering

The University of British Columbia
Vancouver, Canada

Date 4 June 1996

Abstract

Slurry phase reactors employing dispersed metal sulfide catalysts offer the potential of high conversion with minimal coke yield for the hydrocracking of heavy oil. Currently, the dispersed catalysts are prepared by the addition of organometallic compounds to the heavy oil feed, but this synthesis technique offers little control over the size of the catalyst particles. Colloidal suspensions of a wide range of metals and metal compounds in hydrocarbons can be prepared from water-soluble metal salts dissolved within the water pools of a microemulsion. This synthesis technique allows for the simple control of particle size, a factor which together with their narrow size distribution makes these colloids potentially attractive as dispersed heavy oil hydrocracking catalysts.

The synthesis of reduced metal and metal sulfide colloids in the water pools of the water/polyoxyethylene-4-laurylether/hexane microemulsion was investigated in the present study. The sizes of the reverse micelles were determined by dynamic light scattering (DLS), while the reduced Ni, Co and Fe colloids and the Ni, Co and Fe sulfide colloids were characterized by DLS, transmission electron spectroscopy (TEM), energy dispersive x-ray spectrometry (EDX) and x-ray photoelectron spectroscopy (XPS). The catalytic activity of the metal sulfide catalysts was also determined using the hydrocracking of diphelylmethane as a model reaction.

The water:surfactant ratio (ω) and metal ion concentration were found to be the key factors affecting the size of the reverse micelles in the water/PE4LE/hexane system. Monodisperse Co and Fe colloids with sizes ranging from 10-23 nm were prepared in the microemulsion system by the addition of N_2H_4, and the size of the metal colloids was found to be directly related to ω.

Ni, Co and Fe sulfide colloids were prepared in reverse micelles using 5% H_2S in H_2, and XPS analysis identified NiS and CoS_2 on the surface of these colloids. The metal sulfides proved difficult to characterize due to their extreme sensitivity to atmospheric oxygen. The Fe sulfide colloids oxidized readily, and could not be identified using XPS. The NiS and CoS_2 colloids had average sizes of 67 and 71 nm respectively (as determined by TEM), and were more polydisperse than the reduced metal colloids prepared in the same system.

The metal sulfide catalysts prepared in the water/polyoxyethylene-4-laurylether/hexane microemulsion were found to be less active for the hydrocracking of diphenylmethane than a dispersed catalyst prepared from the decomposition of Co naphthenate. The crystallite size was similar for both catalyst preparations (20-30 nm), suggesting that diffusion limitations may have controlled the rate of reaction in the case of the aggregated metal sulfide catalyst prepared in the microemulsion.

Table of Contents

List of Tables

List of Figures

Acknowledgements

First of all I would like to thank my supervisor Dr. Kevin Smith for his support, enthusiasm and guidance throughout my research.

I would like to acknowledge the Alberta Department of Energy for their generous financial support of this project.

Special thanks must also go to Dr. Barbara Frisken of the Department of Physics, Simon Fraser University for performing the light scattering measurements; and to Mary Mager of the Department of Metals and Materials Engineering, U.B.C. for helping me with the TEM work.

I would also like to thank the fellow members of my research group for the valuable assistance which they have given me with my experimental work, and for creating a pleasant and stimulating work environment.

In closing I would like to dedicate this thesis to my parents, for all the loving support, advice and encouragement which they have always given me over the years.

Chapter 1: Introduction

1.1 Motivation for the study

A significant portion of the world's fossil fuel reserves exist as hydrocarbons referred to as heavy oils. Heavy oils are defined in terms of their physical properties as mixtures of hydrocarbons which have a viscosity of 10^2 - 10^5 mPa.s, a density of 934-1000 kg/m^3 and an API gravity of 10-20. They originate from various sources including coal liquids, shale oils, oil sands and crude distillate bottoms. Canadian reserves of heavy oil in the Cold Lake and Athabasca regions of Alberta are estimated at between 2000-3000 billion barrels, compared to conventional oil reserves in the Middle East of 1500 billion barrels. Clearly these vast reserves of heavy oil in Alberta will supply an increasing portion of the worlds energy needs in the future, and it is essential that processes are developed to profitably pretreat these heavy oils.

Heavy oils contain high levels of sulfur, metals and cokeable materials. The presence of these contaminants means that heavy oils must be upgraded to lighter products which can be pumped and processed more easily in conventional oil refineries (Del Bianco *et al.* 1993). The aim of the upgrading process is to increase the H:C ratio of the feed stock, as well as to remove the heteroatoms and metals (Laine and Trimm, 1982). The H:C ratio of heavy oil can be increased by either coking, or catalytic hydrocracking. Coking is currently the most common method used, but catalytic hydrocracking processes have gained increasing popularity in recent times due to their higher conversion (>90%), higher distillate yield and lower severity compared to coking processes (Dautzenberg and De Deken, 1985).

Most catalytic hydrocracking processes utilize Co, W, Ni and Mo sulfide catalysts supported on alumina (Gates *et al.*, 1979). However, commercial heavy oil hydrocracking

processes which employ these supported catalysts experience extremely high rates of catalyst deactivation due to the deposition of coke and metals in the catalyst pores (Oelderik *et al.*, 1989; Ternan, 1983). These operational problems associated with supported catalysts have led to the development of 'slurry phase' reactors which use unsupported or 'dispersed phase' metal sulfide catalysts (Del Bianco *et al.*, 1993). The key advantage of dispersed catalysts is their ability to suppress coke formation. Since the catalyst particles are extremely small and highly dispersed within the heavy oil, the interparticle distance is radically reduced. As a result, the catalyst particles are able to intercept and hydrogenate free radical intermediates which would otherwise condense to form coke (Bearden and Aldridge, 1981). In addition, the extremely small size (typically sub-micron) of dispersed catalysts results in a large increase in specific surface area compared to supported hydrocracking catalysts. Consequently, a much lower catalyst loading can be used in slurry reactors, which may result in decreased catalyst costs.

Dispersed metal catalysts are most commonly prepared by the addition of oil soluble metal salts (organometallics) to the heavy oil feed of the slurry reactor. Although these organometallic precursors yield active hydrocracking catalysts, they provide little control over the size of the dispersed catalyst particles. In addition, the activity of dispersed catalysts is strongly dependent on the solubility of the organometallic additive in the heavy oil, and the choice of catalysts which can be prepared from organometallic precursors is thus fairly limited (Dabkowski *et al.*, 1991; Bearden and Aldridge, 1981; Hirschon and Wilson, 1989). Further understanding of the catalytic action of dispersed catalysts is hampered by the lack of control over particle size and the narrow selection of oil-soluble organometallics which are available. Consequently, there is a need to find a method for synthesizing dispersed catalysts in a hydrocarbon medium whereby the size of the catalyst particles can be easily controlled, and a large range of catalysts can be prepared.

A number of researchers have recently demonstrated that a wide range of metals and metal compounds dispersed in organic solvents can be prepared in the reverse micelles of a microemulsion (see section 2.3). Metal colloids prepared in reverse micelles are a potentially attractive alternative to catalysts prepared from the decomposition of organometallics for a number of reasons. Firstly, a number of studies have shown that the size of colloids synthesized within reverse micelles can be manipulated by simply changing the composition of the microemulsion (Ravet *et al.*, 1984; Nagy *et al*, 1983; Modes and Lianos, 1989; Pileni *et al.*, 1992). In addition, a far wider range of metal compounds, including bimetallic particles, can be synthesized in reverse micelles compared to the decomposition of organometallics. Finally, it is believed that colloidal catalysts prepared in microemulsions of oil-soluble organics can be very easily mixed with heavy oil and attain a far higher dispersion than colloidal catalysts from organometallics.

1.2 Objectives of the present study

The present study focuses on the preparation and characterization of metal and metal sulfide colloids prepared in the water/polyoxyethylene-4-laurylether/hexane microemulsion, and the application of this colloidal catalyst to the hydrocracking of a model compound, diphenylmethane. The current research had a number of more specific objectives:

1. To determine the factors affecting the size of the reverse micelles in the water/ polyoxyethylene-4-laurylether/hexane microemulsion.
2. To establish whether a relationship exists between the size of the reverse micelles in the water/polyoxyethylene-4-laurylether/hexane system and the size of solid colloids synthesized within the reverse micelles. For this purpose, the synthesis of reduced Ni, Co and Fe colloids was initially studied as a model intramicellular synthesis reaction.

3. To determine a suitable technique for the synthesis of metal sulfide colloids in the water/polyoxyethylene-4-laurylether/hexane microemulsion, and whether the size of these metal sulfide colloids can be controlled in the microemulsion. If possible, the metal sulfide species formed during the synthesis reaction were also to be identified.
4. Finally, the catalytic activity of the metal sulfide colloids synthesized in the water/polyoxyethylene-4-laurylether/hexane system was measured. The hydrocracking of a model compound diphenylmethane was studied for this purpose. The relative catalytic activity of these metal sulfide colloids synthesized in reverse micelles compared to catalysts prepared from organometallic compounds was of primary concern in these activity measurements.

Chapter 2 : Literature Review

2.1 Heavy oil upgrading

2.1.1 Introduction

Heavy oil represents an extremely important energy source to both the Canadian and world economies. Currently, 21% of Canada's total petroleum needs are derived from Alberta oil sands (Lupien, 1995). On a global scale, Venezuelan and Canadian heavy oil reserves are approximately 4 times larger than known reserves of conventional crude oil in the Middle East, and there is little doubt that heavy oil will supply an increasing percentage of the worlds energy needs in the future. Consequently, the successful and profitable utilization of these heavy oil reserves is critical to the long term future of the petrochemical industry, and it is essential that processes are developed to handle and pre-treat these heavy feeds.

2.1.2 Heavy oil upgrading processes

Heavy oils contain components which make processing in existing refineries extremely difficult (Del Bianco *et al.*, 1993), including heteroatoms (sulfur, nitrogen, oxygen), metals (nickel and vanadium) and considerable amounts of cokeable materials (referred to as Conradson Carbon Residue, CCR). Consequently, heavy oil must be upgraded to convert the heavy feeds to lower boiling point products which can be pumped and processed more easily. The basic aim of the upgrading process is to increase the H:C ratio in the feed stock, though other process requirements include the reduction of overall molecular weight and the removal of metals and heteroatoms (Laine and Trimm, 1982).

The H:C ratio of heavy oil can be increased by using 2 different approaches: carbon rejection (coking), or hydrogen addition. Coking is a proven method currently favored by most US refiners, and involves removing carbon as coke via a pyrolysis reaction (Del Bianco *et al.*, 1993). Despite their popularity, coking processes suffer from several disadvantages. Firstly, distillate yields are low since a large fraction of the feed is converted to gas and coke. Consequently, a higher crude intake is required to produce an equal quantity of light hydrocarbon product (Dautzenberg and De Deken, 1985). In addition, coking distillates are generally of poor quality (low CCR reduction and poor heteroatom and metal removal) and the large volumes of high sulfur, high metals coke produced present disposal problems (Del Bianco *et al.*, 1993).

2.1.3 Catalytic hydrocracking of heavy oil

Heavy oils can also be upgraded by the catalytic addition of hydrogen. Hydrogen is added to the heavy oil directly, removing inorganic materials and decreasing molecular weight by a hydrogenolysis/hydrocracking mechanism (Laine and Trimm, 1982). Considerable attention has recently been paid to catalytic hydrocracking processes, since they offer potential conversions of over 90%, including the removal of asphaltene coke precursors (Dautzenberg and De Deken, 1985). Hydrocracking processes are operated under less severe conditions than coking operations (430-460 °C compared to >500 °C in the case of coking), resulting in improved process economics in most cases (Sanford, 1996). Catalytic hydrocracking processes utilize metal sulfide catalysts to provide a source of hydrogen radicals (H•) through the catalytic dissociation of H_2. Hydrogen radicals (H•) promote bond cleavage reactions and control the retropolymerization processes, thus reducing the production of coke (Del Bianco *et al.*, 1993). In most catalytic hydrocracking processes, combinations of the sulfides of Co, Mo, Ni and W, supported on

alumina are used (Weisser and Landa, 1970; Gates *et al.*, 1979). Thomas and co-workers proposed the following mechanism for the generation of H• by iron sulfide (Thomas *et al.*, 1982):

$$FeS_2 \rightarrow FeS + S$$

$$S + H_2 \rightarrow H\bullet + HS\bullet$$

$$HS\bullet + H_2 \rightarrow H\bullet + H_2S$$

$$H_2S + FeS \rightarrow FeS_2 + H_2$$

Catalytic hydrocracking catalysts can be divided into two main groups: supported catalysts and unsupported or dispersed catalysts. At present, all commercial hydrocracking processes utilize supported catalysts in fixed bed reactors, with the exception of the LC-Fining (Van Driesen and Caspers, 1979) and the H-Oil (Eccles, 1982) processes which are based on ebullating bed technology.

Commercial heavy oil hydrocracking processes employing supported catalysts experience unacceptably high rates of catalyst deactivation (Oelderik *et al.*, 1989). Four factors contribute in varying degrees to the deactivation: the deposition of clay / mineral matter, the formation of coke on the catalyst surface, the deposition of metal sulfides in the catalyst pores, and thermal sintering of the catalyst (Ternan, 1983). In general, the deposition of metals and coke are the most critical factors leading to catalyst deactivation (Oelderik *et al.*, 1989). In many cases the high rate of catalyst deactivation and high consumption of catalyst adversely affect the economic feasibility of processes using supported hydrocracking catalysts.

2.2 Dispersed catalysts for heavy oil hydrocracking

2.2.1 Introduction

The chronic deactivation of supported heavy oil hydrocracking catalysts has prompted the development of processes using unsupported catalysts (Del Bianco *et al.*, 1993). These 'dispersed phase' catalysts are extremely small metal sulfide particles (typically sub-micron) dispersed within the heavy oil. The dispersed catalysts cannot be used in conventional fixed or ebullating bed reactors due to the combined problems of high pressure drops and increased bed plugging. Consequently, a new reactor technology referred to as the 'slurry phase' reactor has been developed to utilize the extremely small catalyst particles. A slurry phase reactor is essentially a 3 phase fluidized bed with the catalyst completely fluidized by the upward motion of the gas/liquid (Dautzenberg and De Deken, 1984). The reactor differs from a conventional fluidized bed in that the catalyst passes through the reactor with the feed, and in most cases it is not recovered or recycled back to the reactor. A comparison between the basic characteristics of fixed, ebullating and slurry phase reactors is given in Table 2.1.

Table 2.1 : Comparison between heavy oil hydrocracking reactor technologies (Dautzenberg and De Deken, 1984).

	Fixed Bed	Ebullating Bed	Slurry Phase
Vol % Catalyst	60	40	1
Catalyst Size, mm	1.5 x 3	0.8 x 3	.002
Particles/cm^3	120	250	2.4×10^9
Interparticle Distance, mm	—	1.6	0.008

The use of dispersed phase catalysts offers several distinct advantages over supported catalysts for heavy oil hydrocracking:

1. Firstly, since the catalyst has no pore structure, deactivation resulting from pore diffusion limitations and metals deposition is not a problem (Bearden and Aldridge, 1981).
2. Secondly, the extremely small catalyst particle size results in a considerable increase in specific surface area when compared to supported catalysts. Consequently, a much lower catalyst loading (<1000 ppm by weight) can be used, leading to decreased catalyst costs.
3. Since the catalyst is highly dispersed within the heavy oil (interparticle distances are very small), the ability of the catalyst particles to intercept and hydrogenate free radical intermediates is greatly increased. Consequently, dispersed catalysts are highly effective in suppressing coke formation (Del Bianco *et al.*, 1993; Bearden and Aldridge, 1981). Proposed hydroconversion mechanisms in the presence of dispersed catalysts are discussed in section 2.2.2.
4. Aside from their catalytic role, the dispersed catalyst particles serve as nucleation sites for the small amounts of coke which do form. In this manner fouling of the reactor surfaces is prevented (Bearden and Aldridge, 1981).
5. There are several operational advantages associated with slurry reactors employing dispersed catalysts. Catalyst replenishment is simple, and the problems of reactor plugging inherent to fixed bed reactors are solved. In addition, large liquid-phase heat transfer coefficients make temperature control of slurry reactors fairly simple (Dautzenberg and De Deken, 1984).

2.2.2. Hydroconversion mechanisms in the presence of dispersed catalysts

Several researchers have proposed conceptual hydroconversion mechanisms in the presence of dispersed catalysts (Dautzenberg and De Deken, 1984; Bearden and Aldridge, 1981). Such a proposed mechanism is shown in Figure 2.1. Heavy molecules such as asphaltenes and resins undergo a thermally induced free-radical cracking reaction to generate unstable

intermediates (reaction 2). The dispersed catalyst then hydrogenates the unstable radicals to yield oil (reaction 3), rather than allowing free radical coking reactions (e.g. polymerization) to occur via reaction 4. Several researches have used electron spin resonance (ESR) to demonstrate that dispersed catalysts derived from molybdenum naphthenate reduce the concentration of free radicals in heavy petroleum feed stocks (Rudnick, 1987; Varghese, 1986; Rudnick and Audeh, 1986). Consequently, the main catalytic effect of dispersed metal catalysts is to reduce the amount of coke formed during the hydrocracking reaction.

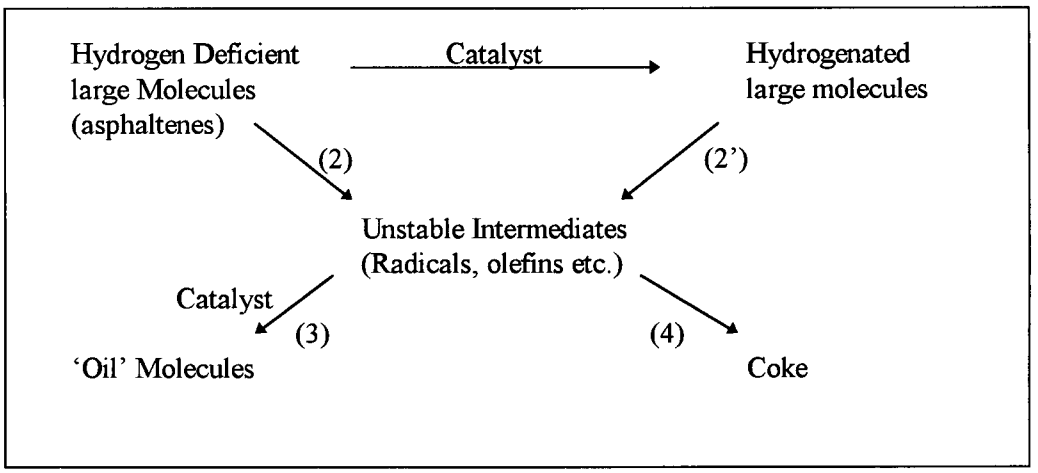

Figure 2.1 : Reaction mechanism in the presence of disperse catalysts (Dautzenberg and De Deken, 1984).

Sanford *et al.* (1995) found that a similar mechanism also applies to supported heavy oil hydrocracking catalysts. The researchers found that supported metal catalysts lose their hydrotreating function very rapidly under hydrocracking conditions. In this context, hydrotreating refers to the reaction whereby an organic molecule (such as one containing an aromatic ring) is activated on one active site of the catalyst, whilst hydrogen is activated on another site, usually remote from the aromatic ring. The activated hydrogen then migrates to the activated aromatic and adds across a double bond, resulting in the saturation of that bond. Once the supported metal

catalysts lose their hydrotreating function, they essentially become a source of activated hydrogen, with a similar catalytic mechanism to that of dispersed catalysts.

2.2.3 The synthesis of dispersed metal catalysts

A number of methods exist for the synthesis of sub-micron dispersed metal catalysts, including flame pyrolysis of organometallic compounds with ethylene (Andres *et al.*, 1983; Hager *et al.*, 1994), and low temperature vapor condensation (Bradley *et al.*, 1991). However, these methods are complex and impractical for large scale industrial application. The most common synthesis method involves the direct addition of finely divided inorganic powders, water soluble or oil-soluble metal salts to the heavy oil feed (Del Bianco *et al.*, 1993). These metal precursors include:

- Inorganic metal compounds such as metal oxides, metal alloys, phosphomolybdic acid and ammonium tetrathiomolybdate (oil-insoluble).
- Metal salts of organic amines and quaternary ammonium compounds (oil-insoluble).
- Organometallic salts of organic acids such as naphthenates and resinates (oil soluble).
- Organomatallic compounds such as phthalocyanines, dithiocarbamates, dithiophosphates and alkyl molybdate (oil soluble).

The metal constituents of these compounds are transition metals (Mo, Co, Ni, Fe, Cr etc.). In the case of oil-soluble metallic compounds, the active form of the catalyst is generated 'in-situ': the oil-soluble compound first dissolves within the oil and subsequently, under suitable thermal conditions, decomposes in the presence of H_2S and other sulfur containing compounds in the heavy oil to yield metal sulfide catalyst particles (Del Bianco *et al.*, 1993). Researchers have found that the temperature profile (Utz *et al.*, 1989; Lett *et al.*, 1989), the method of addition (Liu *et al.*, 1994), and the partial pressure of H_2S (Derbyshire *et al.*, 1986; Anderson and

Bockrath, 1984) can affect this decomposition reaction. However, these effects are highly complex and have not been comprehensively studied (Del Bianco *et al.*, 1993).

2.2.4 Effect of precursor solubility on catalyst activity

A number of researchers have found that dispersed catalysts synthesized from oil soluble metal salts are more active than those resulting from oil insoluble compounds. Dabkowski and co-workers (1991) conducted hydrocracking experiments on Arabian heavy residues using dispersed catalysts derived from organometallic compounds of varying solubility. The researchers found that distillate yield, demetallization activity and desulfurization activity increased with increasing precursor solubility, whereas coke yield decreased with increasing solubility.

Bearden and Aldridge (1981) conducted similar hydrocracking experiments on heavy crude oil using the M-COKE process, and found that catalysts from oil soluble Mo naphthenate and $Mo(CO)_6$ gave higher desulfurization activity, higher CCR conversion and lower coke yields than oil-insoluble MoO_3 and MoS_2.

Hirschon and Wilson (1989) found that dispersed catalysts derived from oil soluble $Mo_2(OAc)_4$ and $Cp_2Mo_2(\mu\text{-}SH)_2(\mu\text{-}S)_2$ gave higher conversion of coal to liquids than oil-insoluble tetrathiomolybdate impregnated from aqueous solution.

2.2.5 Size distribution of dispersed catalysts

Researchers have studied the size distributions of dispersed metal catalysts derived from organometallic precursors using a number of different techniques. Bulk particle size was generally determined by microscopic techniques, including scanning electron microscopy (SEM) and transmission electron microscopy (TEM), whereas crystallite size was generally determined using x-ray diffraction (XRD) and Mössbauer Spectroscopy. Takemura and Okada (1988) investigated

the size of Ni crystallites resulting from the decomposition of nickel acetate in coal liquefaction feed. XRD analysis gave crystallite sizes ranging from 14.6 to 28.5 nm. The researchers also found that the Ni crystallite size increased with both decomposition temperature and nickel concentration. In addition the researchers found that the specific activity of the Ni catalyst increased linearly with crystallite diameter.

Liu *et al.* (1994) investigated MoS_2 synthesized in heavy oil from various oil-soluble and oil-insoluble Mo precursors. XRD analysis gave average crystallite sizes of 4-5 nm in the perpendicular direction, and 4-7 nm in the lateral direction, and the solubility of the metal salt did not have a dramatic effect on crystallite size. Bulk particle sizes (as determined by SEM and TEM) were found to be in the range of 1-2 μm.

Kim and co-workers characterized dispersed catalysts resulting from the decomposition of molybdenum naphthenate in coal liquefaction model systems (Kim *et al.*, 1989). XRD analysis gave crystallite sizes of 2.6 nm in the perpendicular direction and 4.5 nm in the lateral direction. The 'needle-shaped' crystallites displayed a so-called 'rag morphology' previously described by Pecoraro and Chianelli (1981). Bulk catalyst particle sizes were found to range from 50 to 250 nm, and the catalyst surface areas ranged from 150 to 200 m^2/g.

Herrick *et al.* (1990) investigated the decomposition products of $Fe(CO)_5$ for coal/heavy oil co-processing. XRD analysis gave crystallite sizes ranging from 12-20.5 nm. Mossbauer spectroscopy gave crystallite sizes ranging from 5-20 nm. TEM analysis of the bulk catalyst gave particle sizes ranging from 100 to 1000 nm, and the particles displayed a granularity at the 10-50 nm scale.

These studies show that oil soluble organometallics generally decompose to form very small crystallites in the 2-7 nm range. However, it would appear that the individual crystallites

aggregate to much larger bulk particles in the 50 - 3000 nm range. It is unclear whether this aggregation occurs under the reaction conditions, or later during cooling or sample preparation.

2.2.6. Active species of dispersed catalysts

The active metal sulfide species of dispersed catalysts have been well characterized by a number of researchers using XRD, Mössbauer spectroscopy and Fourrier transform infra red (FTIR) spectroscopy. Liu *et al.* (1994), Kim *et al.* (1989), and Curtis and Pellegrino (1989) identified MoS_2 as the active species formed from various molybdenum-based precursors. Anderson and Bockrath (1984) and Herrick *et al.* (1990) identified the non-stoichiometric sulfide $Fe_{1-X}S$ as the active species formed from various iron-based organometallic compounds.

2.2.7. Disadvantages of dispersed catalysts derived from organometallic compounds

Although organometallic precursors yield active catalysts for the hydrocracking of heavy oil, this synthesis technique suffers from a number of drawbacks. Firstly, there is little evidence in the literature to suggest that the catalyst particle size can be controlled when synthesized from these precursors. Hence, there is no information in the literature on the relationship between dispersed catalyst size and activity. In addition, the requirement for the organometallic precursors to be soluble in the heavy oil limits the choice of catalysts which can be synthesized from these precursors.

Consequently, further understanding of the factors affecting the activity of dispersed catalysts is hampered by this apparent lack of control over particle size. Hence there is a need to find an alternate synthesis technique for dispersed catalysts in a hydrocarbon medium which allows for control over the catalyst particle size, and allows more flexibility with respect to the choice of metals which can be synthesized.

2.3 Preparation of metal colloids in reverse micelles

2.3.1 Introduction

A novel technique for the preparation of metal colloids dispersed in organic solvents has been developed in recent years. Monodisperse suspensions of a wide range of metals and metal compounds have been prepared by the precipitation of water-soluble metal salts dissolved within the water pools of a microemulsion. This synthesis technique allows for the simple control of particle size, a factor which together with their narrow size distribution makes these colloids potentially attractive catalysts (Boutonnet *et al.*, 1991).

2.3.2 Emulsions and microemulsions

An emulsion is generally defined as a mixture of two immiscible liquids wherein one of the liquids is broken into small particles and dispersed within the second liquid (Shaw, 1992). This produces a tremendous increase in the interfacial free energy of the system and makes emulsions thermodynamically unstable. This thermodynamic instability means that phase separation is usually rapid without the presence of an emulsifying agent to stabilize the system (Shaw, 1992). In nearly all emulsions, one of the phases is aqueous and the other a hydrocarbon or 'oil'. If the oil is the dispersed phase, then the emulsion is termed 'oil-in-water' (O/W); and if the aqueous medium is the dispersed phase, then the emulsion is termed 'water-in-oil' (W/O). There are three types of emulsions based on the size of the dispersed particles (Rosen, 1978): (i) macroemulsions, opaque emulsions with particles larger than 400 nm; (ii) miniemulsions, blue-white with particle sizes in the 100-400 nm range; (iii) microemulsions, transparent dispersions with particles smaller than 100 nm.

A microemulsion is usually defined as an emulsion of water, oil and an amphiphile/surfactant which forms a single optically isotropic and thermodynamically stable liquid

solution (Danielsson and Lindman, 1981). The surfactant molecules adsorb to the interface between the immiscible liquids, and stabilize the dispersed phase by lowering the interfacial surface tension and free energy of the system (Shaw, 1992; Pillai *et al.*, 1993). With the interfacial tension (γ_{OW}) close to zero, microemulsions form spontaneously and are thermodynamically stable (Shaw, 1992). In addition, the surfactant layer decreases the rate of coalescence of the dispersed liquid particles by forming mechanical, steric and/or electrical barriers around them. Microemulsions are also classified as oil-in-water or water-in-oil, with surfactants self-assembled around droplets of the dispersed phase in either case. Surfactant-stabilized water pools in a hydrocarbon environment (i.e. O/W microemulsion) are often referred to as inverse or reverse micelles (Fendler, 1987).

2.3.3 Colloid formation in reverse micelles.

Extremely small (<10 nm diameter) monodisperse metallic colloids can be prepared in-situ in the aqueous pools of W/O microemulsions (Fendler, 1987). A summary of examples cited in the literature is presented in Table 2.2. Water soluble metal salts are incorporated into the aqueous droplets of the microemulsion, and the metal/metal compound is then precipitated in the microheterogeneous environment by the addition of a suitable precipitation/reduction agent (Boutonnet *et al.*, 1982; Martino *et al.*, 1994). Confinement within the microenvironment of the reverse micelle limits particle growth (Fendler, 1987), since the surfactant interface provides a spatial constraint on the reaction volume (Martino *et al.*, 1994). Following precipitation, the colloidal particles are stabilized against flocculation by the surfactant (Fendler, 1987; Henglein, 1989) and can remain dispersed in suspension for extended periods (Boutonnet *et al.*, 1982).

Table 2.2 : Examples of metals and inorganic compounds prepared in reverse micelles.

Authors	Colloids	Microemulsion System(s)[1]	Precipitation Agent	Particle Size (nm)
Boutonnet *et al.* (1991)	Pt	Water/PEGDE/Hexadecane	N_2H_4	3 ± 0.5
Boutonnet *et al.* (1982)	Pt, Rh, Pd, Ir	Water/CTAB/Octanol Water/PEGDE/Hexane	N_2H_4 / H_2	Pt : 2.5-3 Rh : 3 Ir : 3
Pillai *et al.* (1993)	$BaCO_3$	Water/CTAB/Octane	NH_4CO_3	5 - 15
Pileni and Lisiecki (1993)	Cu	Water/AOT/Alkane	N_2H_4 / $NaBH_4$ (in micelle)	3 - 28
Martino *et al.* (1991)	Fe, Pd, FeS_2	Water/DDAB/Toluene Water/$C_{12}E_4$/Octane Water/Ph_9E_6/Cyclohexane	$LiBH_4$ Li_2S	Fe: 1.5±0.2 Pd: 1.8±0.2 FeS_2: 3.1±0.1
Ravet *et al.* (1987)	Ni_2B, Co_2B, Ni-Co-B	Water/CTAB/n-Hexanol	$NaBH_4$	3 - 7
Nagy *et al.* (1983)	Ni_2B	Water/CTAB/n-Hexanol	$NaBH_4$	4 - 7
Pileni *et al.* (1992)	CdS	Water/AOT/iso-Octane	H_2S / Na_2S (in micelle)	2 - 4

A number of different precipitation/reduction agents have been used to prepare colloids in reverse micelles, the choice of the particular reducing agent depending largely on the type of metal compound being synthesized. These agents can be divided into 3 broad categories:

1. Liquid reducing agents added directly to the microemulsions. Examples of liquid reducing agents reported in the literature include hydrazine hydrate $N_2H_4.xH_2O$ (Boutonnet *et al.*, 1982 and 1991), aqueous solutions of various metal borohydrides including $LiBH_4$ and $NaBH_4$

[1] Note: PEGDE, $C_{12}E_4$ and Ph_9E_6 represent the non-ionic surfactants pentaethyleneglycoldodecylether, butylethylene glycol n-dodecyl ether and polyoxyethylene(6) nonylphenol; CTAB, DDAB and AOT represent the ionic surfactants cetyltrimethylammonium bromide, didodecyldimethylammonium bromide and surfactant bis(2-ethylhexyl) sulfosuccinate respectively.

(Nagy *et al.*, 1983; Ravet *et al.*, 1984 and 1987; Martino *et al.*, 1994) and aqueous solutions of lithium sulfide Li_2S (Martino *et al.*, 1994).

2. Gaseous precipitation agents added either in a static pressurized system or a flow system. Examples include H_2 (Boutonnet *et al.*, 1982), H_2S (Meyer *et al.*, 1984; Lianos and Thomas, 1987; Petit *et al.*, 1990; Pileni *et al.*, 1992) and CO_2 (Kon-no *et al.*, 1984; Kandori *et al.*, 1986).
3. Reverse micelle entrapped reducing agents. The dispersed droplets in a microemulsion continuously collide, coalesce and decoalesce, resulting in the continuous exchange of solute content (Flecher *et al.*, 1987). This exchange process can be utilized to react/precipitate different chemical species contained within different water pools. Two identical microemulsions containing the metal salt and the reducing agent dissolved within the water pools are mixed, resulting in the precipitation of solid colloids upon exchange of the reverse micelle contents. Examples of micelle entrapped reducing agents include NH_4CO_3 (Pillai *et al.*, 1993), $N_2H_4.xH_2O$ (Pileni and Lisiecki, 1993) and Na_2S (Petit and Pileni, 1988).

Colloid formation in reverse micelles is a complex process involving interplay between nucleation, microcrystal formation, intermediate growth (Ostwald ripening), coagulation and flocculation, and no single mechanism has been agreed upon in the literature (Fendler, 1987). A number of researchers have proposed a simple statistical mechanism for crystal growth in reverse micelles (Ravet *et al.*, 1987; Nagy *et al.*, 1983). The proposed mechanism is based on a number of fundamental assumptions (Ravet *et al.*, 1987):

- Metal ions are statistically distributed through the water cores of a microemulsion according to a gaussian distribution (Vold and Vold, 1983).
- A minimum number of metal ions are required to form a stable nucleus.
- The nucleation step is always slower than the growth process.

A diagrammatic representation of the proposed mechanism for the formation of metal borides is given in Figure 2.2.

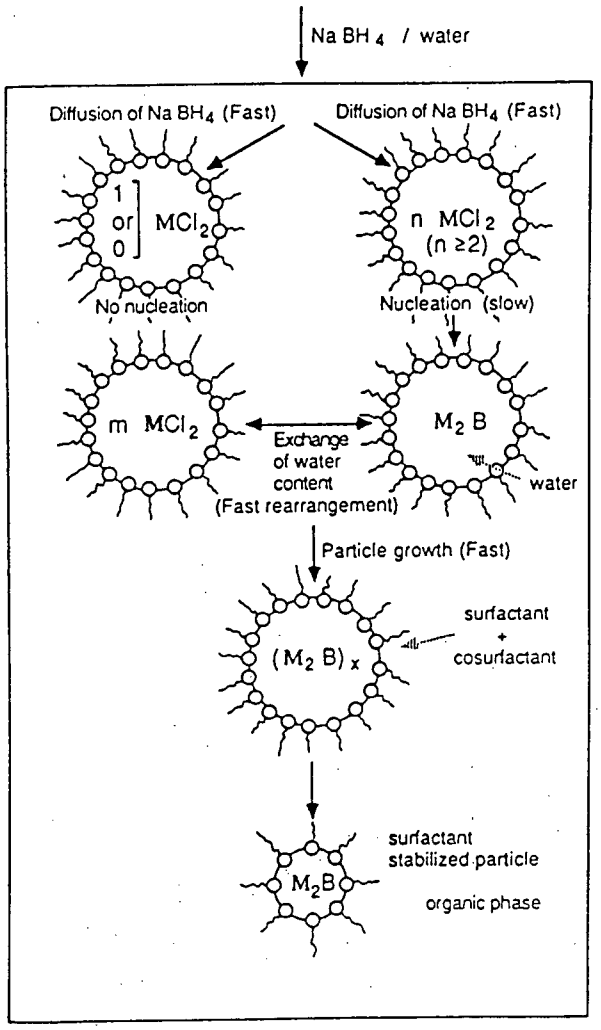

Figure 2.2 : Proposed mechanisms for metal boride formation in reverse micelles (Ravet *et al.*, 1987; Nagy *et al.*, 1983).

At the very beginning of the reduction process, nucleation occurs only in those water pools which contain more than the minimum number of metal ions required to form a stable nucleus. Following the initial nucleation step, additional ions are brought into contact with the existing nuclei through dynamic exchange between the water cores. These additional ions participate in the growth process, but no new nuclei are formed at this time since the nucleation process is much slower than particle growth. Consequently, the nuclei formed at the beginning of

the reduction grow at the same rate and ultimately form colloids of the same size (Ravet *et al.*, 1987; Nagy *et al.*, 1983). Cluster growth terminates when the colloids reach a critical size where the surface tension of the reverse micelle prevents further material entering and adding to the colloids (Steigerwald and Brus, 1989). According to this mechanism, the colloid size depends on a number of factors, including: the number of water cores containing enough ions to form stable nuclei, the rate of rearrangement of the system, and the ability of the reducing agent to diffuse into the solution and reach the water pools before system rearrangement.

2.3.4 Factors affecting the size of reverse micelles and colloids

A number of factors affect the size of reverse micelles and the size of colloids synthesized therein. It is important to identify these factors since they allow one to manipulate the size (and therefore the surface area) of colloids synthesized using the reverse micelle technique.

The most obvious factor which affects the size of reverse micelles is the water:surfactant ratio in the microemulsion (ω). A number of researchers have found that the water pool size increases in a linear fashion with increasing ω (Ravet *et al.*, 1984; Kizling and Stenius, 1987; Nagy *et al.*, 1983, Modes and Lianos, 1989; Pileni *et al.*, 1992). This relationship is illustrated in Figure 2.3 (a) for the water/CTAB/n-Hexanol microemulsion. The observed trend has been found to apply to both ionic (Ravet *et al.*, 1984) and non-ionic (Kizling and Stenius, 1987) surfactant systems. A number of systems have been well characterized; for example, $R_W(Å)=1.5*\omega$ for the water/AOT/Alkane system (Pileni *et al.*, 1985), and $R_W(Å)=3.6+0.52*(\%\ Water)$ for the water/CTAB/n-Hexanol system (Nagy *et al.*, 1983). The trend of increasing water pool size with increasing ω is relatively simple to explain. For a fixed amount of surfactant the interfacial area which can be stabilized by the surfactant is fixed. Consequently, new water pools cannot be

formed if ω is increased, and the water pools must swell to accommodate extra water added to the system.

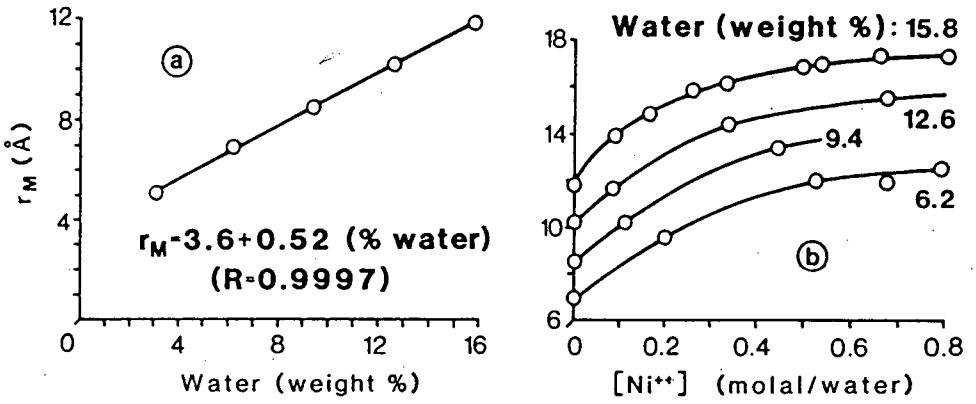

Figure 2.3 : Variation of the average radius (r_M) of the water cores in the water/CTAB/n-Hexanol microemulsion as a function of (a) water content and (b) Ni(II) concentration (Nagy *et al.*, 1982).

Researchers have also found that the size of colloidal particles precipitated in reverse micelles increases with increasing ω, and this trend has been found to apply to all surfactant types and reducing agents (Ravet *et al.*, 1984; Nagy *et al.*, 1983, Modes and Lianos, 1989; Pileni *et al.*, 1992). This trend is illustrated in Figure 2.4. for Ni_2B colloids synthesized in the water/CTAB/n-Hexanol microemulsion. Nagy *et al.* explained this trend in terms of their mechanism of colloid formation (discussed in section 2.3.3). Particle growth in a reverse micelle ceases when the particle reaches a critical size where the surface tension of the surfactant layer keeps the reverse micelle intact, thus preventing further material exchange between water pools. This implies that the critical nucleus size depends on the reverse micelle size, which in-turn depends on the water:surfactant ratio ω (Steigerwald and Brus, 1989). Consequently, increasing ω yields larger particles.

The second factor which affects reverse micelle size is the concentration of metal ions within the water pools. A number of researchers have found that water pool size increases with an increasing metal ion concentration, tending to a limiting water pool size at very high concentrations (Ravet *et al.*, 1984; Nagy *et al.*, 1983; Ravet *et al.*, 1987). This trend is illustrated in Figure 2.3 (b). Ravet *et al.* explained this phenomenon for the case of Co(II) and Ni(II) ions in the ionic surfactant system water/CTAB/n-Hexanol (Ravet *et al.*, 1984). The authors found that one or two hexanol molecules participate in the co-ordination shells of tetrahedral Co(II) and Ni(II) complexes. Consequently, an increase in the concentration of metal ions in the water pool leads to an increase in number of hexanol molecules at the surfactant interface, and thus to an increase in the interfacial free energy of the system. An increase in the interfacial free energy of the system in turn leads to an increase in the reverse micelle size.

The effect of metal ion concentration on the size of reverse micelles in microemulsions of non-ionic surfactants has not been directly reported in the literature. However, it is possible to deduce the effect of metal ion concentration in these systems by examining the effect of metal ions on the hydrophilic/lipophilic balance (HLB) of non-ionic polyoxyethylene (POE) based surfactants. Researchers have shown that different electrolytes affect the HLB of nonionic surfactants in different ways, depending on the nature of the electrolyte (Schick M. J., 1987). Schott found that nitrate salts of multivalent cations (e.g. $Ni(NO_3)_2$, $LiNO_3$, $Mg(NO_3)_2$) form stable complexes with oxygen atoms in the POE chains of nonionic POE based surfactants, as shown below:

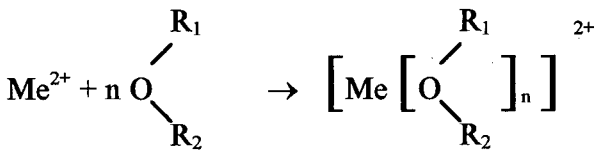

Schott found that this complex formation resulted in a so-called 'salting in' effect, raising the cloud point and HLB of the nonionic surfactant. The increase in HLB of the surfactant was found to be proportional to the metal ion concentration in the system (Schott, 1973).

The effect of the HLB on the size of reverse micelles of nonionic surfactants can be deduced by examining the effect of temperature on the HLB and reverse micelle size. A number of researchers have found that the HLB of POE based non-ionic surfactants decreases with increasing temperature (Schick, 1987; Shaw, 1992). Kizling and Stenius found that increasing temperature (decreasing HLB) leads to a decrease in the size of the reverse micelles in the nonionic surfactant system water/PEGDE/hexadecane (Kizling and Stenius, 1987). These two experimental observations imply that a decrease in HLB results in a decrease in reverse micelle size, and an increase in HLB leads to an increase in reverse micelle size. This in turn implies that increasing the concentration of certain metal ions (e.g. $Ni(NO_3)_2$) within reverse micelles of nonionic surfactants will lead to an increase in the HLB of the surfactant molecules at the interface, thus leading to an increase in the size of the reverse micelles.

The concentration of metal ions dissolved within reverse micelles also has an effect on the size of the colloidal particles precipitated within the reverse micelles. Ravet *et al.* (1984) and Nagy *et al.* (1983) studied the precipitation of Co_2B and Ni_2B particles in the water/CTAB/n-Hexanol system and found that a complex relationship exists between particle size and metal ion concentration (see Figure 2.4).

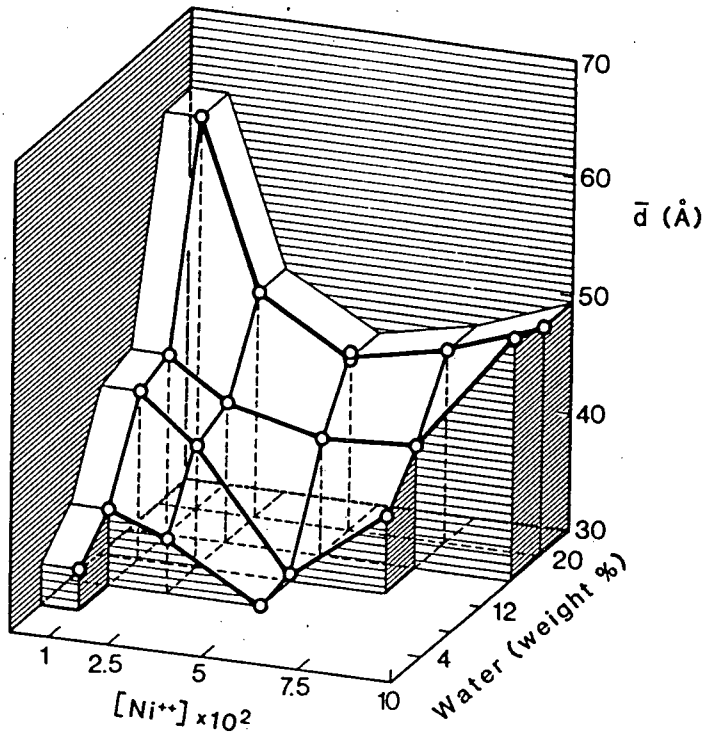

Figure 2.4 : Variation of the average diameter (d in Å) of the nickel boride particles prepared in water/CTAB/n-Hexanol as a function of water content and Ni(II) concentration (Nagy *et al.*, 1982).

As illustrated in Figure 2.4, a minimum particle size was found, with particle size increasing with increasing ion concentration at high metal concentrations. Ravet *et al.* explain this phenomena using the statistical mechanism for colloid formation in reverse micelles discussed in section 2.3.3. The size of particles formed in reverse micelles is inversely proportional to the number of nucleation sites formed at the beginning of the reaction. At low ion concentration, only a few water cores contain the minimum number of ions necessary to form a nucleus. Hence, few nuclei are formed at the very beginning of the reduction and the size of the particles formed is quite large. The researchers found that as ion concentration increases, the distribution of precursor ions in the reverse micelles changes, and the number of nuclei obtained by reduction increases faster than the total number of ions in the system. This results in a decrease in the particle size to a minimum. When more than 80% of the water cores have enough ions to form

stable nuclei, the number of nuclei formed remains quasi constant with increasing ion concentration. Hence, the size of the particles formed increases again.

A number of other factors also affect the size of reverse micelles and the colloids synthesized therein. Kizling and Stenius (1987) found that the size of the reverse micelles in the non-ionic water/PEGDE/Hexadecane system decreased with increasing temperature between 22 and 38 °C. Further increases in temperature lead abruptly to phase separation. The observed trend was probably linked to changes in the hydrophobic/lipophobic balance (HLB) experienced by non-ionic surfactants at elevated temperatures (Overbeek *et al.*, 1984). A number of researchers have also found that the amount of reducing agent affects the size of the colloids formed (Nagy *et al.*, 1983; Pileni *et al.*, 1992). In general, the researchers found that larger particles were formed when the cation/anion ratio was ≈ 1, and that the particle size decreased when the reducing agent was in excess. Finally, the type of micellar system used has an effect on the size of the solid particles precipitated in reverse micelles. The viscosity of the hydrocarbon continuous phase and the characteristics of the surfactant (e.g. hydrophobic/lipophobic balance) affect the morphology of the surfactant interface, the rate of exchange of reactants between water pools, and hence the size of the particles formed (Steigerwald and Brus, 1989).

2.3.5 Catalytic activity of colloids synthesized in reverse micelles

The small size and monodisperse nature of dispersed particles prepared in reverse micelles make them attractive as potential catalysts. A number of researchers have investigated the use of colloidal metal/metal compounds synthesized in reverse micelles as catalysts for a number of hydrogenation and hydrogenolysis reactions.

Nagy *et al.* (1983) and Ravet *et al.* (1984) investigated the hydrogenation of 1-heptene using Ni_2B and Co_2B colloids prepared in the water/CTAB/n-Hexanol microemulsion. The

reactions were performed *in-situ* in a mixture ethanol and a microemulsion containing the metal boride colloids. The researchers obtained quite different results for the different catalysts. The activity of the Ni_2B colloids was found to be greater than Raney catalysts prepared in ethanol by 'conventional' methods. The presence of surfactant in the reaction system did not appear to affect the activity of the Ni_2B catalyst (Nagy *et al.*, 1983). However, the researchers found that the CTAB surfactant had a depleting effect on the catalytic activity of Co_2B colloids synthesized in the same way. In this case 2 nm Co_2B colloids showed lower activity for the hydrogenation of 1-heptene than 250 nm Co_2B prepared in ethanol (Ravet *et al.*, 1984).

Boutonnet *et al.* investigated the hydrogenation and isomerization of 1-butene using platinum colloids in a microemulsion, and microemulsion-generated platinum supported on pumice (Boutonnet *et al.*, 1986; Boutonnet *et al.*, 1987). The researchers found that the deposition of microemulsion-generated Pt particles on a solid support provided an excellent catalyst for the hydrogenation and isomerization of 1-butene. However, considerably less catalytic activity was observed when the same reaction was performed in the microemulsion phase. The authors claim that the surfactant coating hindered the accessibility of 1-butene and hydrogen to the catalyst surface.

Martino *et al.* (1994) investigated the catalytic activity of various metals prepared in microemulsions in three separate reactions: (i) hydrogenolysis of naphthylbibenzylmethane (a coal liquefaction model compound), (ii) hydropyrolysis of coal, and (iii) coal liquefaction. The researchers found that the presence of surfactant pyrolysis byproducts in reaction (i) resulted in a loss in catalyst activity. They attributed this loss in activity to the scavenging of hydrogen by the surfactant byproducts, as well as possible chemical and steric poisoning by the surfactant. The effect of surfactant was found to be less pronounced in reactions (ii) and (iii), and colloidal Pd

prepared in the water/DDAB/Toluene system was as active as commercial MoS_2 for the hydropyrolysis of coal.

In conclusion, the catalytic activity of colloidal metal particles synthesized in reverse micelles appears to be highly dependent on the particular reaction, type of metal and type of surfactant used, especially if the reaction is performed *in-situ* in the microemulsion suspension. Evidence in the literature suggests that the presence of surfactant either depletes or has no effect on the catalytic effect of colloidal catalysts in reverse micelles, depending on the particular system studied.

2.3.6 Preparation of dispersed hydrocracking catalysts in reverse micelles

The application of metal colloids prepared in reverse micelles as dispersed heavy oil hydrocracking catalysts holds a number of potential advantages over dispersed catalysts prepared from organometallics. Firstly, a number of researchers have demonstrated that the size of solid colloids prepared in reverse micelles can be controlled and manipulated, whereas there is little evidence in the literature to suggest that the size of catalyst particles synthesized from organometallics can be controlled. Consequently, the relationship between dispersed catalyst size and activity may potentially be investigated using dispersed catalysts prepared in reverse micelles. Secondly, the range of catalysts which can be prepared from organometallics is limited by the solubility of the organometallics in the heavy oil. No such restriction applies to colloidal catalysts prepared in microemulsions, and it is believed that these catalysts can be well dispersed or mixed within the heavy oil feed, especially if the organic component of the microemulsion is highly soluble in the heavy oil.

Chapter 3 : Experimental Methods

3.1 Microemulsion preparation and colloid synthesis

3.1.1 Microemulsion preparation

The present work focused on the water-in-oil microemulsion water/polyoxyethylene-4-laurylether/n-hexane. Polyoxyethylene-4-laurylether (Sigma Chemical Company) and n-hexane (Aldrich Chemical Company, HPLC Grade) were used as received. Microemulsions were prepared with either cobalt nitrate ($Co(NO_3)_2.6H_2O$, Sigma Chemical Company, 99.4%), nickel nitrate ($Ni(NO_3)_2.6H_2O$, Aldrich Chemical Company) or ferric nitrate ($Fe(NO)_3.9H_2O$, Fisher Scientific, 99.0 %) dissolved within the water pools of the microemulsions. Both the water:surfactant ratio (ω) and the metal ion concentration in microemulsions were varied for each of the metals investigated. A full list of the microemulsions prepared is presented in Appendix 1.1. A number of water/polyoxyethylene-4-laurylether/decahydronaphthalene (Decahydronaphthalene, Sigma Chemical Company, 98%) microemulsions were also prepared for a preliminary series of activity measurements. This issue is discussed further in section 3.4.3.

In a typical preparation, specified volumes of polyoxyethylene-4-laurylether (PE4LE) and hexane were pre-mixed. The appropriate volume of a metal nitrate solution of specified concentration was added to the PE4LE/hexane mixture. The system was equilibrated by mixing with a magnetic stirrer for a period of 12 hours. Metal salt solutions of varying concentration were prepared from stock solutions of known metal ion concentration. The stock solutions were assayed using atomic absorption by ACME Analytical Laboratories, Vancouver. The preparation procedure allowed for the precise control of the water:surfactant ratio in the microemulsion and

metal ion concentration within the water pools of the microemulsion. After preparation, the microemulsions were stored in sealed bottles in a refrigerator at 3-4 °C.

3.1.2 Synthesis of reduced metal colloids

Reduced nickel, cobalt and iron colloids were prepared in water/PE4LE/hexane microemulsions following the procedure used by Boutonnet *et al.* (1982). A typical preparation procedure involved adding hydrazine hydrate ($N_2H_4.xH_2O$, Aldrich Chemical Company, 55 wt% N_2H_4) drop-wise to a microemulsion containing a metal salt dissolved within the water pools. A 5:1 molar ratio of $[N_2H_4]$:[Metal] was used to ensure the complete reduction of the metal species in the microemulsion (Martino *et al.*, 1994). In addition, the size of colloids precipitated in reverse micelles is minimized when the reducing agent is in excess (Nagy *et al.*, 1983; Pileni *et al.*, 1992). The microemulsions were stored in sealed bottles following reduction.

3.1.3 Synthesis of metal sulfide colloids using dimethyl disulfide

The high temperature synthesis of metal sulfide colloids in the water/PE4LE/hexane microemulsion using dimethyl disulfide (DMDS) was investigated in the early part of this study. These experiments were performed in a 300 mL Autoclave Engineers EZE-SEAL batch reactor, heated by a jacket furnace and temperature controller. The reactor contents were mixed by a magnetically driven impeller with an accompanying speed controller. A schematic diagram of the batch reactor system is given in Figure 3.1. A typical synthesis experiment involved adding dimethyl disulfide ($(CH_3)_2S_2$, Aldrich Chemical Company, 98 %) equivalent to 3 wt% sulfur to 100 mL of a water/PE4LE/hexane microemulsion containing either nickel, cobalt or iron nitrate dissolved within the waterpools. The mixture was then placed in the reactor, the reactor was purged with N_2 (UHP, Medigas) and pressurized to 790 kPa (100 psig) with H_2 (UHP,

Medigas). The reactor was then heated to 210 °C at a temperature ramp rate of 1.5 °C/min, and held at this temperature for 2 hours. At the end of the reaction time, the jacket furnace was removed and the reactor was quenched using the internal water-cooled cooling coil.

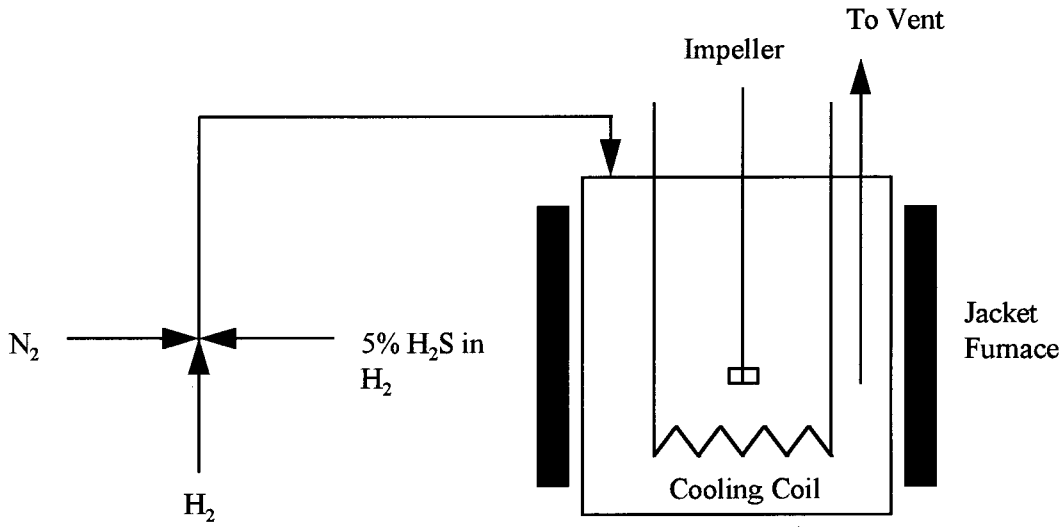

Figure 3.1 : Flow diagram of batch autoclave system used for colloid synthesis and activity measurements.

3.1.4 Synthesis of metal sulfide colloids using H_2S

Nickel, cobalt and iron sulfide colloids were prepared in water/PE4LE/hexane microemulsions using H_2S at room temperature. In a typical experiment, 100 mL of a water/PE4LE/hexane microemulsion containing either nickel, cobalt or iron nitrate (dissolved within the waterpools) was placed in the reactor and the reactor was purged with nitrogen. The reactor was then pressurized to 7 MPa (1000 psig) with a 5% mixture of H_2S in H_2 (Medigas) and stirred at ± 500 rpm. The reaction proceeded for a specified reaction time of either 2 or 6 hours. At the end of the reaction, the reactor was vented and the metal sulfide suspension was removed.

3.2 Micelle characterization by dynamic light scattering (DLS)

A number of techniques have been used to measure the size of reverse micelles in microemulsions, including dynamic light scattering (Boutonnet *et al.*, 1982; Kizling and Stenius, 1987; Wilcoxon *et al.*, 1993), small angle neutron scattering (Robinson *et al.*, 1984), small angle x-ray scattering (Pileni *et al.*, 1985) and ^{19}F-NMR spectroscopy of labeled probe molecules in the micellar solution (Ravet *et al.*, 1984; Ravet *et al.*, 1985). In the present study, dynamic light scattering (DLS) was used to determine the size of the reverse micelles in the water/PE4LE/hexane microemulsion. The DLS measurements and analysis were performed by Dr. Barbara Frisken in the Department of Physics, Simon Fraser University. The DLS equipment consisted of a He/Ne laser (λ = 633 nm) as a light source, a cell holder and an ALV 'Multi-μ' autocorrelator. The microemulsion samples were diluted in hexane and placed in 20 mm vials in the cell holder. The method used by Kizling and Stenius (1987) and Chang and Kaler (1986) was followed to determine the size of the reverse micelles in solution. The normalized intensity correlation function $g^{(2)}(\tau)$ was analyzed by the method of cumulants, and $g^{(2)}(\tau)$ was fit with a simple monomodal expression:

$$g^{(2)}(\tau) = B + A\exp(-2\bar{\Gamma}\tau + \mu\tau^2)$$

Where, τ = delay time (s)

A = Constant (depending on the geometry of the light scattering apparatus)

$B \approx 1$

$\bar{\Gamma}$ = Average decay rate (1/s)

$\bar{\Gamma}$ and μ were determined from the exponential regression, and the apparent diffusion coefficient of the scattering units (D_{app}) was calculated using the equation:

$$D_{app} = \frac{\bar{\Gamma}}{q^2}$$

Where, the scattering wave vector q is defined as follows:

$$q = \frac{4\pi n}{\lambda} \mathrm{Sin}\left(\frac{\Theta}{2}\right)$$

Here, Θ = Scattering angle (90°)

λ = Wavelength of the scattered light

= 633 nm

Chang and Kaler (1986) have shown that the apparent diffusion coefficient $D_{app} \approx D_o$ (intrinsic diffusion coefficient) for this type of system. Consequently, the hydrodynamic radii (r_H) of the reverse micelles in the microemulsion were calculated directly from the Stokes-Einstein equation:

$$r_H = \frac{kT}{6\pi\eta D_{app}}$$

Where, η = Solvent viscosity

The parameter $\frac{\mu}{\Gamma^2}$ gives a measure of the relative variance of the monomodal distribution, a value of 0.05 or less indicating an acceptable degree of monodispersity

The size of the reverse micelles in each microemulsion was measured 3 times and the average diameter was calculated for each sample. The standard deviation in the measured diameter was also calculated in each case. This standard deviation gave an estimate of the instrumentational error in the measurement of the reverse micelle diameters.

3.3 Colloid characterization

3.3.1 Dynamic light scattering (DLS)

The particle sizes of the reduced metal colloids synthesized within reverse micelles were determined by dynamic light scattering (DLS). The experimental procedure was the same as that used to measure the size of the reverse micelles (described in section 3.2). However, the DLS

data were analyzed in a slightly different way. A multi-modal particle size distribution was assumed in the regression of the normalized intensity correlation function. Consequently, a distribution of particle sizes could be detected and characterized using DLS.

3.3.2 Transmission electron microscopy (TEM)

The particle sizes of the reduced metal and metal sulfide colloids synthesized within reverse micelles were also determined by transmission electron microscopy (TEM). A Hitachi H-800 electron microscope operating in the transmission mode at 100 kV was used. TEM samples were prepared following the method used by Boutonnet *et al.* (1982) and Wilcoxon *et al.* (1993). Samples were deposited directly onto carbon coated Mo, W or Au grids by the application of 1-2 droplets (2-5 μL) of the colloid-containing microemulsion. The grids were then either examined as prepared, or dried in a vacuum oven at 120 °C and 2 torr for a period of 12 hours. The grids were examined using the electron microscope, and an attempt was made to examine and photograph many representative portions of the grid in order to determine the average particle size. The approximate average particle sizes were obtained from a histogram of the number vs. size of all the particles photographed.

3.3.3 Energy dispersive x-ray spectrometry (EDX)

Elemental analysis of the particles observed by TEM was performed using an Ortec EEDS II energy disperse X-Ray spectrometer operating in tandem with the Hitachi H-800 electron microscope. The electron microscope was operated in the scanning transmission mode (STEM) for the EDX analysis.

3.3.4 X-Ray diffraction (XRD)

Phase analysis of the metal sulfide colloids synthesized in the reverse micelles was performed by powder x-ray diffraction. A Siemens D5000 powder diffractometer using Cu Kα radiation (λ = 1.5406 Å) at 40 kV and 30 mA was used, and the analysis was performed at room temperature (22 °C). The metal sulfide colloids were extracted from the microemulsions following the method described by Boutonnet *et al.* (1991): Twice excess tetrahydrofuran (THF, Aldrich Chemical Company, HPLC grade) was first added to the microemulsions containing the metal sulfide colloids, causing the colloids to aggregate and settle from suspension over a period of approximately 12 hours. The colloid-free supernatant was decanted off and the settled colloids were washed 3-4 times with fresh THF to remove excess surfactant. The washed colloids were then dried in a vacuum oven at 22 °C and 2 torr for 12 hours. The dried samples were finally ground into a fine powder and mounted on an acrylic sample holder ready for XRD analysis. The metal sulfide species present were identified by comparing the XRD spectra obtained with standard spectra of various metal sulfide compounds. Siemens peak matching and identification software was also used to aid in the identification of the metal species present.

The spent catalysts from the model compound activity tests were also analyzed using XRD, in order to identify the metal species present and determine the average crystallite sizes. The spent catalyst was allowed to settle in the liquid reactor product, and was then removed from the liquid using a pipette. The concentrated catalyst 'slurry' was then deposited drop-wise on a glass slide. The first stage of the sample preparation was performed under a nitrogen blanket in a glove box to minimize exposure to the air. The samples were then transferred to a vacuum oven and dried at 22 °C and 2 torr for 12 hours to evaporate the liquid hydrocarbons. The average

crystallite sizes were calculated from the peak width at half-height using the Debye-Scherrer equation:

$$t = \frac{\lambda}{B.Cos\Theta}$$

Where,

$$B = \sqrt{W^2 - w^2}$$

t = Crystallite size (Å) λ = Wavelength (1.5406 Å)

Θ = Peak position (radians) W = Peak width at half height (radians)

w = Instrumental peak broadening (radians)

= 0.2 degrees

3.3.5 X-Ray photoelectron spectroscopy (XPS)

The metal sulfide colloids synthesized in the reverse micelles were also analyzed using x-ray photoelectron spectroscopy (XPS). XPS allows one to identify the chemical species on the surface layer (several atoms thick) of a sample (Delgass *et al.*, 1970). The XPS measurements were made by Dr. Philip Wong, in the Department of Chemistry, UBC. The XPS spectra were measured using a Leybold MAX-200 spectrometer with computer controlled data acquisition. Unmonochromatized Al Kα x-rays (hν = 1486.6 eV) were used. The system pressure was $1.28*10^{-8}$ mbar during the data collection. The XPS system was calibrated using the C 1s line of air-borne carbon (binding energy = 285.0 eV). Charging effects were also measured by the shift in the C 1s line, and were automatically corrected for by the spectrometer software.

Two samples were prepared for each of the metal sulfides analyzed by XPS. The first set was prepared and transported under a helium (UHP, Medigas) blanket in an attempt to prevent exposure to atmospheric oxygen. The samples were exposed to the air briefly when they were

removed from the inert atmosphere of the sample bottle and placed in the XPS sample holder. A typical sample preparation procedure involved depositing 100-200 droplets (0.5 to 1 mL) of the colloid-containing microemulsion onto a 1 cm^2 square of glass fiber filter paper (glass micro-fiber filter paper, Watmann Company). The colloid impregnated square was then transported under a flowing He blanket to a vacuum oven and dried at room temperature (22 °C) and 2 torr for 12 hours. The vacuum oven was flushed with helium prior to evacuation to ensure an inert drying environment. After 12 hours, the dried sample was transported in an air-tight glass bottle to the XPS laboratory. The sample was pre-evacuated overnight at 10^{-4} torr to remove any remaining volatile matter adsorbed on the colloids, and then transferred to the spectrometer for analysis.

The second set of samples was prepared using the same procedure, but the samples were exposed to the air during preparation.

3.3.6 BET surface area measurements

The BET (Brunauer-Emmett Teller) surface area of a number of metal sulfide colloids synthesized in reverse micelles was determined by single point nitrogen adsorption/desorption using a Flowsorb 2300 analyzer. The metal sulfide colloids were recovered from the microemulsion using the method outlined in section 3.3.4. A pre-weighed sample of the recovered catalyst was then placed in a quartz sample tube and degassed under flowing N_2 at 130 °C for 20 minutes. The sample tube was then connected to the Flowsorb unit for the surface area measurements. The surface area of the sample was determined by the adsorption of N_2 from a 70:30 volumetric mixture of He and N_2 at -195 °C, and then by the subsequent desorption of the adsorbed N_2 monolayer at room temperature. The specific surface area of the sample was calculated by dividing the average of the adsorption and desorption surface area values by the weight of the sample.

3.4 Activity measurements

3.4.1 Reaction system

A series of catalyst activity measurements was conducted to determine the catalytic activity of nickel, cobalt and iron sulfide colloids synthesized within the water/PEEL/hexane microemulsion. The hydrocracking of a model compound, diphenylmethane (DPM), was chosen as a model reaction for this purpose. A number of researchers have used this model reaction to determine the relative catalytic activity of various hydrocracking catalysts (Wei *et al.*, 1992; Stenberg *et al.*, 1983; Sweeny *et al.*, 1987). These studies have shown that metal sulfides promote the cleavage of the alkyl-aromatic carbon-carbon bond in DPM, producing benzene and toluene as the reaction products:

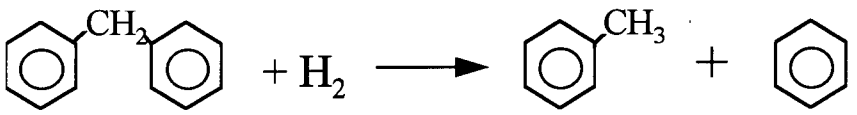

This reaction is attractive as a model compound reaction for a number of reasons. Firstly, the product distribution obtained allows one to differentiate between the hydrocracking and hydrogenation activity of the catalyst being tested. Secondly, the reactant and product molecules are well defined, and the concentration of these species can be easily determined by gas chromatography (GC).

3.4.2 Modeling of the reaction system

Previous studies on the hydrocracking of DPM using metal sulfide catalysts have been conducted at temperatures ranging from 400 °C to 450 °C, and reaction pressures ranging from 10.4 to >20.8 MPa (Wei *et al.*, 1992; Stenberg *et al.*, 1983; Sweeny *et al.*, 1987). Given the physical limitations of the batch reactor used for the hydrocracking experiments ($P < 20.8$ MPa at 426 °C), it was important to determine the pressure and phase equilibrium of the reaction mixture

at the final reaction conditions. The ASPEN process simulation package version 5.5 (ASPEN Technology Inc.) was used for these calculations. A detailed description of the ASPEN simulation is given in Appendix 1.3.

3.4.3 Experimental apparatus and methods

The activity measurements were conducted in the batch autoclave reactor described in section 3.1.3. Two slightly different experimental methods were used for the activity measurements. A preliminary set of activity measurements was conducted *in situ* in water/PE4LE/decahydronaphthalene microemulsions containing metal sulfide catalyst colloids. A typical experiment involved placing 135 mL of a water/PE4LE/decalin microemulsion with a particular metal salt dissolved within the reverse micelles of the microemulsion into the reactor. The reactor was then pressurized with 5% H_2S in H_2 at room temperature (22 °C) and 7 MPa for 2 hours to synthesize the metal sulfide catalyst colloids within the reverse micelles. Next, the reactor was vented, and 15 mL (15.015 g) of DPM (Aldrich Chemical Company, 99%) was added to the suspension of metal sulfide colloids in the microemulsion. The reactor was then repressurized to 2.2 MPa (300 psig) with 5% H_2S in H_2 and heated to 430 °C at a temperature ramp rate of 5 °C/min (Autoclave Engineers recommend a temperature ramp rate of less than 7°C/min to avoid exposing the reactor vessel to excessive thermal shock). The reactor temperature was maintained at 430 °C for 2 hours. After 2 hours, the furnace was removed and the reactor was air-cooled until the temperature dropped to 250 °C (about 15 min). The reactor was then quenched using the internal water cooled cooling coil.

The reactor vessel and reactor internals (impeller, cooling coil and thermocouple housing) were carefully cleaned between successive activity measurements in an attempt to remove any

catalyst adhering to the metal surfaces. The reactor vessel and internals were first cleaned with soap, water and steel wool to remove any solid deposits on the metal surfaces. The surfaces were then further cleaned using Brasso®, a petroleum based abrasive metal polish. Finally, the reactor and internals were rinsed with hexane and dried overnight at room temperature.

A second set of activity measurements was conducted using a slightly different experimental procedure. Metal sulfide colloids were synthesized in a water/PE4LE/hexane microemulsion following the procedure outlined in section 3.1.4, and then extracted from the microemulsion and dried following the method outlined in section 3.3.4. The extracted metal sulfide colloids were then used as the catalyst in the DPM hydrocracking reaction. A typical experiment involved first mixing 120 mL of Decalin (Sigma Chemical Company, 98%) and 15.015g of Diphenylmethane. A 5 mL sample of the mixed reactor feed was then removed for analysis by gas chromatography (GC). A specified amount of the extracted catalyst powder was added to the remaining 120 mL of decalin/DPM, and this mixture was placed in the reactor. Presulfiding with 5% H_2S in H_2 at room temperature (22 °C) and 7 MPa for 2 hours followed. The pressure was then reduced to $\pm$ 2.4 MPa (340 psig) and the reactor was heated to 400 °C at a temperature ramp rate of 5 °C/min using the electric jacket furnace. The reaction temperature was maintained at 400 °C for 3 hours. After 3 hours, the furnace was removed and the reactor was cooled following the procedure described above. As with the first set of activity measurements, the reactor and internals were cleaned between successive runs to remove residual catalyst.

Activity measurements were also conducted with dispersed metal catalysts synthesized from organometallic precursors such as iron pentacarbonyl ($Fe(CO)_5$, Aldrich Chemical Company) and Co naphthenate (Sigma Chemical Company, 8 wt% Co). The same procedure was used as that described above for the second set of activity experiments, with the organometallic

precursors replacing the colloidal metal sulfide catalyst. A full list of all the activity experiments conducted is presented in Appendix 1.2.

3.4.4 Analysis of the activity test products using gas chromatography.

The reaction products from the activity measurements were identified by gas chromatography (GC). A Varian 3400-CX gas chromatograph with a flame ionization detector (FID) was used. The GC was equipped with a 3.2 mm x 2.1 m column (Chromatographic Specialties Inc.) packed with 5% OV-17 on Chromosorb WAW-DMCS. The temperature program used is given in Appendix 1.4. Helium (UHP, Medigas) was used as a carrier gas at a flowrate of 30 cm^3/min. The GC analyses was performed by the manual injection of 1 µl of liquid reactor product into the column using a 10 µl miro-syringe. The micro-syringe was rinsed thoroughly with decalin between injections. Each sample was injected three times, and the average peak area of the three injections was used to calculate the concentration of each component in the sample.

n-Decane (Fisher Scientific, 99.8%) was used as an internal standard to quantify the amounts of DPM, benzene and toluene in the reactor product. 3.611 mL of n-decane (approximately equivalent to a 36:1 volumetric ratio of decane:liquid product) was added to the liquid reaction products before the reactor was unloaded. The resulting mixture was then unloaded into a septum-capped glass bottle and stored at 4 °C in a refrigerator.

A number of calibration curves were generated in order to relate the concentrations of benzene, toluene and DPM in the liquid reactor product to the amount of internal standard added to the sample. Standard calibration mixtures of n-decane (Fisher Scientific, 99.8%), DPM (Aldrich chemical company, 99%), decalin (Sigma chemical company, 98%), benzene (Fisher Scientific, A.C.S. reagent grade) and toluene (Fisher Scientific, A.C.S. reagent grade) were

prepared in proportions similar to those expected in the reactor product. In total, eight calibration standards were prepared corresponding to DPM conversions ranging from 0% to 20 %. A table of the compositions of the calibration standards is given in Appendix 1.5. Each calibration mixture was injected into the GC three times, and the average peak area of each of the components present was determined in each case. The calibration curve for each component n was generated by plotting:

$$\frac{\text{Area of Component n Peak}}{\text{Area of Decane Peak}} \quad \text{vs.} \quad \frac{\text{Moles of Component n in Mixture}}{\text{Moles of Decane in Mixture}}$$

Two sets of calibration curves were prepared in order to determine the effect of continued use on the calibration of the column. The first set was prepared before the activity measurements were started, and the other set was prepared mid-way through the experimental work. The raw data and both sets of calibration curves are presented in Appendix 1.6. A least squares regression was performed on the data to determine the calibration equations from the data. The calibration equations were calculated in the following form:

$$\frac{A_i}{A_{C10}} = a * \frac{M_i}{M_{C10}} + c$$

Where, A_i = Area of component i

A_{C10} = Area of the n-decane internal standard

M_i = # of moles of component i in the reactor product

M_{C10} = # of moles of n-decane added to the reactor product

The calibration equations obtained are presented in Table 3.1.

The benzene and toluene calibration curves were both linear, with negligible scatter in the data points (R^2 values of 0.998 and 0.999 respectively). The results of the recalibration indicate that the calibration of the GC with respect to benzene and toluene did not change with time. The

DPM calibration curves show more scatter than those of benzene and toluene, and the R^2 value of the linear fit to the data was lower (R^2 = 0.89). The lower apparent accuracy of the DPM calibration curves may be attributed to saturation of the FID detector, due to the high relative concentration of DPM in the GC injections. The recalibration results for DPM display the same scatter as the initial calibration.

3.4.5 Calculation of conversion

The conversion for each activity measurement was calculated based on: i) the amount of DPM consumed in the reaction, ii) the amount of benzene produced, and iii) the amount of toluene produced. The equations used to calculate the conversions are given in Appendix 1.7. For each experiment, the number moles of DPM in the reactor feed was determined by GC analysis of the 5 mL sample taken from the reactor feed. The amounts of DPM, benzene and toluene in the reactor product were determined by GC analysis following the method described in section 3.4.4.

Table 3.1 : Calibration curves used to calculate the number of moles of benzene, toluene and DPM in the reactor product.

Component	a	c	R^2
Benzene	0.5931	-0.0032	0.9984
Toluene	0.6971	-0.0057	0.9997
DPM	1.4872	-0.8807	0.8941

Chapter 4 : Catalyst Preparation and Characterization

4.1 Microemulsion preparation

4.1.1 Introduction

A key advantage of preparing dispersed hydrocracking catalysts in reverse micelles is the proposed link between the size of the reverse micelles and the size of the colloidal catalyst synthesized therein. Consequently, it was important to first establish the factors which influence the size of the reverse micelles in the water/polyoxyethylene-4-lauryl ether/hexane system, as these factors may ultimately be used to exercise control over the catalyst particle size.

Little information has been published in the literature on the water/polyoxyethylene-4-lauryl ether/hexane system. Polyoxyethylene-4-lauryl ether (or PE4LE) is a non-ionic surfactant with the chemical formula $C_{12}H_{25}(OC_2H_4)_4OH$. The aliphatic $C_{12}H_{25}$ group is hydrophobic and solubilizes in the hexane phase, whilst the hydrophilic $(OC_2H_4)_4OH$ group solubilizes within the aqueous phase of the microemulsion. Some work has been published in the literature on the water/PEGDE/hexane system (Boutonnet *et al.*, 1982), and the water/PEGDE/hexadecane system (Kizling and Stenius, 1987). Given the structural similarities between PE4LE ($C_{12}H_{25}(OC_2H_4)_4OH$) and PEGDE ($C_{12}H_{25}(OC_2H_4)_5OH$), it was expected that the water/PE4LE/hexane system would show similar characteristics to the water/PEGDE/hexane system.

4.1.2 Factors affecting the size of reverse micelles in the water/PE4LE/hexane system

Previous studies on the preparation of microemulsions have shown that 3 key factors affect the size of the reverse micelles within the microemulsion, namely: the water:surfactant ratio

(ω), the concentration of metal ions within the reverse micelle, and the type of metal dissolved within the reverse micelle (see section 2.3.4). Consequently, the effect of these 3 factors on the size of the reverse micelles in the water/PE4LE/hexane system was investigated. A number of microemulsions of varying ω and metal ion concentration were prepared, with Ni, Fe or Co nitrates dissolved within the water pools. Ni, Co and Fe were chosen since combinations of these metals are commonly used as heavy oil hydrocracking catalysts. The hydrodynamic diameters of the reverse micelles were determined by dynamic light scattering (DLS). The DLS results are presented in Table 4.1. The average hydrodynamic diameter and the standard deviation in the measured diameter are quoted for each microemulsion (see section 3.2 for a more detailed description of these parameters). The parameter μ/Γ^2 gives an indication of the relative degree of polydispersity of the reverse micelles, a value of 0.05 or less indicating an acceptable degree of monodispersity.

The hydrodynamic diameters of the reverse micelles were similar to those reported by Kizling and Stenius for the water/PEGDE/dodecane system (Kizling and Stenius, 1987). The researchers reported reverse micelle hydrodynamic diameters ranging from 12-18 nm (at 22 °C) for microemulsions containing 4-7 weight % water. In general, the reverse micelles in the water/PE4LE/hexane system displayed a fair degree of monodispersity. μ/Γ^2 (a measure of the variance in the diameters) was generally less than 0.1 for the microemulsions investigated, indicating a fairly narrow distribution of reverse micelle sizes.

A number of water/PE4LE/decahydronaphthalene (DHN) microemulsions were also prepared for the preliminary set of activity measurements (see section 3.4.3). The hydrodynamic diameters of the reverse micelles of this system were determined by dynamic light scattering, and the results are presented in Table 4.2. The diameters of the reverse micelles in the

water/PE4LE/decahydronaphthalene microemulsions were slightly larger than reverse micelles of identical ω and metal ion concentration in the water/PE4LE/hexane system. These slight differences in reverse micelle size were to be expected due to the differences in solubility of the surfactant in hexane and decahydronaphthalene.

Table 4.1 : Hydrodynamic diameters of reverse micelles in the water/PE4LE/hexane system.

#	Metal dissolved in reverse micelle	ω (vol/vol)	Metal ion conc. in reverse micelle (mol/L)	Avg. hydrodynamic diameter of rev. micelle (nm)	μ/Γ^2 (Relative variance)
6	Ni	0.066	1.6	11.4 ± 0.2	0.05
1	Ni	0.066	3.1	12.9 ± 0.2	0.04
7	Ni	0.066	4.7	14.4 ± 0.2	0.1
12	Ni	0.099	3.1	20.4 ± 0.2	0.09
4	Co	0.033	3.1	2 Phases	-
8	Co	0.040	3.1	12.4 ± 0.2	0.07
10	Co	0.050	3.1	12.2 ± 0.2	-
2	Co	0.066	3.1	13.2 ± 0.2	0.05
11	Co	0.083	3.1	15.8 ± 0.2	0.08
9	Co	0.099	3.1	21.8 ± 0.2	0.1
5	Co	0.132	3.1	2 Phases	-
13	Co	0.066	1.6	12.4 ± 0.4	0.08
14	Fe	0.066	1.6	13.0 ± 0.4	0.05
3	Fe	0.066	2.8	13.6 ± 0.2	0.08
15	Fe	0.099	2.8	18.8 ± 0.2	0.1

Table 4.2 : Hydrodynamic diameters of reverse micelles in the water/PE4LE/DHN system.

#	Metal dissolved in reverse micelle	ω (vol/vol)	Metal ion conc. in reverse micelle (mol/L)	Avg. hydrodynamic diameter of rev. micelle (nm)	μ/Γ^2 (Relative variance)
17	Ni	0.066	3.1	14.2 ± 0.2	0.1
18	Co	0.066	3.1	14.2 ± 0.2	0.1

The effect of ω (water:surfactant on a volumetric basis) on the size of the reverse micelles in the water/PE4LE/hexane system is shown in Figure 4.1. The data presented in Figure 4.1 indicate that the size of the reverse micelles increased with increasing ω, and the trend was consistent for all three metals dissolved within the water pools. This result concurs with previous studies on a number of microemulsion systems, including water/CTAB/hexanol (Nagy *et al.*, 1983), water/AOT/alkane (Pileni *et al.*, 1985) and water/PEGDE/hexadecane (Kizling and Stenius, 1987). The sizes of the reverse micelles presented in Figure 4.1 do not display the precise linear dependence on ω reported in previous studies. There is no obvious explanation for the lack of linearity in the data at this point.

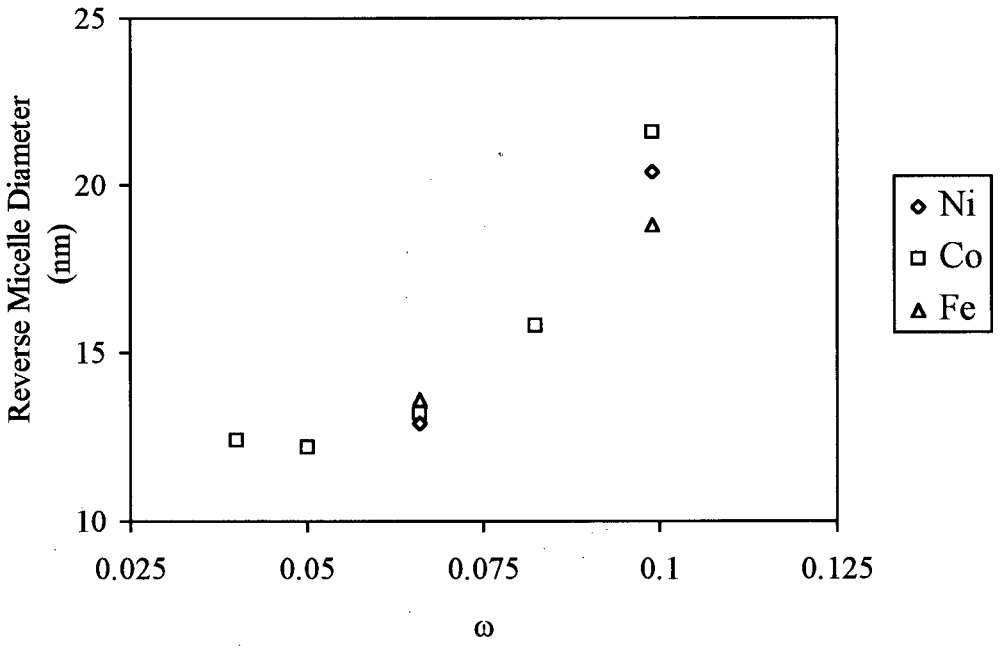

Figure 4.1 : Effect of ω on the hydrodynamic diameters of reverse micelles in the water/ PE4LE/hexane system (temperature = 22 °C, $[M^{2+}]$ in water pool = 3.1 mol/L, 94.4 vol % hexane).

It was also observed that stable, optically transparent microemulsions could only be prepared between ω = 0.03 and ω = 0.1. Phase separation occurred with microemulsions #4 and

#5 at values of ω outside these limits. This observation agrees with previous studies conducted by Kizling and Stenius (1987) and Boutonnet *et al.* (1982) on non-ionic microemulsions. Boutonnet *et al.* found that a certain minimum amount of water was required to form clear, stable microemulsions in the water/PEGDE/hexane system with H_2PtCl_6 dissolved within the water pools. This would explain the observed phase separation in the water/PE4LE/hexane system at values of $\omega < 0.03$. Kizling and Stenius found that a minimum concentration of PEGDE was required to form stable reverse micelles in the water/PEGDE/hexadecane system. The researchers claim that a minimum number of surfactant molecules is required to form a structure which can accommodate water between the ethylene oxide chains without the occurrence of extensive water/hydrocarbon contact. This would explain the phase separation at values of $\omega > 0.1$ (i.e. insufficient surfactant). The observed phase separation implies that the system imposes a natural limit on the size of the water pools which can be achieved. The data in Figure 4.1 indicate that the minimum water pool size for the water/PE4LE/hexane system was 12.2±0.2 nm at 22 °C.

The effect of metal ion concentration within the reverse micelles on the hydrodynamic diameter of the reverse micelles is shown in Figure 4.2. A microemulsion with $[Fe^{3+}] = 4.5$ mol/L could not be prepared since iron nitrate reached its solubility limit at about 3 mol/L. A cobalt microemulsion with $[Co^{2+}] = 4.5$ mol/L was also not prepared. Nevertheless, the data in Figure 4.2 illustrate that the reverse micelle size increased with increasing metal ion concentration within the water pool. This result confirms the proposed relationship between metal ion concentration and reverse micelle size in nonionic surfactant systems discussed in section 2.3.4. It would appear that increasing the concentration of multivalent metal nitrates within the reverse micelles of a nonionic surfactant led to an increase in the HLB of the surfactant molecules at the interface, which in turn led to an increase in the size of the reverse micelles. It should be noted that

increasing the metal ion concentration over the range considered in this study did not have as strong an effect on reverse micelle size as increasing ω (e.g. increasing metal ion concentration from 1.5 to 4.5 mol/L only resulted in an increase in reverse micelle size of 4 nm).

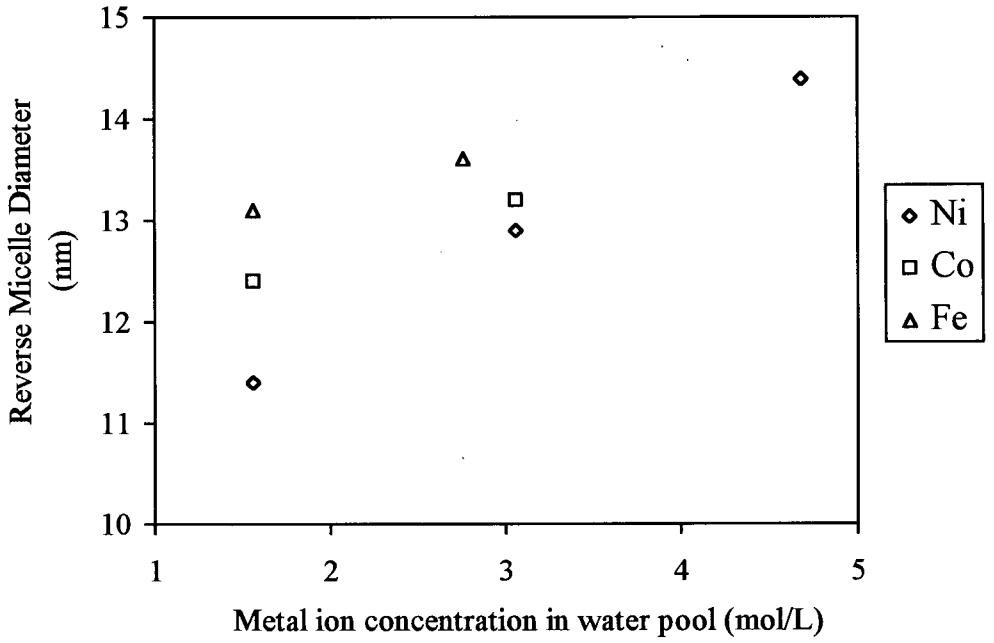

Figure 4.2 : Effect of metal ion concentration within the water pool on the hydrodynamic diameter of the reverse micelles in the water/PE4LE/hexane system (temperature = 22 °C, ω = 0.066, 94.4 vol % hexane).

The data in Figure 4.2 also indicate that the type of metal species had some effect on the size of the reverse micelle. For all metal ion concentrations, the water pools containing Fe^{3+} were larger than those containing Ni^{2+} and Co^{2+}. This effect has not been reported in the literature for microemulsions of nonionic surfactants. However, the observed trend can be qualitatively explained using the same arguments used to relate metal ion concentration to reverse micelle size. Schott (1973) claimed that the 'salting-in' effectiveness of metal salts in POE based nonionic surfactants can be qualitatively correlated to the heat of hydration of the metal salt. Consequently, the differences in the heats of hydration of $Ni(NO_3)_2$, $Co(NO_3)_2$ and $Fe(NO_3)_3$ could have led to

differences in the extent of 'salting-in' of the surfactant molecules at the interface of the reverse micelles. As discussed in section 2.3.4, these differences in the extent of 'salting-in' would have lead to differences in the HLB of the surfactants, which could account for the differences in reverse micelle size with metal species observed in Figure 4.2.

4.2 The synthesis of reduced metal colloids in the water/PE4LE/hexane system.

4.2.1 Introduction

Once the factors influencing the size of the reverse micelles in the water/PE4LE/hexane system had been identified, it was necessary to investigate the relationship between reverse micelle size and the size of colloidal catalysts synthesized therein. The synthesis of reduced Ni, Co and Fe colloids was initially studied as a model intra-micellular precipitation reaction. Although zero valent metal is not the active species of dispersed heavy oil hydrocracking catalysts, the model intra-micellular reaction was easy to study, and the reduced metal colloids were stable and could be easily characterized using DLS.

4.2.2 Characterization of reduced metal colloids

Reduced metal colloids were prepared in the microemulsions described in Table 4.1 by the addition of hydrazine ($N_2H_4.xH_2O$), using the method outlined in section 3.1.2. The reduction of the microemulsions containing Ni^{2+} was characterized by a colour change from light green to colourless, whilst the Co^{2+} containing microemulsions changed from pink to orange. The Fe^{2+} microemulsions changed from a light yellow colour to dark orange upon reduction. In all cases, the suspensions of the reduced metal colloids were stable and optically transparent after reduction. The sizes of the reduced Ni, Co and Fe colloids synthesized using hydrazine were determined by dynamic light scattering (DLS). The results are presented in Table 4.3. The DLS

data were analyzed using both monomodal and multimodal particle size distributions to determine whether a distribution of particle sizes was present.

Table 4.3 : Reduced metal colloid sizes as determined by DLS.

#	Metal	ω	Metal ion Concentration (mol/L)	Monomodal Fit		Multimodal Fit	
				Particle Diameter (nm)	μ/Γ^2	D1 (nm)	D2 (nm)
6	Ni	0.066	1.6	12.2 ± 0.2	0.06		
1	Ni	0.066	3.1	126 ± 20	0.2	142.8	11.2
7	Ni	0.066	4.7	200 ± 40	0.17	248	14.4
12	Ni	0.099	3.1	100 ± 10	0.2	139	16.8
4	Co	0.033	3.1	2 Phase			
8	Co	0.040	3.1	12.6 ± 0.2	0.05		
10	Co	0.050	3.1	12.6 ± 0.4	0.1		
2	Co	0.066	3.1	22 ± 1	0.2		
11	Co	0.083	3.1	not measured			
9	Co	0.099	3.1	23.4 ± 0.2	0.1		
5	Co	0.132	3.1	2 Phase			
13	Co	0.066	1.6	12.2 ± 0.4	0.03		
14	Fe	0.066	1.6	15.2 ± 0.2	0.05		
3	Fe	0.066	2.8	17.8 ± 0.2	0.05		
15	Fe	0.099	2.8	20.6 ± 0.2	0.1		

In general, the size distributions of the reduced Co and Fe colloids were reasonably well described by a monomodal fit, with $\mu/\Gamma^2 \leq 0.1$ in most cases. The sizes of the Co and Fe colloids ranged from 10 to 20 nm. By contrast, the reduced Ni size distributions were not well described by a monomodal fit ($\mu/\Gamma^2 \approx 0.2$). The data from samples #1, #7 and #12 were better described by a bimodal size distribution, with both large particles > 100 nm, and smaller 10-20 nm colloids. It would appear that the 10-20 nm Ni colloids formed initially in the reverse micelles aggregated to larger 100-200 nm sized particles. Boutonnet *et al.* (1982) reported similar results for the synthesis of Pd, Rh and Ir colloids in water/PEGDE/hexane microemulsions using H_2. The

researchers were able to prepare 5 nm sized Pd colloids with H_2, but they found that the Rh and Ir colloids aggregated to larger particles which settled from suspension. The observed differences between the sizes of the reduced Ni and the reduced Co and Fe colloids may have been due to differences in the relative rates of reduction and nucleation during the reduction reaction. For example, a slow rate of reduction in the case of Ni may have allowed the Ni colloids to aggregate during the reduction reaction.

The Ni colloids prepared in microemulsion #6 were an exception to the trend described above. In this case the reduced colloids were small (12.2 nm) and fairly monodisperse (μ/Γ^2 = 0.02). The small size of the reduced Ni colloids prepared in microemulsion #6 appears to suggest that the low concentration of metal ions in the water pool (1.6 mol/L) had a moderating effect on the apparently uncontrolled particle growth which occurred in the other Ni microemulsions.

The relationship between the size of the reverse micelle and the size of the reduced metal colloids synthesized therein is presented in Figure 4.3. The data points representing microemulsions #1, #7 and #12 (extremely large Ni particle sizes) were not included in Figure 4.3 since the mechanism of colloid formation in these three cases was probably different, resulting in uncontrolled particle growth. Although there is some scatter in the data, a clear trend of increasing colloid size with increasing reverse micelle size is evident. This result concurs with a number of studies published in the literature which suggest that particle growth within reverse micelles is spatially constrained by the intrinsic size of the reverse micelle (Ravet *et al.*, 1984; Nagy *et al.*, 1983; Modes and Lianos, 1989; Pileni *et al.*, 1992). The small amount of scatter in the data of Figure 4.3 may have been due to imperfect mixing/distribution of N_2H_4 during the reduction reaction. A number of researchers claim that a low [reducing ion]:[metal ion] ratio results in the formation of large colloids (Nagy *et al.*, 1983; Pileni *et al.*, 1992). Consequently, imperfect mixing of N_2H_4 could have resulted in local variations in the concentration of N_2H_4

during the reduction reaction, which in turn could have lead to the formation of larger than expected colloids in some of the reduced samples.

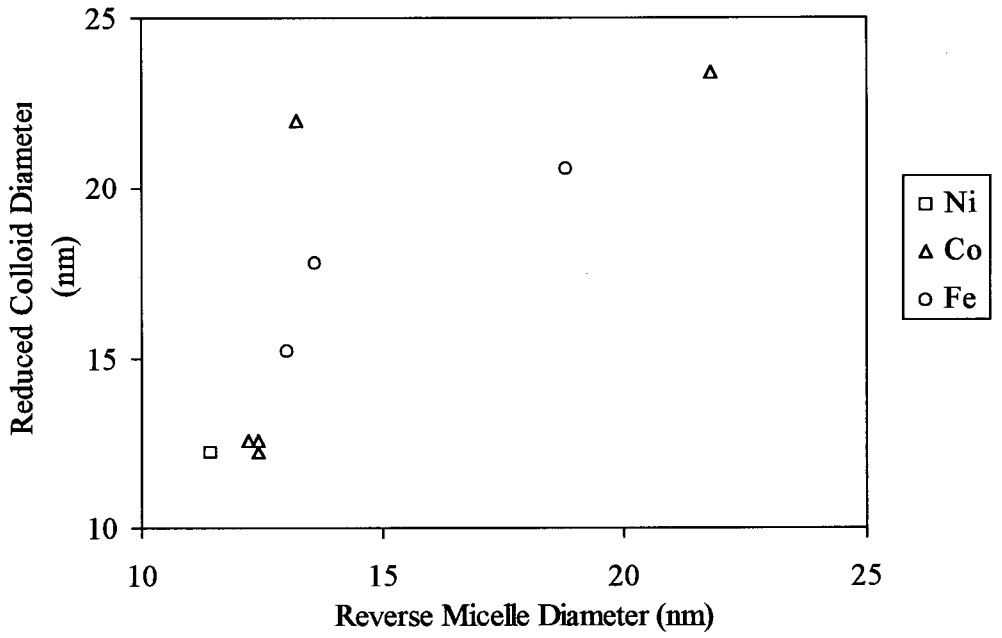

Figure 4.3 : Relationship between reverse micelle size and reduced metal colloid size.

Since light scattering is an indirect method of determining particle size, some particle size measurements were made using transmission electron microscopy (TEM) to check the reduced metal colloid sizes given by DLS. TEM photographs of reduced Co and Fe colloids prepared in microemulsions #2 and #3 are presented in Appendix 2.1. The size distributions of the Co colloids present in TEM photographs #925 and #926 are given Figure 4.4. The two size distributions of the Co colloids in photographs #925 and #926 are fairly similar, both in terms of their general shape and the average particle diameter. This indicates that the colloid samples shown in the two photographs were representative of the larger colloid population. Table 4.4 gives the average sizes and standard deviations of the particles in each photograph. The size distributions are fairly narrow, with standard deviations (expressed as a percentage of the mean particle size) of 27% and 22% respectively. Martino *et al.* (1994) reported δ/d values of 5-15 % for Fe, Pd and FeS_2

colloids prepared in the various microemulsion systems (see Table 2.2), whilst Boutonnet *et al.* (1991) reported a δ/d value of 15 % for Pt colloids prepared in the water/PEGDE/hexane system. Energy disperse x-ray (EDX) spectra of a typical reduced Co colloid in photo #925 and a typical reduced Fe colloid in photo #929 are shown in Appendix 2.2. A cobalt peak and an iron peak are present in each spectrum, though they are of low intensity due to the extremely small size of the colloids analyzed. Gold TEM grids were used for this analysis, accounting for the gold peak observed.

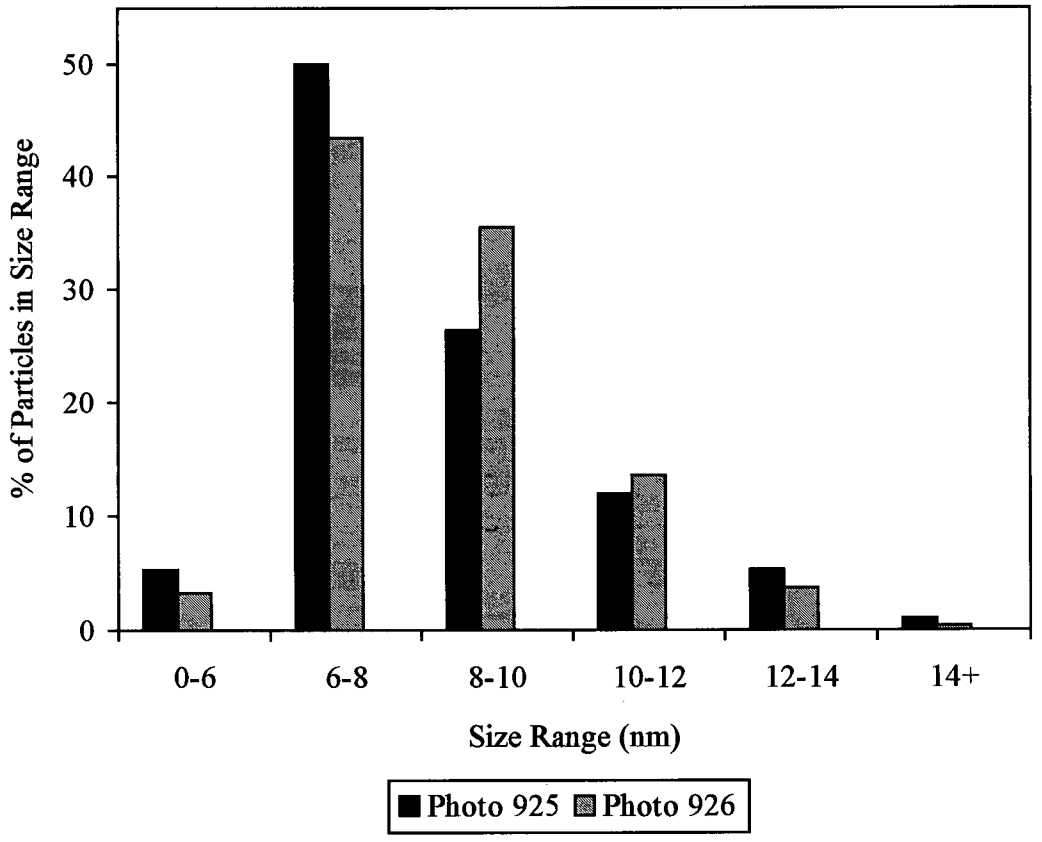

Figure 4.4 Size distribution of Co colloids present in TEM photographs #925 and #926

Table 4.4 : Statistical analysis of the reduced Co colloid sizes in photographs #925, #926 and the reduced Fe colloid sizes in photograph #929.

Photo #	Number Average Particle Diameter d (nm)	Standard Deviation δ (nm)	δ/d
925 (Co)	8.4	2.3	0.27
926 (Co)	8.7	1.9	0.22
929 (Fe)	10.7	3.1	0.29

Figure 4.5 shows the size distribution of the Fe colloids in photograph #929 and the size distribution of the Co colloids in photographs #925 and #926. The data in Figure 4.5 indicate that the Fe colloids synthesized in the reverse micelles of the water/PE4LE/hexane system were slightly larger than the Co colloids synthesized in the same system. The sizes of the reverse micelles in the microemulsions used were very similar (d = 13.2 nm for Co, d = 13.6 nm for Fe). As with the reduced Ni particles, the slight differences in the sizes of the Co and Fe colloids may have been caused by differences in the relative rates of reduction and particle formation.

It should be noted that DLS gave a slightly larger average particle size compared to TEM for the same sample of reduced Co and Fe colloids. This discrepancy between the microscopic and light scattering results illustrates that these two techniques essentially measure different physical quantities. TEM provides a direct measurement of the colloid size only, whilst light scattering gives a measurement of the size of the metal colloid plus the layer of surfactant molecules which surrounds the colloids in suspension. If one assumes that PE4LE surfactant molecules are at least 2.6 nm in length, and that they surround the suspended colloids in a monolayer, then a net diameter of at least 13 nm is to be expected for the 8 nm colloid plus surfactant covering.

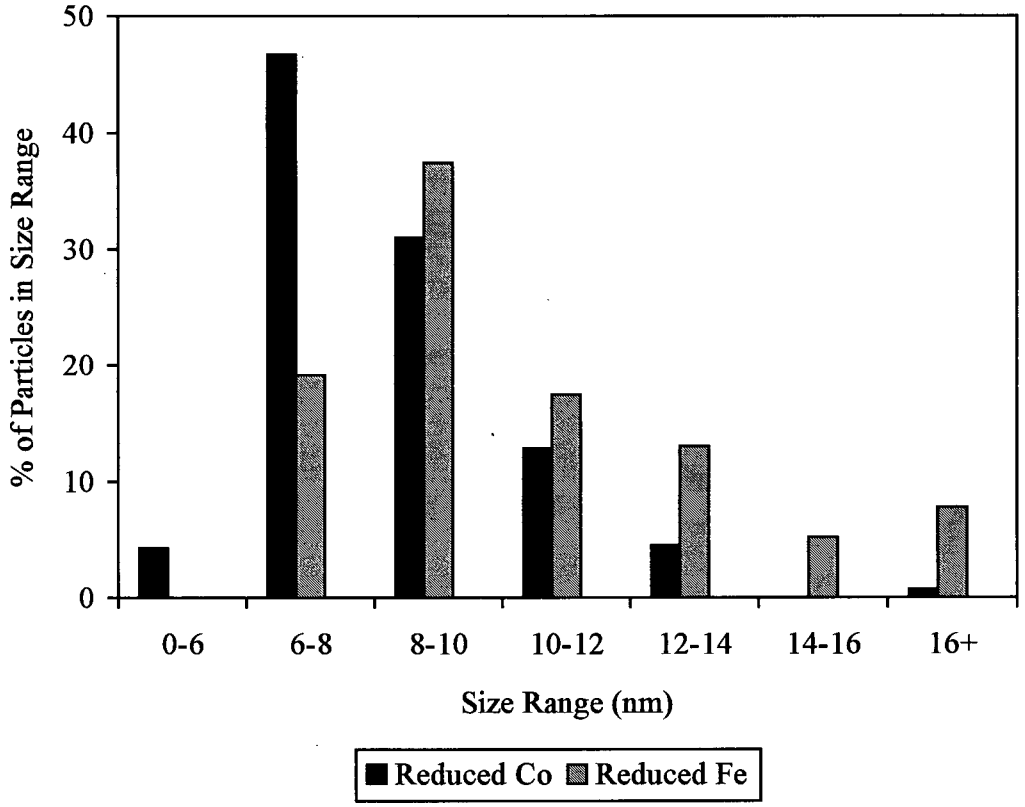

Figure 4.5 : Size distributions of reduced Fe and Co colloids prepared in water/PE4LE/hexane microemulsions

4.3 Synthesis of metal sulfide colloids using dimethyl disulfide.

Once the synthesis of reduced metal colloids in the water/PE4LE/hexane system was demonstrated, the focus of the research shifted to the synthesis of metal sulfide colloids. A number of researchers have shown that metal sulfides are the active form of dispersed heavy oil hydrocracking catalysts (see section 2.2.6). Consequently, the direct intramicellular synthesis of metal sulfide colloids is of more practical significance than the synthesis of zero valent metal colloids.

The synthesis of nickel sulfide colloids in the water/PE4LE/hexane system using dimethyl disulfide ($(CH_3)_2S_2$) was initially investigated. Dimethyl disulfide (DMDS) is an organic sulfiding agent commonly used to presulfide supported metal catalysts used in fixed bed heavy oil

hydrocracking processes. The results of the synthesis reactions with DMDS are presented in Table 4.5. An EDX spectrum of the solid reaction products are presented in Appendix 2.3.

Table 4.5 : Results of the nickel sulfide colloid synthesis experiments using DMDS.

Reaction Temperature (°C)	Average Particle Size	Elements detected by EDX
150	1 mm	Ni
210	1 mm	Ni, S (2:1 ratio)

The results presented in Table 4.5 indicate that DMDS was not an effective sulfiding agent below its decomposition temperature of 207 °C. No sulfur was detected by EDX analysis in the solid product of the synthesis reaction performed at 150 °C, but sulfur was detected in the product of the reaction at 210 °C. Severe particle aggregation was observed in both the experiments, and the solid particles obtained were generally in the millimeter size range or larger. This aggregation was probably due to the phase separation of the microemulsion at the elevated reaction temperatures, resulting in the formation of bulk aqueous and organic phases. The temperature sensitivity of microemulsions of non-ionic polyoxyethylene based surfactants has been reported by a number of researchers (Overbeek *et al.*, 1984; Kizling and Stenius, 1987; Shaw, 1993). Kizling and Stenius found that phase separation occurred in the water/PEGDE/hexadecane system at temperatures ranging from 32 °C to 42 °C, depending on the water content of the microemulsion. Phase separation at elevated temperature in microemulsions of non-ionic surfactants is thought to be due to a decrease in the hydrophilic-lipophilic balance (HLB) of the surfactant (Overbeek *et al.*, 1984) . The hydration of the lyophilic poly(ethylene oxide) groups decreases with increasing temperature, resulting in the surfactant becoming less hydrophilic - i.e. HLB decreases. Phase separation finally occurs when the solubility of the

surfactant in the aqueous phase decreases to a point where the surfactant can no longer occupy the interface between the aqueous and organic phases.

The temperature sensitivity of microemulsions (as illustrated in the results presented in Table 4.5) has a number of important implications for the synthesis of colloidal hydrocracking catalysts in reverse micelles. Organic sulfiding agents such as DMDS which require high reaction temperatures are completely unsuitable for the synthesis of nm sized metal sulfide colloids in reverse micelles. Clearly, any precipitation reaction to prepare metal sulfide colloids in reverse micelles must take place at a relatively low temperature (< 30 °C) to maintain the structural integrity of the microemulsion. This temperature restriction has important implications for the synthesis of this type of catalyst in industrial settings.

4.4 Synthesis of metal sulfide colloids using H_2S

4.4.1 Introduction

The results of the catalyst synthesis experiments with DMDS clearly indicated that any precipitation reaction in reverse micelles of non-ionic surfactants must be conducted close to ambient temperature (20-30 °C). Consequently, the focus of the research shifted to finding a suitable low-temperature sulfiding agent. Two sulfiding agents have been used by previous researchers to prepare metal sulfide colloids in reverse micelles at room temperature, namely: H_2S, and reverse micelle entrapped S^{2-} ions (see Table 2.2). Metal sulfide synthesis using reverse micelle entrapped S^{2-} is a controlled and well characterized technique, but it is only suited to laboratory scale preparations. Colloid preparation with H_2S gas is presumably a more robust technique, and thus more suited to large industrial scale applications. Consequently, the preparation of metal sulfide colloids was investigated using 5% H_2S in H_2. A 5% mixture of H_2S in H_2 is a typical gas composition found in a refinery H_2 stream.

Sulfides of Ni, Co and Fe were prepared in reverse micelles of the water/PE4LE/hexane system following the procedure outlined in section 3.1.4. Details of the experiments performed are presented in Appendix 2.4. Fairly lengthy reaction times of 2 and 6 hours were used to account for the low rates of reaction expected at room temperature. Published data on the solubility of H_2S in hexane (Fogg, 1988) indicate that the mole fraction of H_2S in the liquid phase $x_{H2S} > 0.04$ at the reaction conditions (22 °C, partial pressure of H_2S = 300 kPa). Consequently, external mass transfer limitations were assumed to be negligible in the reaction system. The colloids synthesized in experiments #26, 27, 28 and 29 were characterized by EDX and x-ray photoelectron spectroscopy (XPS) in an attempt to determine the metal sulfide species formed during the synthesis reaction. Experiments #30, 31 and 32 were repeats of experiments #26, 27 and 29, and the colloids synthesized in these experiments were characterized by TEM in order to establish the size distributions of the particles formed.

4.4.2 Physical characterization of metal sulfide colloids using TEM and EDX.

The colloids synthesized in experiments #30, 31 and 32 were characterized by TEM in order to establish the size distributions of the particles formed. The synthesis of nickel sulfide colloids in the microemulsions containing Ni^{2+} (experiments #26 and #30) was characterized by a colour change from light green to dark green/black, whilst the Co^{2+} containing microemulsions (experiments #27 and 31) changed from pink to dark purple/black . The Fe^{2+} microemulsions (experiments #28, 29 and 32) changed from a light yellow colour to dark yellow/black.

The metal sulfide suspensions were unstable when exposed to air, and generally changed colour from clear-black to the colour of the original microemulsion over a period of 12 hours. The colour change was probably due to reoxidation of the metal sulfide colloids by atmospheric oxygen. Pileni *et al.* (1992) found that CdS colloids prepared in the water/AOT/iso-octane system

reoxidized (photocorroded) in the presence of oxygen and light according to the following reaction:

$$CdS + 2O_2 \xrightarrow{h\nu} CdSO_4 \rightarrow Cd^{2+} + SO_4^{2-}$$

The sensitivity of the metal sulfide suspensions meant that the colloid sizes could not be determined using dynamic light scattering. Consequently, TEM was the only method used to determine the size of the metal sulfide colloids.

Photographs of the metal sulfide colloids synthesized are shown in Appendix 2.5. The size distributions of the nickel sulfide and cobalt sulfide colloids synthesized in experiments #30 and 31 are presented in Figure 4.6. Unfortunately, decent size distributions of the Fe sulfide colloids synthesized in experiment #32 could not be obtained. The size distribution of the nickel sulfide colloids was taken from the colloids in photographs #127, 130, 132 and 134 (194 particles), whilst the size distribution of the cobalt sulfide colloids was taken from the colloids in photographs #138 and 142 (622 particles). A simple statistical analysis of the Ni sulfide and Co sulfide particle sizes is given in Table 4.6. An explanation of the terms in Table 4.6 is given in Appendix 2.6. The surface area average particle diameters ($\bar{d}_{SA}$) of the colloids were calculated for purposes of comparison with the results of the BET surface area measurements (as discussed in section 4.4.4). EDX spectra of typical colloids seen in Appendix 2.5 are presented in Figures 4.7 to 4.10.

The preparation of metal sulfide colloids with H_2S appears to have been accompanied by some degree of aggregation or uncontrolled particle growth. In all cases, the metal sulfide colloids were far larger than the zero-valent metal colloids prepared in identical microemulsions (see Table 4.3). The nickel sulfide and cobalt sulfide colloids were also significantly larger than the CdS

colloids prepared by Pileni *et al.* (1992) in the ionic surfactant system water/AOT/iso-octane using 100% H_2S ($d \approx 4$ nm).

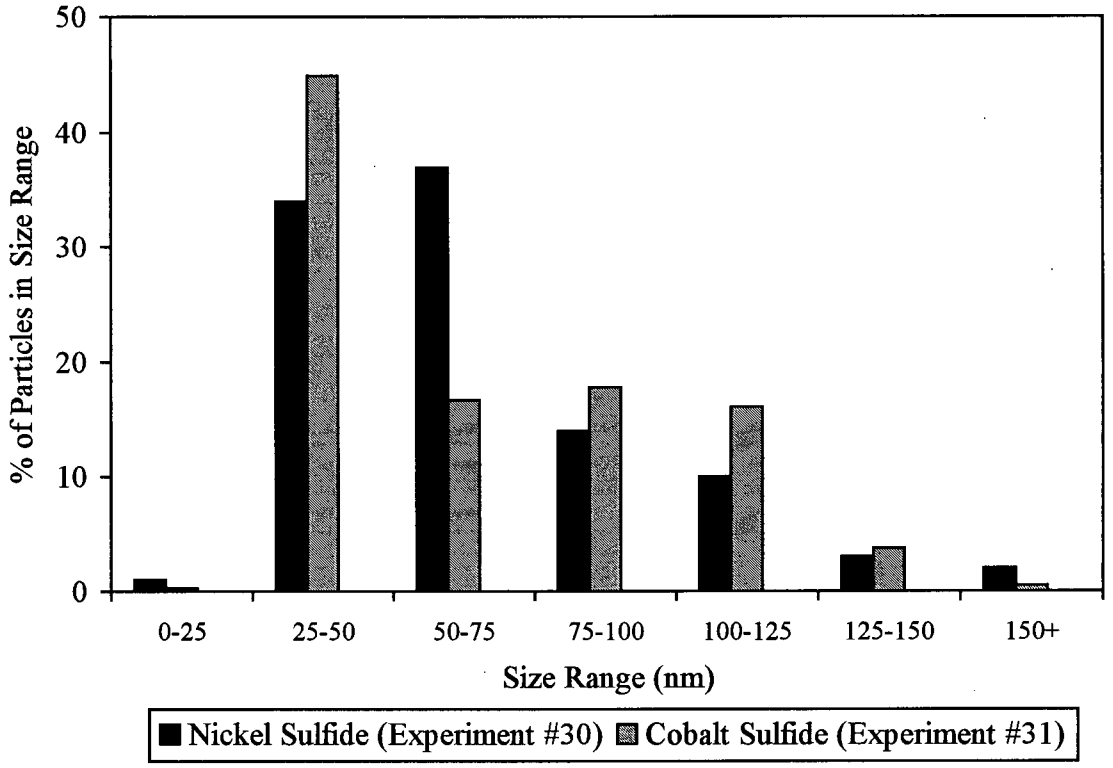

Figure 4.6 : Size distributions of nickel sulfide and cobalt sulfide colloids synthesized in experiments #30 and #31 (Microemulsions: $\omega = 0.066$, $[M^{2+}] = 3.1$ mol/L).

Table 4.6 : Simple statistical analysis of the Ni sulfide particle sizes in photographs #127, 130, 132 and 134 and the Co sulfide particle sizes in photographs #138 and 142.

	NiS Exp.#30	CoS_2 Exp. #31
Number Average Particle Diameter $\overline{d}_n$ (nm)	67	71
Number Standard Deviation δ_n (nm)	31	32
Average Surface Area $\overline{SA}$ (nm^2)	17069	18268
Surface Area Average Particle Diameter $\overline{d}_{SA}$ (nm)	74	76

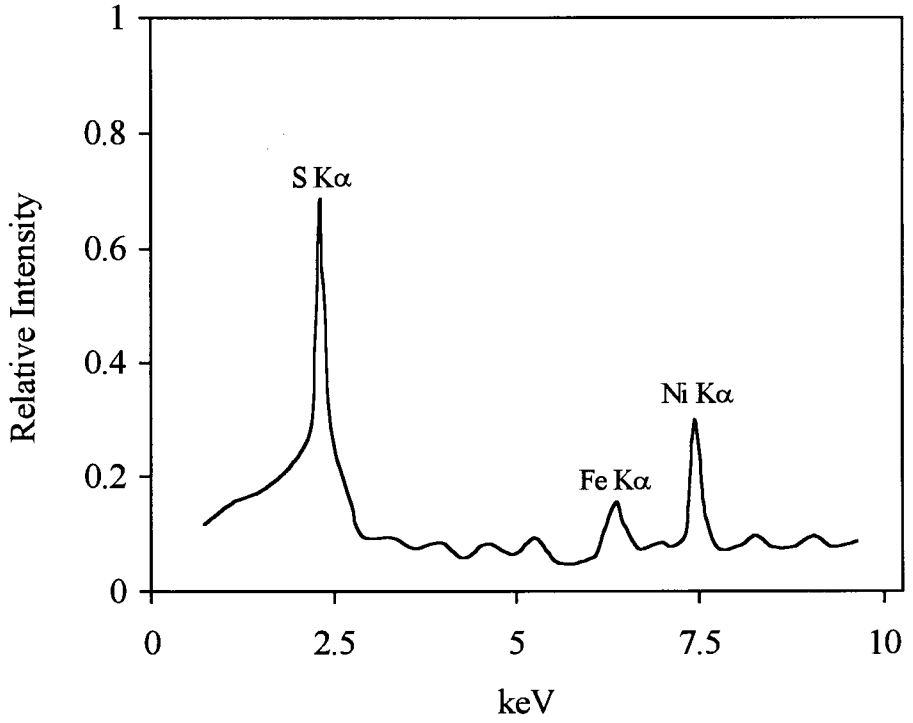

Figure 4.7 : EDX elemental analysis of a colloid from experiment #026 (Ni microemulsion, 7 MPa 5% H_2S in H_2, 22 °C, 6 hours)

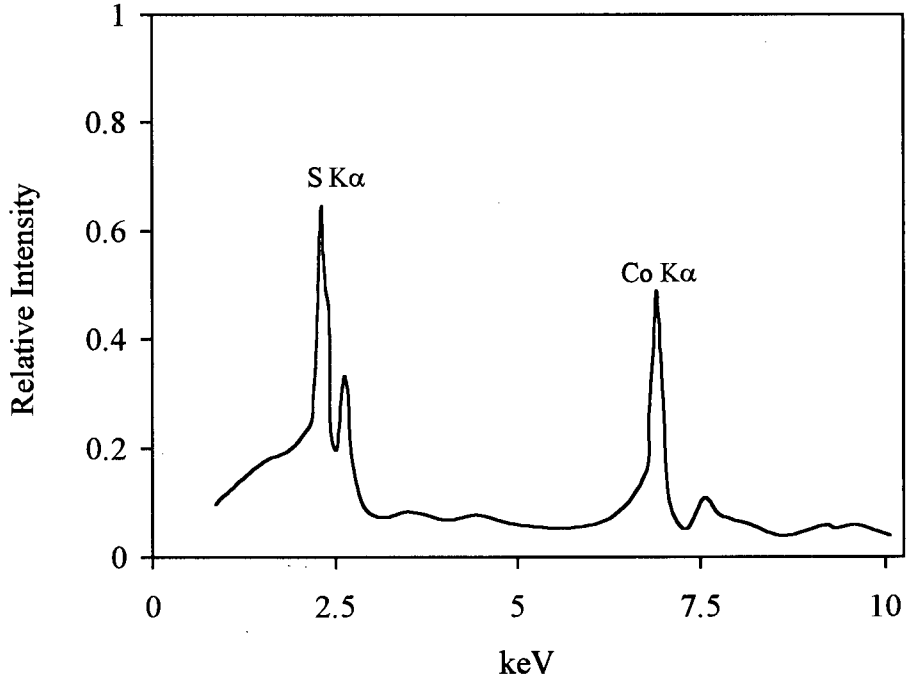

Figure 4.8 : EDX elemental analysis of a colloid from experiment #027 (Co microemulsion, 7 MPa 5% H_2S in H_2, 22 °C, 6 hours)

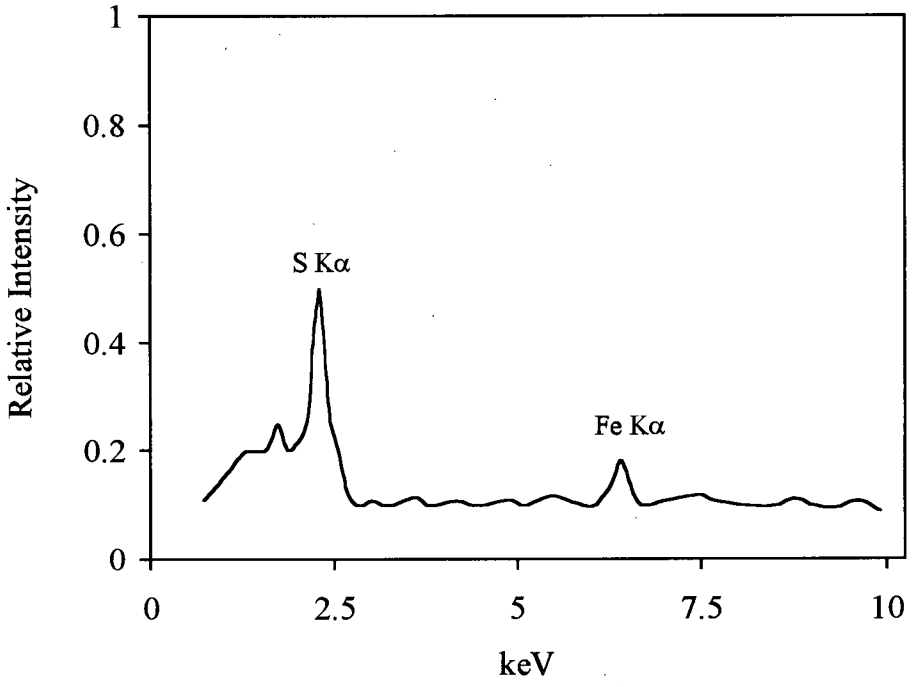

Figure 4.9 : EDX elemental analysis of a colloid from experiment #028 (Fe microemulsion, 7 MPa 5% H_2S in H_2, 22 °C, 2 hours)

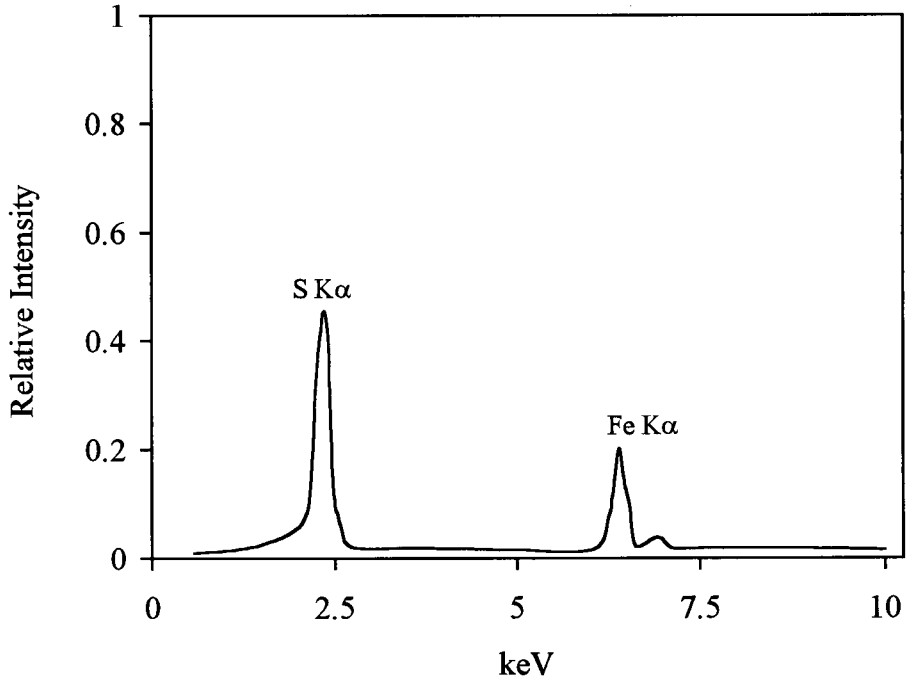

Figure 4.10 : EDX elemental analysis of a colloid from experiment #029 (Fe microemulsion, 7 MPa 5% H_2S in H_2, 22 °C, 6 hours)

The size distributions of the nickel sulfide and cobalt sulfide particles presented in Figure 4.6 indicate that the particle sizes ranged from 25 to 150 nm in both cases. The Co sulfide particles displayed a distinct bimodal distribution, with a large number of smaller colloids in the 25-50 nm range, and larger particles in the 75 to 125 nm range. This trend is clearly apparent in photograph #141. The Ni sulfide particles did not display a distinct bimodal distribution, and most of the nickel sulfide colloids were in the 25-75 nm size range. Photograph #131 shows a magnified image of 100-120 nm Ni sulfide particles. It would appear that the particles display a granularity at the 10 nm scale, indicating that the particles may be made up of smaller 10 nm colloids. This hypothesis is supported by the presence of very faint 10-15 nm sized particles in photograph #131.

In conclusion, the results indicated that the synthesis of nickel sulfide and cobalt sulfide in the reverse micelles of the water/PE4LE/hexane microemulsion was accompanied by aggregation and excessive particle growth beyond the confines of the reverse micelles. As in the case of the synthesis of reduced Ni colloids with hydrazine, the observed aggregation may have been due to a low rate of reaction, which would have given the colloids sufficient time to interact and coalesce. The differences between the size distributions of the Ni sulfide and Co sulfide colloids may also have been due to differences in the rate of reaction between the two metals.

The EDX results indicated the presence of metal-sulfur containing compounds in each of the samples analyzed. The relative areas of the sulfur and metal peaks indicated that the sulfur:metal ratio in the bulk was > 1. However, it was not possible to further identify the metal sulfide compounds present in each sample from the EDX results alone. In addition, since EDX analysis only identifies elements heavier than sodium (n = 23), it was not possible to identify the presence of other metal compounds (e.g. metal oxides) in the samples. Consequently, another

analysis technique was required to adequately characterize the metal sulfide compounds formed using H_2S.

4.4.3 Characterization of metal sulfide colloids using XPS

X-Ray Photoelectron Spectroscopy (XPS) was used in an attempt to identify the metal sulfide species prepared in the water/PE4LE/hexane system using H_2S. It should be noted that XPS is a surface sensitive technique, and tells very little about the nature of the bulk material. The effect of exposure to air after preparation was also investigated using XPS. As explained in section 3.3.5, two samples were prepared for each of the metal sulfides analyzed by XPS. The first set was prepared and transported under a helium blanket in an attempt to prevent exposure to atmospheric oxygen. The second set of samples was prepared using the same procedure, but the samples were exposed to the air during preparation.

The XPS results are presented in Figures 4.11 to 4.16. Standard binding energies of various Ni, Co and Fe compounds are presented in Appendix 2.7 for reference. Figures 4.11 and 4.12 show the XPS spectra of samples prepared from experiment #026 (H_2S sulfiding of a Ni microemulsion). The spectrum of the sample prepared under He indicates that a mixture of NiS and NiO was present on the colloid surfaces after sulfiding. The presence of NiO is difficult to explain, given the lack of oxygen in the reacting system. It is believed that the surfaces of the NiS colloids were partially oxidized by exposure to O_2 present in the He supply, or by atmospheric oxygen from the accidental exposure to air during sample preparation. The differences between the spectra of the 'air-free' and 'air-exposed' samples further illustrate the air sensitivity of the NiS colloid surfaces. Both the NiS peak at 853 eV (Figure 4.11) and the S^{2-} peak at 162 eV (Figure 4.12) are absent from the spectra of the air-exposed sample, indicating that the surfaces of the NiS colloids oxidized to NiO upon exposure to the air.

Figures 4.13 and 4.14 show the XPS spectra of samples prepared from experiment #027 (H_2S sulfiding of a Co microemulsion). The peak at 780.5 eV in spectrum (a) of Figure 4.13 indicates the presence of a Cobalt-Oxygen compound (either CoO or $Co(OH)_2$) on the surface of the sulfided colloids. However, the peak at 162.7 eV in spectrum (a) in Figure 4.14 clearly indicates the presence of sulfur as S^{2-} (i.e. sulfur in a metal-sulfur bond), suggesting that CoS_2 was present on the particle surface. Exposure to air had little effect on the Co $2p_{3/2}$ spectrum, whilst the S 2p spectrum showed a clear shift from a Metal-Sulfur bond to a Metal-SO_4 bond. From these spectra, it would appear that both cobalt oxide and cobalt sulfide were initially present on the surface of the colloids. The S 2p spectra indicate that the cobalt sulfide species on the surface of the colloids was oxidized to $CoSO_4$ upon exposure to the air.

Figures 4.15 and 4.16 show the XPS spectra of samples prepared under He from experiments #028 and #029 (H_2S sulfiding of Fe microemulsion). In both cases, the surface species appeared to be either Fe_2O_3 or Fe_3O_4, and the S 2p spectrum was flat in both cases (the S 2p spectrum of experiment #026 was included in Figure 4.16 for purposes of comparison). It would appear that the surfaces of the sulfided iron colloids were completely oxidized to Fe_2O_3 or Fe_3O_4 during the sample preparation procedure.

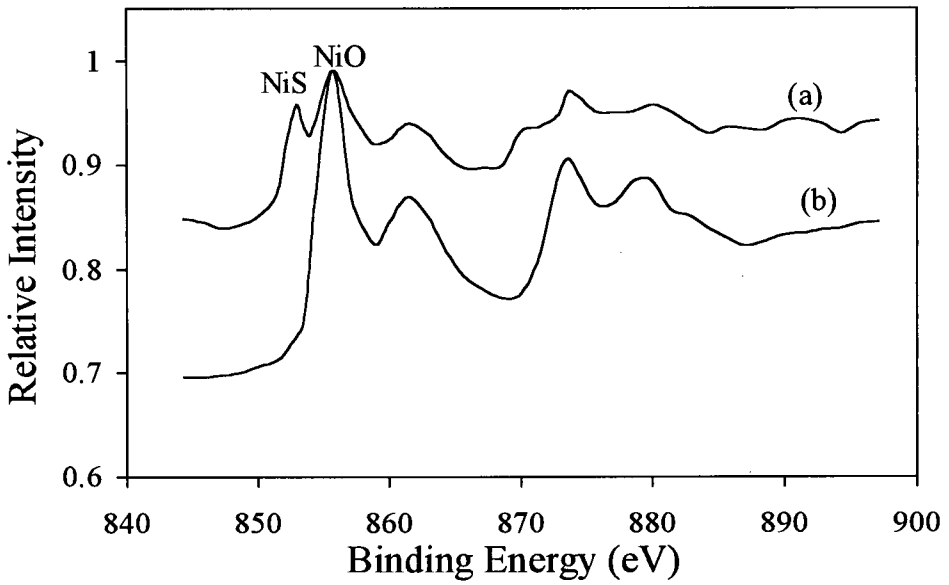

Figure 4.11 : Experiment #026 - XPS Scan of Ni $2p_{3/2}$ region. (a) Sample prepared under He, (b) Sample exposed to air.

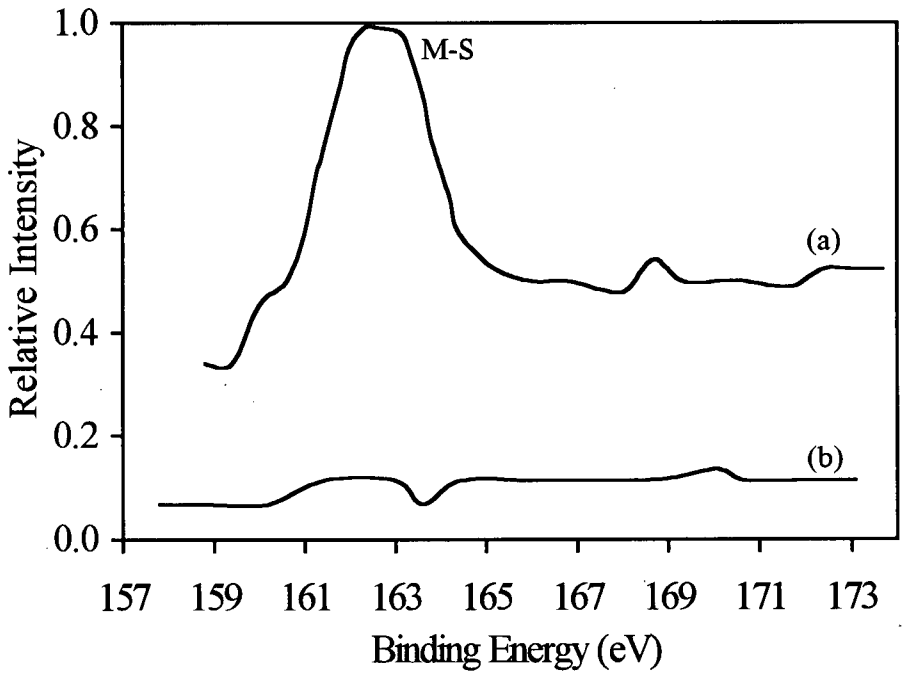

Figure 4.12 : Experiment #026 - XPS Scan of S 2p region. (a) Sample prepared under He, (b) Sample exposed to air.

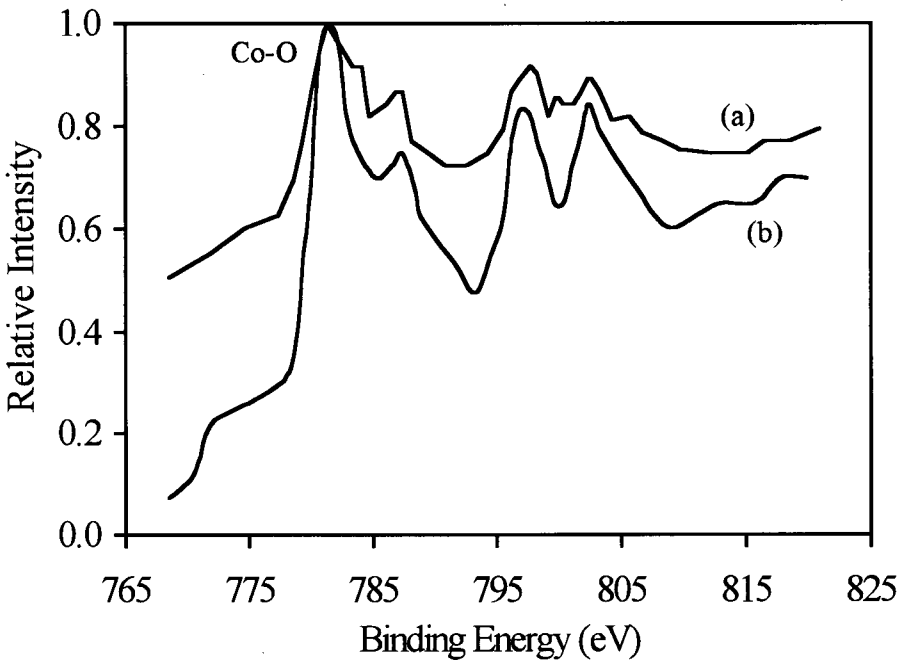

Figure 4.13 : Experiment #027 - XPS Scan of Co $2p_{3/2}$ region. (a) Sample prepared under He, (b) Sample exposed to air.

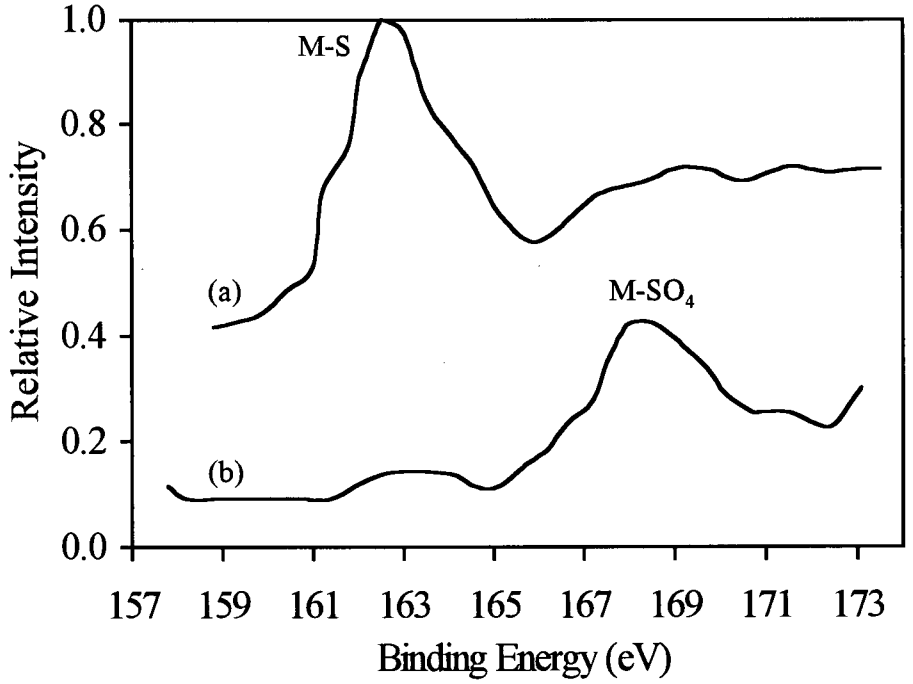

Figure 4.14 : Experiment #027 - XPS Scan of S 2p region. (a) Sample prepared under He (b) Sample exposed to air.

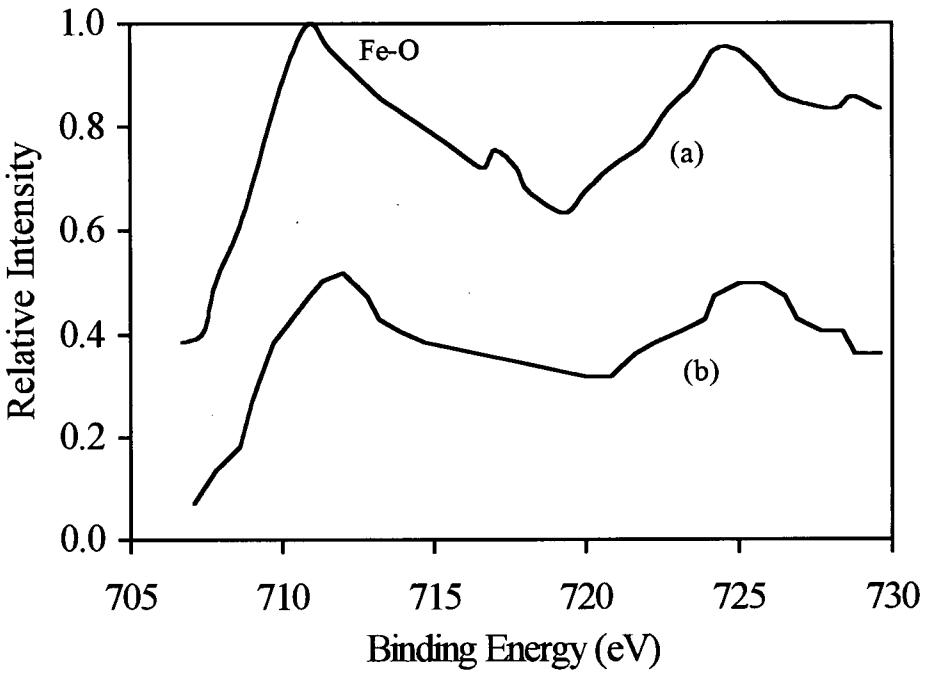

Figure 4.15 : Experiments #028 and #029 - XPS Scan of Fe $2p_{3/2}$ region. (a) #029, sample under He, (b) #028, sample under He.

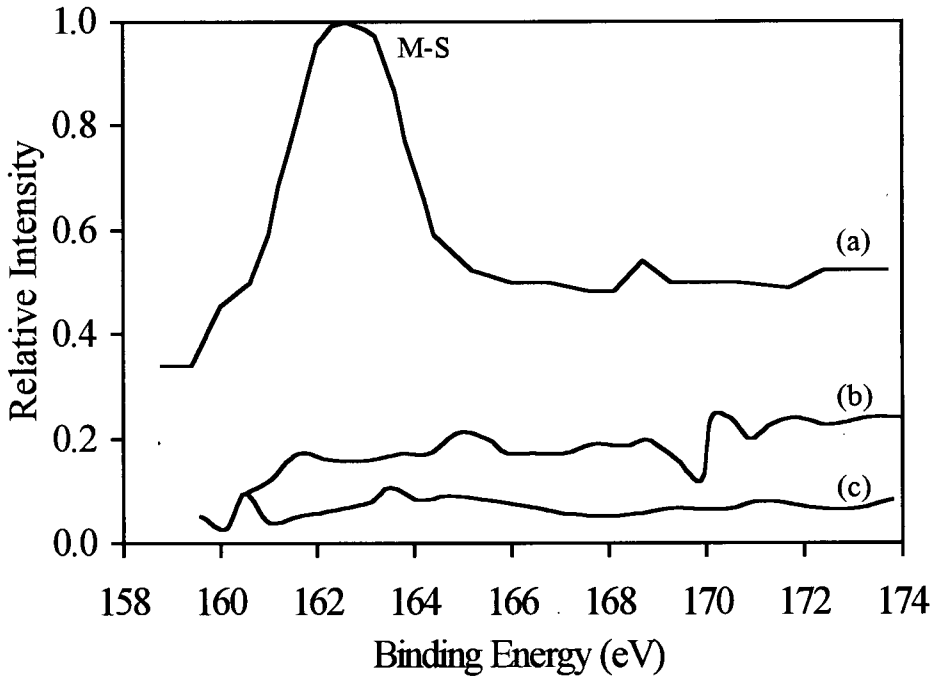

Figure 4.16 : Experiments #028 and #029 - XPS Scan of S 2p region. (a) S 2p scan from Figure 4.11 (b) #029, sample under He, (c) #028, sample under He.

4.4.4 Characterization of metal sulfide colloids using BET surface area measurement

The surface area of a sample of cobalt sulfide colloids prepared in an experiment identical to experiment #31 was measured using N_2 adsorption. As mentioned before, the metal sulfide colloids were recovered from the microemulsion using tetrahydrofuran, following the method outlined in section 3.3.4. The surface area of the sample was found to be 25 m^2/g from both the N_2 adsorption and desorption measurements. Assuming that the sample was made up of non-porous spheres, this specific surface area corresponded to a average particle size of 56 nm. (details of the surface area calculations and calculations of average particle size are presented in appendix 2.8). The specific surface area as determined the BET surface area measurement (25 m^2/g) was slightly larger than the specific surface area calculated from the TEM measurements[1] (18 m^2/g). This indicates that the CoS_2 colloids had some internal porosity which resulted in the higher specific surface area as determined by N_2 adsorption/desorption.

4.5 Summary of the major findings on colloidal catalyst preparation in reverse micelles

The experimental work outlined thus far has described the synthesis of colloidal heavy oil hydrocracking catalysts in the reverse micelles of the water/PE4LE/hexane microemulsion. The water:surfactant ratio (ω) and the metal ion concentration in the reverse micelle were identified as the key factors affecting the size of the reverse micelles in the water/PE4LE/hexane system. The smallest reverse micelles (11.4±0.2 nm in diameter) were obtained by minimizing both ω and the metal ion concentration.

A direct relationship was demonstrated between reverse micelle size and the size of reduced metal colloids synthesized in the reverse micelle, and fairly monodisperse Co and Fe

[1] TEM Measurements of CoS_2 particle size (see section 4.4.2): The S.A. average particle size of 76 nm for the recovered CoS_2 corrresponded to a specific surface area of 18 m^2/g.

colloids were prepared with sizes ranging from 10-23 nm. This result suggests that the size of reduced metal colloids prepared in the water/PE4LE/hexane system can be controlled by simply adjusting the water to surfactant ratio (ω) in the microemulsion. The reduced Ni aggregated to much larger 100-200 nm sized particles, indicating that the rate of reduction also affects the size of solid colloids synthesized in microemulsions.

The water/PE4LE/hexane system was found to be sensitive to increases in temperature, indicating that the synthesis of colloidal catalysts in reverse micelles must be performed at room temperature (20-30 °C). Ni, Co and Fe sulfide colloids were prepared in the water/PE4LE/hexane system using H_2S at room temperature (22 °C), but this synthesis method was characterized by particle growth beyond the confines of the microemulsion. The size of the Ni and Co sulfide colloids (as determined by TEM) ranged from 25 to 150 nm, and were smaller than similar bulk catalyst particles prepared by the decomposition of organometallic compounds (see section 2.2.5). BET surface area measurements confirmed the particle size measurements made by TEM.

Bulk EDX analysis of the metal sulfide colloids showed strong S peaks in all three metal species. However, the exact metal sulfide species prepared in the water/PE4LE/hexane system using H_2S could not be identified using EDX. XPS analysis identified NiS and CoS_2 species on the surfaces of the Ni and Co sulfide samples. However, the XPS analysis also revealed that the metal sulfide colloids were extremely sensitive to oxygen. Strong peaks of NiO, $CoO/Co(OH)_2$ and Fe_2O_3/Fe_3O_4 were identified in each of the samples respectively.

Chapter 5 : Activity Measurements

5.1 Introduction

The final phase of the research involved an investigation of the catalytic activity of the metal sulfide colloids prepared by the reverse micelle technique. The relative activity of these metal sulfide colloids, compared to metal sulfide catalyst particles prepared by the decomposition of organometallic compounds, was of primary concern in this investigation. A series of catalyst activity measurements was conducted to determine the hydrocracking activity of the catalysts. As mentioned in section 3.4.1, the hydrocracking of a model compound diphenylmethane (DPM) was chosen for this purpose. Two sets of activity measurements were conducted, the first set using metal sulfide colloids in the microemulsion, and the second set using metal sulfide colloids recovered from the microemulsion. The spent catalyst from the activity measurements was characterized using XRD in an attempt to determine the active species present in each case.

5.2 Phase equilibrium of the reaction system

The phase equilibrium of the reaction system was modeled using the ASPEN simulation package in order to determine the pressure and vapor/liquid distribution of the components in the reactor at the final conditions. A simplified reaction system of decahydronaphthalene/H_2S/H_2 was used in the simulation. Water/PE4LE/decahydronaphthalene (or decalin) microemulsions were used for the first set of activity measurements since decalin is less volatile than hexane, and thus more likely to remain in the liquid phase at the reaction conditions. In addition, decalin is an inert diluent commonly used in DPM hydrocracking experiments (Wei *et al.*, 1992). DPM and PE4LE were not included in the simulation since the ASPEN component database did not have the

required thermodynamic parameters for these compounds. Details of the ASPEN simulations are presented in Appendix 3.1. A summary of the simulation results using the Redlich-Kwong-Soave (RKS) equation of state is presented in Table 5.1. According to the simulation results, the reaction mixture became supercritical between 405 and 410 °C. However, the presence of DPM and PE4LE (which have a lower relative volatility than decalin) in the reaction mixture probably raises the critical temperature of the system. The ASPEN simulation was only performed once the first set of activity measurements had been conducted, and prompted a reduction in reaction temperature from 430 °C to 400 °C.

Table 5.1 : Simulation results for the simplified reaction system (135 ml Decalin, 165 ml 5% H_2S in H_2, initial pressure = 2.2 MPa (314 psi))

Temperature (°C)	Final Pressure (psi)	Fraction of decalin in liquid phase
390	1055	0.95
400	1100	0.97
405	1130	0.98
410	System supercritical	

5.3. Preliminary activity measurements

A preliminary set of activity measurements was conducted in water/PE4LE/decalin microemulsions containing metal sulfide colloids. As explained in section 5.2, decalin microemulsions were used for the activity measurements since decalin is less volatile than hexane, and thus more likely to remain in the liquid phase at the reaction conditions. The sizes of the reverse micelles in the water/PE4LE/decalin system were determined by dynamic light scattering (DLS), and the results are presented in Table 4.2. The diameters of the reverse micelles in the water/PE4LE/decalin microemulsions (#17 and #18 in Table 4.2) were similar to those of water/PE4LE/hexane microemulsions of identical composition (#1 and #2 in Table 4.1).

Consequently it is believed that the metal sulfide colloids prepared in the decalin system (and used in the preliminary activity measurements) were of similar size to the metal sulfide colloids prepared in the hexane system.

The results of the preliminary activity measurements are presented in Table 5.2. The conversions based on the number of moles of benzene formed were generally found to be the same as the conversions based on the number of moles of toluene formed. Consequently, the conversions are reported on the basis of the number of moles of benzene or toluene formed (B,T). The conversions are also reported on the basis the number of moles of DPM converted during the reaction. The first order rate constants based on the conversion with respect to benzene/toluene are also presented for each experiment, since the first order rate constants allow for the direct comparison of experiments with different metal loadings. A sample calculation of the rate constant for experiment #8 (in Table 5.2) is given in Appendix 3.2. Details of each activity measurement, including the temperature/pressure profiles and GC analyses are presented in Appendix 3.3.

Table 5.2 : Results of the preliminary activity measurements conducted in water/PE4LE/ decalin microemulsions (vol. microemulsion = 120 ml, $\omega = 0.066$, mass DPM = 15.015g, initial pressure = 2.2 MPa, reaction temperature = 430°C, reaction time = 2 hours)

Exp. #	Catalyst	Metal Loading (ppm)	Sulfiding Time (hours)	% Conv. (B, T basis)	% Conv. (DPM basis)	First order rate constant based on B, T basis ($cm^3/g/h$)
8	Co sulfide	620	2	5	8	49
9	Co sulfide	620	6	6	8	51
11	Blank microemulsion[1]	-	2	5	12	-
13	Fe sulfide	520	6	4	12	43
14	Fe sulfide [2]	520	6	4	9	47

[1] Thermal cracking
[2] elemental S added corresponding to a 4:1 mol ratio S:Fe

The cobalt sulfide (experiments #8 and #9) and iron sulfide (experiments #13 and #14) colloids prepared in water/PE4LE/decalin microemulsions did not show significant catalytic activity when compared to the thermal cracking experiment conducted with a microemulsion containing only water (experiment #11). The differences of 2-3% in the conversion based on DPM are not considered to be significant, and can probably be attributed to inaccuracies in the DPM calibration curve used to calculate the concentration of DPM (as discussed in section 3.4.4). The differences between the conversion based on DPM and the conversion based on toluene are not readily explained. The benzene and toluene may have cracked to lighter products during the reaction, accounting for the lower-than-expected concentration of these compounds in the liquid reaction products.

The general inactivity of the metal sulfide catalysts in the preliminary activity measurements may have been due to a 'poisoning' effect caused by byproducts of surfactant pyrolysis. As mentioned in section 2.3.5, Martino *et al.* (1994) found that surfactant pyrolysis byproducts resulted in a loss of catalyst activity in the hydrogenolysis of naphthylbibenzylmethane (NBM) using both FeS_2 colloids prepared in a water/PE4LE/octane microemulsion[1], and Fe colloids prepared in water/DDAB/toluene. The authors attributed this loss in activity to the scavenging of hydrogen by the surfactant byproducts, as well as possible chemical and steric poisoning by the surfactant. In addition, the authors found that the catalytic activity of a commercial catalyst (Shell 324) for the hydrogenolysis of NBM decreased with increased doping with the surfactant DDAB.

The formation of surfactant byproducts during the preliminary activity measurements is clearly illustrated in Figures 5.1, 5.2 and 5.3. Figure 5.1 shows a GC trace of a typical reaction

[1] The colloidal FeS_2 catalyst was freeze dried and used as particle-embedded surfactant powder in the activity measurements.

feed (microemulsion plus DPM) for the preliminary activity measurements. The decalin, PE4LE (surfactant) and DPM peaks are clearly identified[2]. Figure 5.2 shows the GC trace of a mixture of benzene, toluene, decalin, PE4LE and DPM corresponding to a 5% theoretical conversion of DPM to benzene and toluene. Figure 5.3 shows the GC trace of an actual reaction product from the preliminary activity measurements (experiment #13). Clearly, a number of peaks other than those of the theoretical reaction products (benzene and toluene) are present in Figure 5.3. These peaks probably represent the pyrolysis byproducts of the surfactant PE4LE. In addition, the surfactant peak (retention time ≈ 7.5 min) in Figure 5.3 is far smaller than the corresponding peak in Figure 5.1, indicating that the surfactant was converted to other byproducts during the reaction.

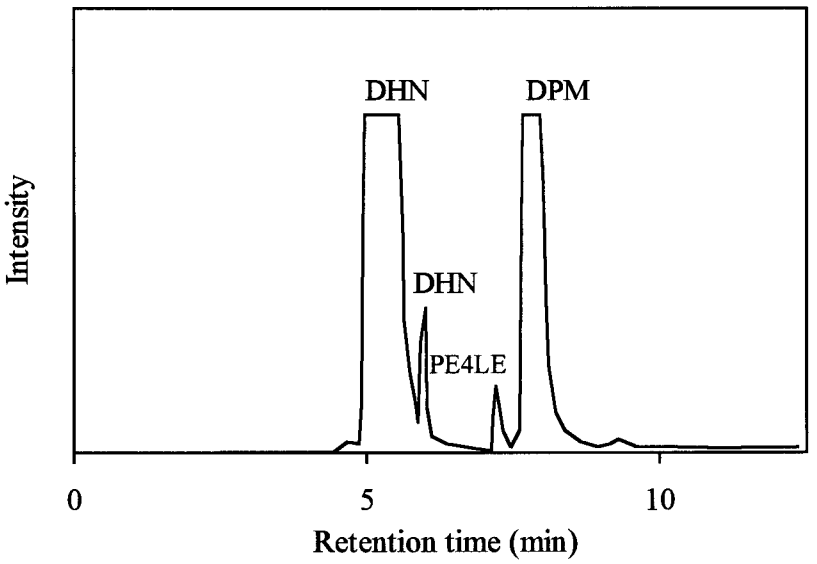

Figure 5.1 : GC trace of a typical reaction feed for preliminary activity measurements. (DHN = decalin, PE4LE = polyoxyethylene-4-lauryl ether, DPM = diphenylmethane).

[2] Decalin has 2 peaks corresponding to the cis- and trans- isomers.

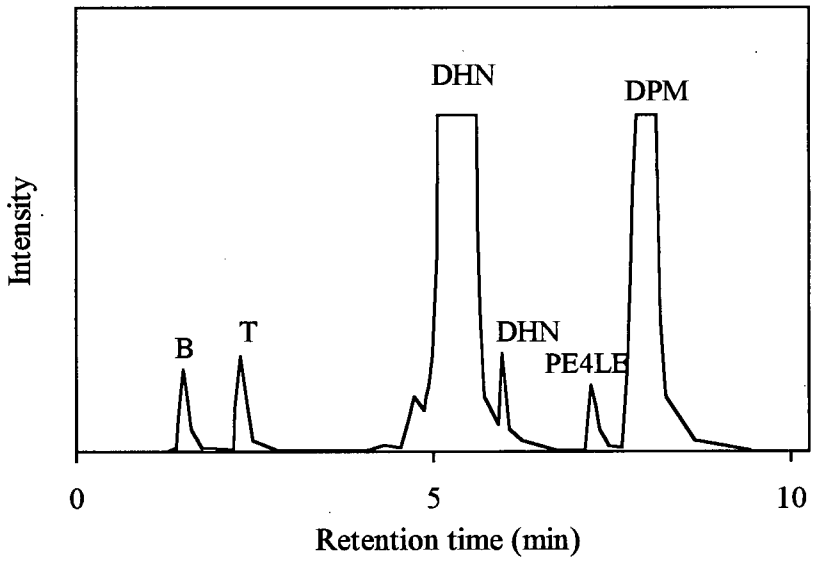

Figure 5.2 : GC trace of a mixture of Benzene (B), Toluene (T), Decalin (DHN), PE4LE and DPM corresponding to 5% conversion of DPM to benzene and toluene.

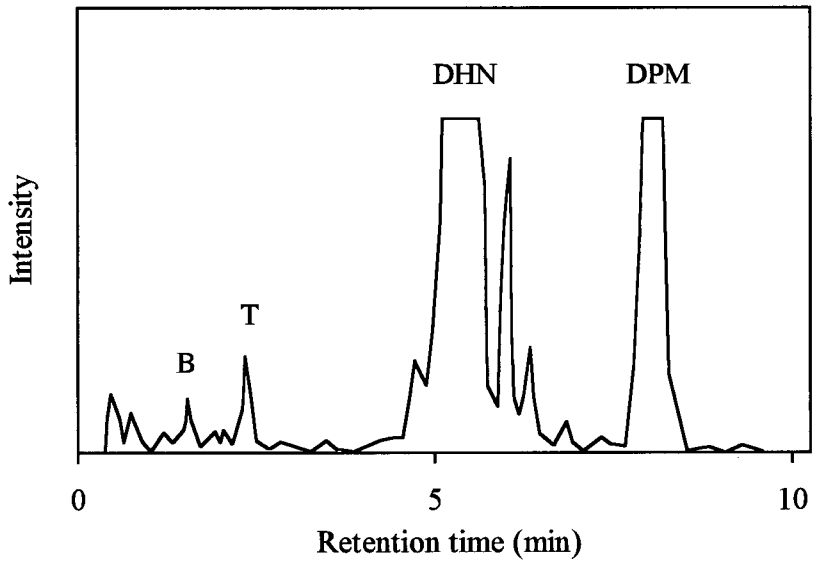

Figure 5.3 : GC trace of a typical reaction product from the preliminary activity measurements (B = benzene, T = toluene, DHN = decalin, DPM = diphenylmethane).

The results in Table 5.2 also indicate that increasing the catalyst synthesis time ('sulfiding time' in Table 5.2.) from 2 to 6 hours had little effect on the activity of the Co sulfide colloidal catalyst (compare experiments #8 and #9). This result indicates that either: i) increasing the colloid synthesis time has little effect on the physical characteristics or the yield of the colloidal catalyst particles, or ii) the 'poisoning' effect of the surfactant or surfactant byproducts is strong enough to mask any effect that increased catalyst synthesis time might have on catalyst activity. The addition of extra elemental sulfur (experiment #14) also had little effect on the catalytic activity of the Fe sulfide catalyst synthesized in the water/PE4LE/decalin system. Two previous studies by Wei and co-workers have shown that the addition of extra elemental sulfur has a promotional effect on the hydrocracking of diphenylmethane (Wei *et al.*, 1992) and di(1-naphthyl) methane (Wei *et al.*, 1993) with FeS_2 catalysts. This provides further evidence that the 'poisoning' effect of the surfactant/surfactant byproducts over-rides any catalytic effects in the reaction system.

Given the similarities between the reaction system studied by Martino *et al.* and the system studied in the present work, it seems likely that the presence of surfactant in the DPM reaction system had a similar 'poisoning' effect as that reported by Martino *et al.* (1994). However, the results of the ASPEN simulation indicated that the reaction system may have been supercritical at 430 °C, which also could have resulted in the apparent lack of catalytic activity observed for the Co sulfide and Fe sulfide colloids in this reaction system. Clearly, the reason for the apparent lack of catalytic activity could not be determined from the results outlined in Table 5.2 alone. An additional experiment (#22) was conducted with cobalt sulfide colloids in a water/PE4LE/decalin microemulsion at 400 °C, a temperature which was below the critical point of the system according to the ASPEN simulation results. The results of experiment #22 are presented in Table

5.3. The results of a thermal cracking experiment at 400 °C are also included in Table 5.3 for comparison.

Table 5.3 : Results of the additional activity measurement conducted in water/PE4LE/ decalin microemulsion (vol. microemulsion = 120 ml, ω = 0.066, mass DPM = 15.015g, initial pressure = 2.2 MPa, reaction temperature = 400°C, reaction time = 3 hours)

Exp. #	Catalyst	Metal Loading (ppm)	Sulfiding Time (hours)	% Conv. (B, T basis)	% Conv. (DPM basis)	First order rate constant based on B, T basis ($cm^3/g/h$)
22	Co microemulsion	620	6	1	7	4
15	Thermal	-	6	1	6	-

Again the cobalt sulfide catalyst did not show significant catalytic activity compared to the thermal cracking experiment (experiment #15). Since the activity of the cobalt sulfide catalyst relative to thermal cracking did not increase when the temperature was reduced from 430 °C to 400 °C, it would appear that the lack of catalytic activity observed at 430 °C was not due to the system being in a supercritical state. It would appear that the apparent lack of catalytic activity observed for the Co sulfide and Fe sulfide colloids in this reaction system (as shown in Table 5.2) may be attributed to the presence of surfactant byproducts in the reaction system.

5.4 Activity measurements using recovered colloids

5.4.1 The use of recovered colloids

As discussed in section 5.3, the presence of surfactant and surfactant pyrolysis byproducts made it impossible to perform meaningful catalytic activity measurements with colloidal metal sulfide catalysts in the microemulsions. Consequently, the metal sulfide colloids were recovered from suspension in order to remove the surfactant, and the recovered colloids were then used in a

second set of activity measurements. As explained in section 3.4.3, the colloidal catalysts were prepared in water/PE4LE/hexane microemulsions using H_2S, and then recovered from suspension using tetrahydrofuran (THF). The metal sulfide colloids aggregated during the extraction process with THF. However, a BET surface area measurement of a sample of recovered colloids revealed that the catalyst still had a large specific surface area (see section 4.4.4). Consequently, the recovered catalysts were probably composed of loose aggregates of the original 25-125 nm sized metal sulfide colloids prepared in the reverse micelles.

The iron sulfide colloids oxidized completely to orange-coloured iron oxide (Fe_2O_3 or Fe_3O_4) during the recovery process. Hence, Fe sulfide colloids were not recovered from the microemulsions and no activity measurements were conducted with Fe sulfide. The second set of activity measurements was conducted at a lower temperature of 400 °C. The reduction in reaction temperature was prompted by the results of the ASPEN simulation of components in the reactor, which indicated that a liquid phase may not have been present in the reactor at 430 °C. The reaction time was increased from 2 to 3 hours to compensate for the lower reaction rates expected at 400 °C.

5.4.2 Experimental results

The results of the second set of activity measurements are presented in Table 5.4. Conversions are again reported on the basis of the number of moles of benzene and/or toluene formed, as well as the number of moles of DPM converted during the reaction. The first order rate constant based on the conversion with respect to benzene/toluene is also presented for each experiment. Details of each activity measurement, including temperature/pressure profiles and GC analyses are presented in Appendix 3.4.

Table 5.4 : Results of the second set of catalytic activity measurements. (liquid volume = 130 ml, initial pressure 5% H_2S in H_2 = 2.4 MPa, reaction temperature = 400 °C, reaction time = 3 hours)

Exp. #	Catalyst	Metal Loading (ppm)	ω	ΔP during reaction (psi)	% Conv. (B,T basis)	% Conv. (DPM basis)	Rate constant based on B, T conversion ($cm^3/g/h$)
15	Thermal	-	-	50	1	6	-
16	$Fe(CO)_5$	926	-	50	1	6	2.5
17	Recovered NiS	655	0.066	40	1	9	2.3
18	$Fe(CO)_5$	1000	-	50	1	4	3.8
19	Co naphthenate	1000	-	150	15	15	58.4
20	Recovered CoS_2	1000	0.099	100	3	3	9.3
23	Recovered CoS_2	2000	0.066	50	1	4	1.7

The first order rate constants based on the number of moles of benzene/toluene formed during the reaction were used as the basis for comparison of the relative activities of the various catalysts. The rate constants were calculated using the conversion based on the number of moles of benzene/toluene formed during the reaction since the production of benzene and toluene reflected the true hydrocracking activity of the catalyst. In addition, the calibration of the GC for the detection of benzene and toluene was more accurate (R^2=0.99) than the calibration for the detection of DPM (R^2=0.89).

As with the preliminary activity measurements, the conversion based on the number of moles of DPM converted was generally greater than the conversion based on the production of benzene and toluene. This result tends to suggest that other by-products were produced during the reaction. However, no other significant products were found by GC and MS (mass spectroscopy) analysis of the reaction products. Some gas (CH_4 or C_2H_6) may have been produced during the reactions, accounting for the increase in pressure over the course of the

reaction. The increase in pressure may also have been due to the addition of benzene and toluene to the vapor phase over the course of the reaction. Moreover, the conversion based on benzene was generally the same as the conversion based on toluene. This would tend to indicate that benzene and toluene were stable reaction products, and were not selectively cracked to lighter components.

The catalyst obtained from the decomposition of iron pentacarbonyl (experiments #16 and #18) showed little activity over and above the base thermal activity (experiment #15) for the hydrocracking of DPM. The difference between the results of runs #16 and #18 was within the error associated with the determination of DPM concentration by GC.

The active catalyst obtained from the decomposition of cobalt naphthenate showed the greatest activity for the hydrocracking of DPM. The relatively high conversion was accompanied by a large increase in pressure (150 psi) over the course of the reaction, which indicates that the benzene and toluene products went into the vapor phase at the reaction conditions. In addition, the conversion based on DPM concentration was equal to the conversion based on the production of benzene and toluene, indicating that little or no by-products were formed.

An additional experiment (experiment #21, not shown) was conducted to determine whether benzene or toluene were produced by the decomposition of Co naphthenate in decalin at the reaction conditions. GC traces of the reaction product of experiment #19 and the products of the decomposition of Co naphthenate are presented in Appendix 3.5. The peaks of benzene, toluene, n-decane (the internal GC standard), decalin and DPM are labeled. Clearly, no benzene and toluene are evident in the product of the decomposition of Co naphthenate, indicating that these compounds were not produced by the decomposition of Co naphthenate. The main decomposition products were found at short retention times (0.46 min and 0.998 min), and at retention times from 5.7 min to 5.9 min.

The recovered NiS catalyst (experiment #17) showed little activity over and above thermal cracking. The recovered CoS_2 catalyst in experiment #20 showed some activity, which was again reflected in an increased pressure rise of 100 psi over the course of the reaction. However, the second batch of CoS_2 catalyst showed little activity. The reason for the difference between the activity of the cobalt and nickel sulfide catalysts synthesized by the microemulsion technique and the catalyst from the decomposition of cobalt naphthenate is not obvious. This matter is discussed further in section 5.4.3.

5.4.3 Catalyst characterization using XRD

The spent catalysts from the second set of activity measurements were characterized by x-ray diffraction (XRD) in order to determine the active species and the average crystallite sizes of the catalysts. A sample of the fresh CoS_2 catalyst recovered from the microemulsion was also analyzed by XRD before it was used in experiment #23. The preparation of the XRD samples was conducted in an air-free environment in order to minimize exposure to atmospheric oxygen. The results of the XRD analyses are presented in Table 5.5. The XRD spectra of the samples are presented in Appendix 3.6.

$Fe_{1-X}S$ was identified as the active species resulting from the decomposition of $Fe(CO)_5$ during the activity measurements. This result is consistent with previous studies which also identified the non-stoichiometric sulfide $Fe_{1-X}S$ as the active species formed by the decomposition of iron-based organometallic compounds in sulfur rich hydrocarbon environments (Anderson and Bockrath, 1984; Herrick *et al.*, 1990).

Co_8FeS_8 was identified as the active species resulting from the decomposition of Co naphthenate (spent catalyst from experiment #19). The presence of iron in the catalyst was not

expected, and this iron contaminant may have originated from the stainless steel of the reactor and reactor internals.

Table 5.5 : Summary of the catalyst characterization using XRD.

Experiment / Catalyst Sample	Species Identified	Crystal Plane	Peak Position (2Θ)	Relative peak intensity	Crystallite Size (nm)
#18 - Spent Catalyst ($Fe(CO)_5$ precursor)	$Fe_{1-X}S$	2 0 0	29.82	0.60	> 150 [1]
		2 0 6	33.70	0.66	> 150 [1]
		2 0 12	43.60	1	75
		2 2 0	53.00	0.43	47
#19 - Spent Catalyst (Co naphthenate precursor)	Co_8FeS_8	1 1 1	15.50	0.32	32
		3 1 1	29.79	0.96	20
		2 2 2	31.22	0.33	27
		5 1 1	47.63	0.35	29
		4 4 0	52.13	1	21
#20 - Spent Catalyst	Co_4S_3 / Co_8FeS_8	1 1 1	15.50	0.25	not measured
		3 1 1	29.84	0.95	68
		2 2 2	31.62	1	> 150 [1]
		5 1 1	47.65	0.29	33
		4 4 0	52.12	0.75	32
#23 - Fresh Catalyst Recovered CoS_2	Amorphous	-	-	-	-
#23 - Spent Catalyst	Co_8FeS_8	1 1 1	15.51	0.17	22
		3 1 1	29.98	0.88	29
		2 2 2	31.27	0.31	26
		5 1 1	47.74	0.37	27
		4 4 0	52.19	1	22

[1] No peak broadening was detected over-and-above normal instrumentational broadening in these samples. The estimate of a minimum crystallite size of 150 nm in these samples was based on the assumption that the peak widths can be read off the XRD spectra with an accuracy of ±0.01 degrees.

The spectrum of the spent catalyst from experiment #20 differed slightly from the spectrum of the catalyst from experiment #19. Firstly, the peak at $2\Theta = 15.5°$ was slightly smaller than in the spectra of the catalyst from #19. This peak resulted from the presence of Fe in the crystal matrix, which indicates that the spent catalyst from experiment #20 had a lower level of iron contamination than the spent catalyst from experiment #19. Secondly, the peak at $2\Theta \approx 31.6°$

was more intense and shifted slightly to the right compared to the corresponding peak in the spectrum of the spent catalyst from experiment #19. A good match was more difficult to find for the spent catalyst from experiment #20, the data fit the standard spectra for Co_8FeS_8 and Co_4S_3 equally well.

The XRD spectrum of the spent catalysts formed from the recovered CoS_2 in experiment #23 was very similar to the spectrum of the active species resulting from the decomposition of Co naphthenate (spent catalyst from experiment #19). Again the relative intensity of the peak at $2\Theta=15.5°$ was smaller than in the spectrum of the catalyst from exp. #19.

In conclusion, it would appear that the spent catalysts from experiments #19, 20 and 23 were of very similar crystalline form. The main difference between the catalysts appears to have been in the amount of iron contaminant incorporated in the crystal lattices (as indicated by differences in the relative heights of the peak at $2\Theta=15.5°$). No comparable results could be generated for the NiS catalyst since sufficient spent catalyst could not be collected from the reactor product of activity experiment #17 to obtain a XRD spectrum

XRD analysis revealed that the cobalt sulfide catalyst recovered from the microemulsion (fresh catalyst for experiment #23) was amorphous. No sharp peaks were identified (see XRD spectrum in Appendix 3.6), and the single broad peak present in the XRD spectrum was characteristic of an amorphous solid. Clearly, the cobalt sulfide catalysts in experiments #20 and #23 underwent a phase transition from amorphous CoS_2 to crystalline Co_8FeS_8 during the reaction. This phase transition was accompanied by the formation of 20-30 nm sized crystallites (particles) in the Co_8FeS_8 catalyst (see Table 5.5).

It is interesting to compare the results of the activity measurements (as presented in Table 5.4) with the results of the XRD analysis of the spent catalysts (Table 5.5). Assuming that the catalysts were present as dispersed single crystallites (particles) at the reaction conditions, one

would expect the catalyst activity to have been inversely proportional to the crystallite size. For example, Takemura and Okada (1988) found that the specific activity of dispersed nickel catalysts for coal liquefaction increased with decreasing Ni crystallite size. However, the results in Table 5.5 indicate that there was no clear relationship between the catalyst activity and crystallite size. The crystallite size of the Co_8FeS_8 catalyst resulting from the decomposition of Co naphthenate (experiment #19) was small (20-30 nm), and the catalyst displayed high activity (k = 58 $cm^3/g/h$) as was to be expected. However, the crystallite size of the spent catalyst from experiment #23 was also small, but the catalyst displayed little catalytic activity. In addition, the crystallite size of the spent catalyst from experiment #20 was slightly larger (30-68 nm), but the catalyst was more active than the catalyst from experiment #23.

The lack of a strong correlation between catalyst activity and crystallite size indicates that the rate of reaction was not dependent on the available surface area of catalyst. This suggests that the macrostructure of the catalyst introduced diffusion limitations which controlled the rate of reaction. For example, it is possible that the crystallites of the catalysts in experiments #18, #20 and #23 aggregated into agglomerates, either during the extraction process from the microemulsion, or by exposure to the elevated reaction conditions. Diffusion limitations resulting from the internal porosity would then account for the low activity of the catalyst in experiments #18, #20 and #23. Likewise, it is feasible that the catalyst in experiment #19 was present as dispersed single crystallites which did not suffer from diffusion limitations.

5.5 Summary of the activity measurements performed

The metal sulfide colloids synthesized in reverse micelles showed little catalytic activity for the hydrocracking of DPM when the activity measurements were conducted in water/PE4LE/decalin microemulsions. This lack of activity can be attributed to a poisoning effect

by the surfactant and surfactant pyrolysis byproducts (identified by GC). Martino *et al.* (1994) reported a similar poisoning effect in NBM hydrogenolysis reactions performed in water/$C_{12}E_4$/octane and water/DDAB/toluene microemulsions containing FeS_2 and Fe colloidal catalysts. A second set of activity measurements was conducted with a number of dispersed catalysts prepared from organometallic additives, and the metal sulfide colloids extracted from the microemulsions.

The catalyst obtained from the decomposition of Co naphthenate showed the greatest activity for the hydrocracking of DPM. The active species was identified as Co_8FeS_8, with an average crystallite size of 26 nm. The active species formed from microemulsion-extracted CoS_2 were also identified as Co_8FeS_8, but these catalysts were found to be less active than the Co_8FeS_8 from the decomposition of Co naphthenate. The lack of a correlation between the crystallite size and the catalyst activity suggests that the catalysts from the microemulsion-extracted CoS_2 were present as aggregates with internal porosity which introduced rate controlling diffusion limitations. It would appear that the extraction process made it difficult to measure the intrinsic activity of the metal sulfide prepared in reverse micelles.

Chapter 6 : Conclusions and Recommendations for Future Work

6.1 Conclusions

The synthesis of colloidal heavy oil hydrocracking catalysts in the reverse micelles of the water/PE4LE/hexane microemulsion was investigated in the present study. The factors affecting the size of the reverse micelles were identified, and the synthesis of reduced Ni, Co and Fe colloids and the corresponding metal sulfide colloids in the microemulsion was completed. The metal sulfide species synthesized in the microemulsion with 5% H_2S in H_2 were characterized by TEM, EDX and XPS. Finally, the catalytic activity of the metal sulfide colloids synthesized in the water/PE4LE/hexane microemulsion was investigated using the hydrocracking of a model compound, diphenylmethane. The principle observations and conclusions resulting from this research are listed below:

1. The water:surfactant ratio (ω) and metal ion concentration were identified as the key factors affecting the size of the reverse micelles in the water/PE4LE/hexane microemulsion. Reverse micelles ranging in diameter from 11.4 to 21.8 nm were obtained by varying ω between 0.04 and 0.09.
2. A direct relationship was found between the reverse micelle size and the size of reduced Co and Fe colloids synthesized by the addition of N_2H_4 to water soluble Co and Fe salts dissolved in the water pools of the reverse micelles. The reduced Co and Fe colloids were monodisperse with sizes ranging between 10 and 23 nm, depending on ω. Reduced Ni formed larger 100-200 nm aggregates, suggesting that the rate of reduction also had an effect on the size of metal particles prepared in reverse micelles.

3. High temperature colloid synthesis using dimethyl disulfide was not possible due to the instability of the microemulsion at elevated temperatures. Nickel, cobalt and iron sulfide colloids were prepared in water/PE4LE/hexane microemulsions using 5% H_2S in H_2 at room temperature (22°C). The Ni sulfide and Co sulfide colloids had average sizes of 67 and 71 nm respectively (as determined by TEM), but were more polydisperse than the reduced metal colloids prepared in the same system. Again this result suggests that a low rate of reaction leads to particle growth beyond the confines of the reverse micelles.
4. XPS analysis of the sulfided colloids identified NiS and CoS_2 as the species formed with 5% H_2S in H_2. The XPS analysis illustrated the extreme difficulty encountered when trying to characterize nanometer sized colloids without altering the physical and chemical nature of the colloids during the sample preparation and analysis. The metal sulfide colloids prepared were extremely sensitive to atmospheric oxygen, and strong peaks of NiO, $CoO/Co(OH)_2$ and Fe_2O_3/Fe_3O_4 were detected.
5. The metal sulfide catalysts prepared in reverse micelles showed little activity for the hydrocracking of a model compound DPM when the activity measurements were performed in the microemulsions containing the metal sulfide colloids. This inactivity was ascribed to the poisoning of the catalyst by products of the pyrolysis of the surfactant formed during the reaction. The metal sulfide catalysts were extracted from the microemulsion to avoid the problem of the surfactant, and the extracted catalysts were used in a second set of activity measurements. The catalyst obtained from the decomposition of cobalt naphthenate showed greater activity for the hydrocracking of DPM than NiS and CoS_2 colloids extracted from the microemulsion.
6. The spent catalysts from the activity measurements were characterized by XRD. The active species resulting from Co naphthenate and the extracted CoS_2 were both identified as

Co_8FeS_8. The iron contamination in the catalysts probably resulted from corrosion of the reactor surfaces. No correlation was found between the crystallite size and the catalyst activity, which suggests that the catalysts from the microemulsion-extracted CoS_2 were present as aggregates with internal porosity which introduced rate controlling diffusion limitations. It would appear that the extraction process made it difficult to measure the intrinsic activity of the metal sulfide prepared in reverse micelles.

6.2 Recommendations and Future work

The results of this study indicate that the size of reduced Co and Fe colloids synthesized in the water/PE4LE/hexane microemulsion can be controlled by manipulating the size of the reverse micelles. However Ni, Co and Fe sulfide colloids synthesized in the same system with 5% H_2S in H_2 grew beyond the confines of the reverse micelles. Consequently, reduced metal colloids should be used as catalysts for future heavy oil hydrocracking experiments since one can retain control over the size of the catalyst particles added to the heavy oil. In this case the reduced metal colloids would be sulfided by naturally occurring sulfur in the heavy oil.

Likewise, the colloidal catalysts synthesized in microemulsions should not be extracted from the microemulsions before use. The colloids appear to aggregate during the extraction process, decreasing the dispersion of the catalyst in the liquid phase, and introducing mass transfer effects which make it difficult to determine the intrinsic activity of the colloidal catalyst.

More specifically, the following future work is recommended to further expand on the results of this thesis:

1. Ni, Co and Fe colloids should be prepared in other microemulsions besides the water/PE4LE/hexane system. Other systems which form stable reverse micelles over a wider range of ω values, and form water pools smaller than 12 nm should be investigated. Examples

may include: water/CTAB/alkane, water/AOT/alkane, water/DDAB/toluene and water/Ph_9E_6/ cyclohexane. Investigation of these systems will also allow for the determination of the effect of the solubility of the organic phase of the microemulsion in the heavy oil on the degree dispersion of the colloidal catalyst in the heavy oil.

2. A wider range of metals, possibly including bimetallic colloids (see Ravet *et al.*, 1987) should be prepared by the reverse micelle technique and used as hydrocracking catalysts.
3. The activity of reduced metal colloids synthesized in reverse micelles should be determined for the hydrocracking of heavy oil. The poisoning effect of surfactant byproducts identified in the model compound activity tests may be a serious disadvantage of preparing colloidal catalysts in reverse micelles, and it must be determined whether a similar poisoning effect occurs in heavy oil hydrocracking tests.
4. The spent catalyst form the heavy oil hydrocracking tests must be recovered and characterized. This will indicate whether the size of the original reduced metal colloid added to the heavy oil has any effect on the size of the active catalyst particle present at the reaction conditions. The relationship between crystallite size and hydrocracking activity should be investigated, as this could shed more light on the catalytic action of dispersed catalysts in heavy oil hydrocracking.

References

Anderson R. R., Bockrath B. C., *Fuel*, 1984, 63 (3), p. 329-333.

Andres M., Charcosset H., Chiche P., Davignon L., Djega-Mariadassou G., Joly J., Pregermain S., *Fuel*, 1983, 62, p. 69-72.

Bearden R., Aldridge C. L., *Energy Progress*, 1981, 1, 1-4, p. 44-48.

Boutonnet M., Kizling J., Stenius P., *Colloids and Surfaces*, 1982, 5, p. 209-225.

Boutonnet M., Kizling J., Touroude R., Maire G., Stenius P., *Appl. Catal.*, 1986, 20, p. 163.

Boutonnet M., Kizling J., Mintsa-Eya V., Choplin A., Touroude R., Maire G., Stenius P., *Journal of Catalysis*, 1987, 103, p. 95-104.

Boutonnet M., Kizling J., Touroude R., Maire G., Stenius P., *Catalysis Letters*, 1991, 9, p. 347-354.

Bradley J.S., Millar J. M., Hill E. W., Behal S., *Journal of Catalysis*, 1991, 129, p. 530-539.

Chang N. J. and Kaler E. W., *Langmuir*, 1986, 2, p. 184-190.

Curtis C. W., Pellegrino J. L., *Energy & Fuels*, 1989, 3 (2), p. 160-168.

Dabkowski M. J., Shih S. S., Albinson K. R., *A.I.Ch.E. Symposium Series*, 1991, 87 (282), p. 53-58.

Danielsson I., Lindman B., *Colloids and Surfaces*, 1981, 3, p. 391-392.

Dautzenberg F. M., De Deken J. C., *Catal. Rev. -Sci. Eng.*, 1984, 26 (3&4), p. 421-444.

Dautzenberg F. M., De Deken J. C., *In proceedings of Symposium on Developments in Hydrodemetallization Catalysts, A.C.S. Miami Beach Meeting, April 28 - May* 3, *1985*, p. 8-20.

Del Bianco A., Panariti N., Di Carlo S., Elmouchnino J., Fixari B., Le Perchec P., *Applied Catalysis A: General*, 1993, 94, p. 1-16.

Delgass W. N., Hughes T. R., Fadley C. S., *Catal. Rev.*, 1970, 4, p.179-219.

Derbyshire F., Davis A., Epstein M., Stansberry P., *Fuel*, 1986, 65, p. 1233-1239.

Eccles R. M., *Oil and Gas Journal*, 1982, 80, p. 121.

Fendler J., *Chem. Rev.*, 1987, 87, p. 877-899.

Flecher P. D. I., Howe A. M., Robinson B. H., *J. Chem Soc.,Faraday Trans. 1*, 1987, 83, p.985-1006.

Fogg P. G. T., *Solubility Data Ser.*, 32, 1988.

Gates B.C., Katzer J.R., Schuit G.C.C., *Chemistry of Catalytic Processes*, McGraw - Hill, New York, 1979.

Hager G. T., Bi X. X., Eklund P. C., Givens E. N., Derbyshire F. J., *Energy & Fuels*, 1994, 8, p. 88-93.

Henglein A., *Chem. Rev.*, 1989, 89, p. 1861-1873.

Herrick D. E., Tierney J. W., Wender I., *Energy & Fuels*, 1990, 4, p. 231-236.

Hirschon A. S., Wilson R. B., *Am. Chem. Soc., Prep. Div Fuel Chem.*, 1989, 34 (3), p. 881-885.

Kandori K., Kon-no K., Kitahara A., Fujiwara M., Tamura T., *Proceedings of the Sixth International Symposium on Surfactants in Solution-Modern Aspects, New Delhi, India, Aug 18-22, 1986.*

Kon-no K., Koide M., Kitahara A., *Nippon Kagaku Kaishi*, 1984, 6, p. 815.

Kim H., Curtis C. W., Cronauer D. G., Sajkowski D. J., *Am. Chem. Soc., Prep. Div Fuel Chem.*, 1989, 34 (4), p. 1431-1438.

Kizling J., Stenius P., *Journal of Colloid and Interface Science*, 1987, 118 (2), p. 482-492.

Laine J., Trimm D., *J. Chem. Tech. Biotechnol.*, 1982, 32, p. 813-833.

Lett R. G., Cugini A. V., Utz B. R., Kranstman D., Cillo D. L., Jin G. T., *VI Korea-U.S.A. Joint Workshop on Coal Utilization Technology, October 17-18, 1989.*

Lianos P., Thomas J. K., *Journal of Colloid and Interface Science*, 1987, 117 (2), p. 505-512.

Liu C., Zhou J., Que G., Liang W., Zhu Y, *Fuel*, 1994, 73, 9, p. 1545-1550.

Lupien, M., *Syncrude - Facts and Figures*, 1995, July, Syncrude Canada Ltd.

Martino A., Wilcoxon J. P., Kawola J. S., *Energy & Fuels*, 1994, 8, p. 1289-1295.

Meyer M., Wallberg C., Kurihara K, Fendler J., *J. Chem Soc., Chem Commun.*, 1984, p. 90-91.

Modes S., Lianos P., *J. Phys. Chem.*, 1989, 93, p. 5854-5859.

Nagy J. B., Gourgue A., Derouane E. G., *Preparation of Catalysts III*, 1983, Elsevier, Amsterdam, p. 193-200.

Oelderik J.M., Sie S.T., Bode D., *Applied Catalysis*, 1989, 47, p. 1-24.

Overbeek J. T. G., de Bruyn P. L., Verkoekcx F., 'Microemulsions', in *Surfactants*, Tandros T. F., Ed., Academic Press, London, 1984, p. 111-132.

Pecoraro T. A., Chianelli R. R., *J. Catal.*, 1981, 67, p. 430.

Petit C., Pileni M. P., *J. Phys. Chem.*, 1988, 92, p. 2282-2286.

Petit C., Lixon P., Pileni M. P., *J. Phys. Chem.*, 1990, 94, p. 1598-1603.

Pileni M. P., Lisiecki I., *Colloids and Surfaces A: Physiochemical and Engineering Aspects*, 1993, 80, p. 63-68.

Pileni M. P., Motte L., Petit C., *Chem. Mater.*, 1992, 4, p. 338-345.

Pileni M. P., Zemb T., Petit C. J., *Chem. Phys. Lett.*, 1985, 118, p. 414.

Pillai V., Kumar P., Multani M., Shah D., *Colloids and Surfaces A: Physiochemical and Engineering Aspects*, 1993, 80, p. 69-75.

Ravet I., Gourge A., Gabelica Z., Nagy J. B., *Proceedings of the VIII International Congress on Catalysis, Berlin 1984*, 4, p. 871-878.

Ravet I., Nagy J. B., Derouane E. G., *Preparation of Catalysts*, 1987, Elsevier, Amsterdam, p. 193-200.

Robinson B. H., Topraciaglu C., Dore J., Chieux P., *J. Chem. Soc. Faraday Trans. I*, 1984, 80, p. 13.

Rosen M. J., *Surfactants and Interfacial Phenomena*, John Wiley & Sons Inc., New York, 1978.

Rudnick L. R., Audeh S., *Am. Chem. Soc., Prep., Div. Pet. Chem.*, 1986, 31 (3), p. 686.

Rudnick L. R., *US Patent 4 642 175*, 1987.

Sanford E. C., *Canadian Chemical News*, 1996, 48 (1), p. 21-23.

Sanford E. C., Steer J. G., Muehlenbachs K., Gray M. R., *Energy and Fuels*, 1995, 9, p. 928-935.

Schott H., *Journal of Colloid and Interface Science*, 1973, 43 (1), p. 150-155.

Schick M. J., *Nonionic Surfactants*, Marcel Dekker Inc., New York, 1987, p. 528-530.

Shaw D. J., *Colloid and Surface Chemistry*, Butterworth-Heinemann Ltd., 4th. Ed., Oxford., 1992.

Steigerwald M. L., Brus L. E., *Annu. Rev. Mater. Sci.*, 1989, 19, p. 471-495.

Stenberg V. I., Ogawa T. O., Willson W. G., Miller D., *Fuel*, 1983, 62, p. 1487.

Sweeny P. G., Stenberg V. I., Hei R. D., Montano P. A., *Fuel*, 1987, 66, p. 532-41.

Takemura Y., Okada K., *Fuel*, 1988, 67, p. 1549-1553.

Ternan M., *Canadian Journal of Chemical Engineering*, 1983, 61, p. 689-696.

Thomas M. G., Padrick T. D., Stohl F. V., *Fuel*, 1982, 61, p. 716.

Utz B. R., Cugini A. V., Frammel E. A., *Am. Chem. Soc., Prep. Div Fuel Chem.*, 1989, 34 (4), p. 1423.

Van Driesen R. P., Caspers J., *Hydrocarbon Processing*, 1979, 58 (5), p. 107.

Varghese P., *US Patent 4 581 127*, 1986.

Vold R. D., Vold M. L., *Colloid and interface chemistry*, Addison Wesley, London, 1983, p. 181-186.

Weisser P., Landa S., *Sulphide Catalysts, their Properties and Applications*, Pergamon Press, New York, 1970.

Wilcoxon J. P., Williamson R. L., Baughman R., *J. Chem. Phys.*, 1993, 98 (12), p. 9933-9950.

Wei X., Ogata E., Zong Z., Niki E., *Energy & Fuels*, 1992, 9, p. 868-9.

Wei X., Ogata E., Zong Z., Niki E., *Fuel*, 1993, 72 (11), p. 1547-1552.

Appendices

Appendix 1

1.1 Microemulsions prepared

1.2 List of activity measurements.

1.3 Modeling of the reaction system using ASPEN process simulation package.

1.4 GC temperature program

1.5 GC standard calibration mixtures

1.6 GC calibration data and calibration equations

1.7 Equations for the calculation of conversion

Appendix 1.1 : Microemulsions Prepared

Water/PE4LE/Hexane Microemulsions

#	Metal salt in Water Pool	ω (vol/vol)	Metal Concentration in water pool (mol/l)	Microemulsion Status
1	$Ni(NO_3)_2$	0.066	3.1	OK
2	$Co(NO_3)_2$	0.066	3.1	OK
3	$Fe(NO_3)_3$	0.066	2.8	OK
4	$Co(NO_3)_2$	0.033	3.1	Cloudy
5	$Co(NO_3)_2$	0.132	3.1	2 Phase
6	$Ni(NO_3)_2$	0.066	1.6	OK
7	$Ni(NO_3)_2$	0.066	4.7	OK
8	$Co(NO_3)_2$	0.040	3.1	OK
9	$Co(NO_3)_2$	0.099	3.1	OK
10	$Co(NO_3)_2$	0.050	3.1	OK
11	$Co(NO_3)_2$	0.083	3.1	OK
12	$Ni(NO_3)_2$	0.099	3.1	OK
13	$Co(NO_3)_2$	0.066	1.6	OK
14	$Fe(NO_3)_3$	0.066	1.6	OK
15	$Fe(NO_3)_3$	0.099	2.8	OK
16	$Ni(NO_3)_2$	0.066	3.1	OK
21	$Ni(NO_3)_2$	0.040	3.1	OK
22	$Fe(NO_3)_3$	0.040	2.8	OK

Water/PE4LE/Decahydronaphthalene Microemulsions:

#	Metal salt in Water Pool	w (vol/vol)	Metal Concentration in microemulsion (mol/l)	Microemulsion Status
17	$Ni(NO_3)_2$	0.066	3.1	OK
18	$Co(NO_3)_2$	0.066	3.1	OK
19	$Fe(NO_3)_3$	0.066	2.8	OK
20	$Ni(NO_3)_2$	0.066	3.1	OK

Appendix 1.2 : List of Activity Measurements

Activity Tests conducted in Microemulsions (method 1)

Exp #	Reactor Charge (Volumetric Ratio)	Catalyst (Metal Loading)	Liq.. Vol. (ml)	Sulfiding Cond. (Time/Temp)	I.P. (psig)	Reaction Temp (°C)	Reaction Time (h)
1	Decalin / DPM 8:1	-	90	2 h / 25 °C	1000	430	1
2	Decalin / DPM 8:1	$Fe(CO)_5$ (620 ppm)	90	2 h / 25 °C	1000	430	1
3	M.E. #1/ DPM 8:1	Ni Sulfide (620 ppm)	90	2 h / 25 °C	1000	430	1
8	M.E. #2/ DPM 8:1	Co Sulfide (620 ppm)	135	2 h / 25 °C	300	430	2
9	M.E. #2/ DPM 8:1	Co Sulfide (620 ppm)	135	6 h / 25 °C	300	430	2
11	Blank M.E. / DPM 8:1	-	135	2 h / 25 °C	300	430	2
13	M.E. #3/ DPM 8:1	Fe Sulfide (520 ppm)	135	6 h / 25 °C	300	430	2
14[1]	M.E.#3/ DPM 8:1	Fe Sulfide (520 ppm)	135	6 h / 25 °C	300	430	2
22	M.E.#2/ DPM 8:1	Co Sulfide (620 ppm)	135	6 h / 25 °C	360	400	3

[1] elemental S added

Activity Tests conducted with extracted catalyst (method 2)

Exp #	Reactor Charge (Volumetric Ratio)	Catalyst (Metal Loading)	Liq. Vol. (ml)	Sulfiding Cond. (Time/Temp)	I.P. (psig)	Reaction Temp (°C)	Reaction Time (h)
15	DHN/DPM 8:1	-	130	-	340	400	3
16	DHN/DPM 8:1	Fe(CO)5 926 ppm Fe	130	2 h / 25 °C	325	400	3
17	DHN/DPM 8:1	Extracted NiS 655 ppm Ni	130	2 h / 25 °C	300	400	3
18	DHN/DPM 8:1	Fe(CO)5 1000 ppm	130	2 h / 25 °C	340	400	3
19	DHN/DPM 8:1	Co Naphthenate 1000 ppm Co	130	2 h / 25 °C	340	400	3
20	DHN/DPM 8:1	Extracted CoS_2 1000 ppm Co	130	2 h / 25 °C	360	400	3
21	DHN	Co Naphthenate 1000 ppm Co	130	2 h / 25 °C	340	400	3
23	DHN/DPM 8:1	Extracted CoS_2 2000 ppm Co	130	2 h / 25 °C	350	400	3

Appendix 1.3 : Modeling of the reaction system using ASPEN process simulation package.

The ASPEN process simulation package version 5.5 (ASPEN Technology Inc.) was used to determine the pressure and phase equilibrium of the reaction mixture at the final reaction conditions for these calculations. In other words, for a particular set of initial conditions (T_1, P_1), the final pressure (P_2) and the vapor/liquid distribution (x/y) at the final reaction conditions (T_2) were required. The ASPEN process simulation package version 5.5 (ASPEN Technology Inc.) was used for these calculations. ASPEN cannot be used to simulate static or batch systems. Consequently, an arbitrary time dimension was added to the physical parameters of the system to fulfill this simulation specification (e.g. reactor volume ml was simulated as a flow in ml/s). The ASPEN simulation was performed in 2 steps: Firstly, n (the number of moles of 5% H_2S in H_2 present at the initial conditions (T_1, P_1)) was calculated using a simple mixer block. Once n had been calculated, the reaction system under the initial conditions (T_1, P_1) was fully characterized. This reaction system was then entered into the flashcurve option of ASPEN, and a series of flash calculations were performed at various combinations of T_2 and P_2. The particular pressure P_2 which gave a final volume V_2 = 300 ml defined the vapor/liquid equilibrium of the reaction system under the reaction conditions. This calculation routine was performed for values of T_2 ranging between 400 and 430 °C. The SRK equation of state was used for the simulation.

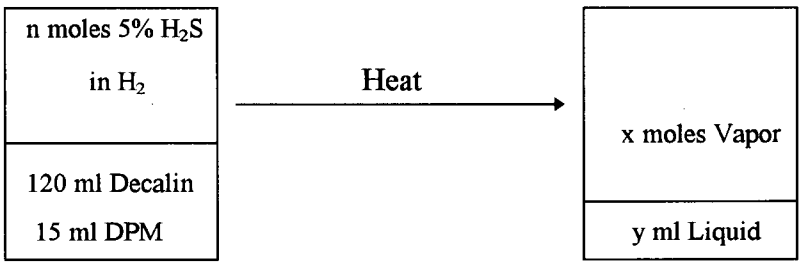

Initial Conditions :	T_1 = 20 °C	Final Conditions :	T_2
	P_1 = 300 psig		P_2
	Total Vol. = 300 ml		Total Vol. = V_2

Appendix 1.4 : Gas Chromatograph Temperature Program

40 °C	1 min
Ramp to 70 °C @ 50 °C/min	
70 °C	2 min
Ramp to 170 °C @ 50 °C/min	
170 °C	5 min
Ramp to 270 °C @ 50 °C/min	
270 °C	2 min

Appendix 1.5 : GC standard calibration mixtures

#	DPM Conv. (%)	Vol. Benzene (ml)	Vol. Toluene (ml)	Vol. DPM (ml)	Vol. DHN (ml)	Vol. C10 (ml)	Total Vol. (ml)
1	0	0	0	4000	32	1	37
2	2.5	53	63	3900	32	1	37.02
3	5	106	127	3800	32	1	37.03
4	7.5	159	190	3700	32	1	37.05
5	10	211	253	3600	32	1	37.06
6	12.5	264	317	3500	32	1	37.08
7	15	317	380	3400	32	1	37.1
8	20	423	506	3200	32	1	37.13

Appendix 1.6 : GC Calibration data and calibration curves

Initial Calibration

Order of Calibration standand injections: 8, 1, 4, 6, 3

Sample #	Repeat #	Benzene Area	Toluene Area	C10 Area	DHN Area	DPM Area	A_B/A_{C10}	A_T/A_{C10}	A_{DPM}/A_{C10}	A_{DHN}/A_{C10}
1	1	0	0	994562	42498980	6299802	0	0	6.334	42.731
	2	0	0	954371	40011637	5784536	0	0	6.061	41.925
	3	0	0	936148	39129864	5674284	0	0	6.061	41.799
	AVG.	0	0	961694	40546827	5919541	0	0	6.152	42.152
3	1	131124	149099	948618	39189217	5412334	0.138	0.157	5.705	41.312
	2	128301	141420	903110	38190713	5326533	0.142	0.157	5.898	42.288
	3	136947	152619	972630	39366026	5313893	0.141	0.157	5.463	40.474
	AVG.	132124	147713	941453	38915318.7	5350920	0.140	0.157	5.689	41.358
4	1	193053	226375	973945	39721228	5079145	0.198	0.232	5.215	40.784
	2	189188	218785	914556	37921009	4886789	0.207	0.239	5.343	41.464
	3	183054	214140	929337	38302532	4999489	0.197	0.230	5.380	41.215
	AVG.	188432	219767	939279	38648256	4988474	0.201	0.234	5.313	41.154
6	1	315506	378987	942871	38632335	4725070	0.335	0.402	5.011	40.973
	2	301867	364227	907939	37861915	4649583	0.332	0.401	5.121	41.701
	3	299522	363172	905632	37832584	4631505	0.331	0.401	5.114	41.775
	AVG.	305632	368795	918814	38108945	4668719	0.333	0.401	5.082	41.483
8	1	592329	686158	1067880	44398543	4985691	0.555	0.643	4.669	41.576
	2	563569	654291	1020812	43195072	4876173	0.552	0.641	4.777	42.314
	3	545502	634454	996294	42630601	4791228	0.548	0.637	4.809	42.789
	AVG.	567133	658301	1028329	43408072	4884364	0.551	0.640	4.752	42.227

Calibration Check - 4/01/96

Order of Injection: 3, 8, 4

Sample #	Repeat #	Benzene Area	Toluene Area	C10 Area	DHN Area	DPM Area	A_B/A_{C10}	A_T/A_{C10}	A_{DPM}/A_{C10}	A_{DHN}/A_{C10}
3	1	95717	114907	745441	30630101	4373046	0.128	0.154	5.866	41.090
	2	95700	114673	719507	29503444	3771662	0.133	0.159	5.242	41.005
	3	91201	110149	701520	28925611	3966629	0.130	0.157	5.654	41.233
	AVG.	94206	113243	722156	29686385.3	4037112	0.130	0.157	5.588	41.109
4	1	139084	169371	731842	29241412	4116917	0.190	0.231	5.625	39.956
	2	140090	170345	733431	29550967	4153986	0.191	0.232	5.664	40.291
	3	141129	171971	740297	29552596	4078272	0.191	0.232	5.509	39.920
	AVG.	140101	170562	735190	29448325	4116392	0.191	0.232	5.599	40.056
8	1	370625	446417	714311	29056086	3519256	0.519	0.625	4.927	40.677
	2	375488	453134	722033	29483768	3645268	0.520	0.628	5.049	40.834
	3	378019	453162	682805	27978764	2501202	0.554	0.664	3.663	40.976
	AVG.	374711	450904	706383	28839539.3	3221909	0.531	0.639	4.546	40.829

Calibration Curves - Initial and Recalibration

Sample #	M_B/M_{C10}	A_B/A_{C10} Initial Calibr.	A_B/A_{C10} Recal.	M_T/M_{C10}	A_T/A_{C10} Initial Calibr.	A_T/A_{C10} Recal.	M_{DPM}/M_{C10}	A_{DPM}/A_{C10} Initial Calibr.	A_{DPM}/A_{C10} Recal.
3	0.232	0.138	0.128	0.232	0.157	0.154	4.407	5.705	5.866
	0.232	0.142	0.133	0.232	0.157	0.159	4.407	5.898	5.242
	0.232	0.141	0.130	0.232	0.157	0.157	4.407	5.463	5.654
4	0.348	0.198	0.190	0.348	0.232	0.231	4.291	5.215	5.625
	0.348	0.207	0.191	0.348	0.239	0.232	4.291	5.343	5.664
	0.348	0.197	0.191	0.348	0.23	0.232	4.291	5.38	5.509
8	0.928	0.555	0.519	0.928	0.643	0.625	3.711	4.669	4.927
	0.928	0.552	0.520	0.928	0.641	0.628	3.711	4.777	5.049
	0.928	0.548	0.554	0.928	0.637	0.664	3.711	4.809	3.663

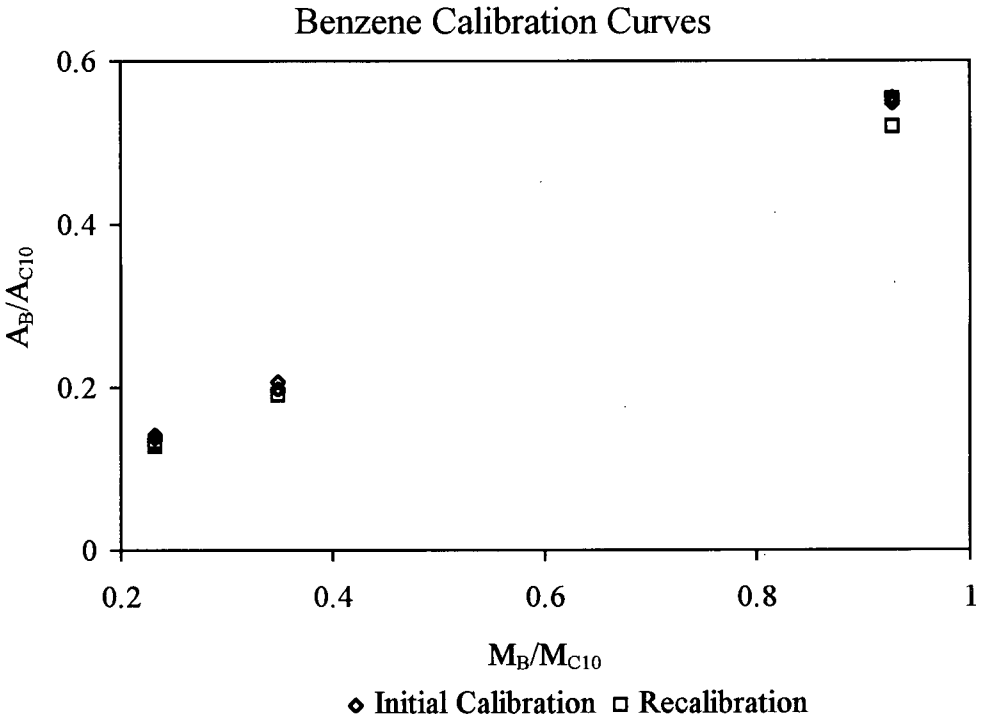
Benzene Calibration Curves
0.6
0.4
0.2
0
A_B/A_{C10}
0.2
0.4
0.6
0.8
1
M_B/M_{C10}
◇ Initial Calibration □ Recalibration

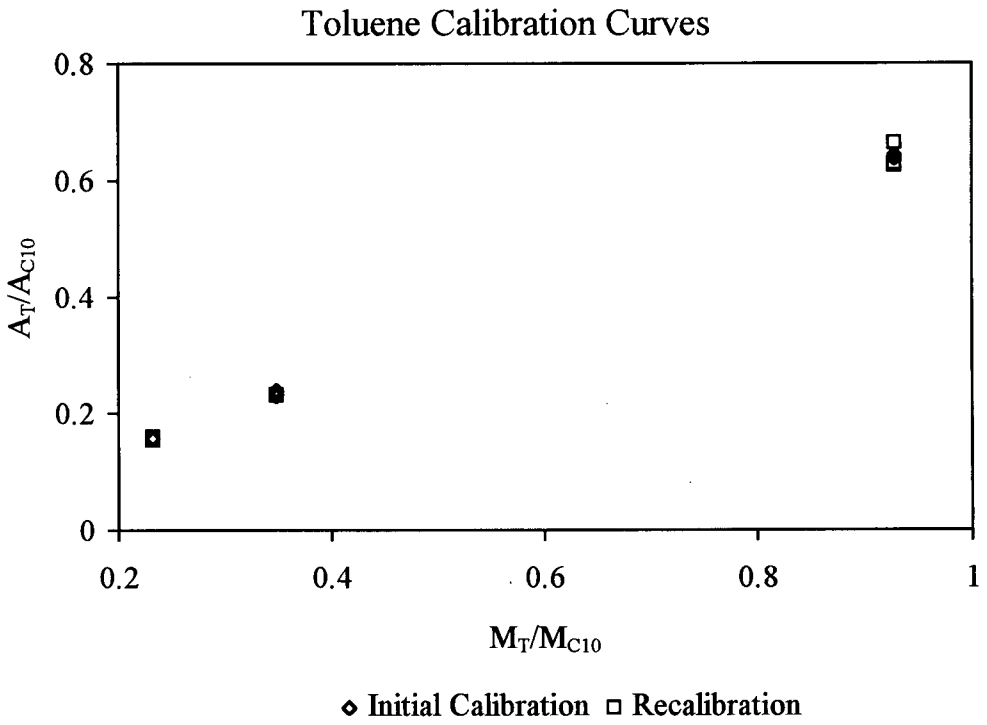
Toluene Calibration Curves
0.8
0.6
0.4
0.2
0
A_T/A_{C10}
0.2
0.4
0.6
0.8
1
M_T/M_{C10}
◇ Initial Calibration □ Recalibration

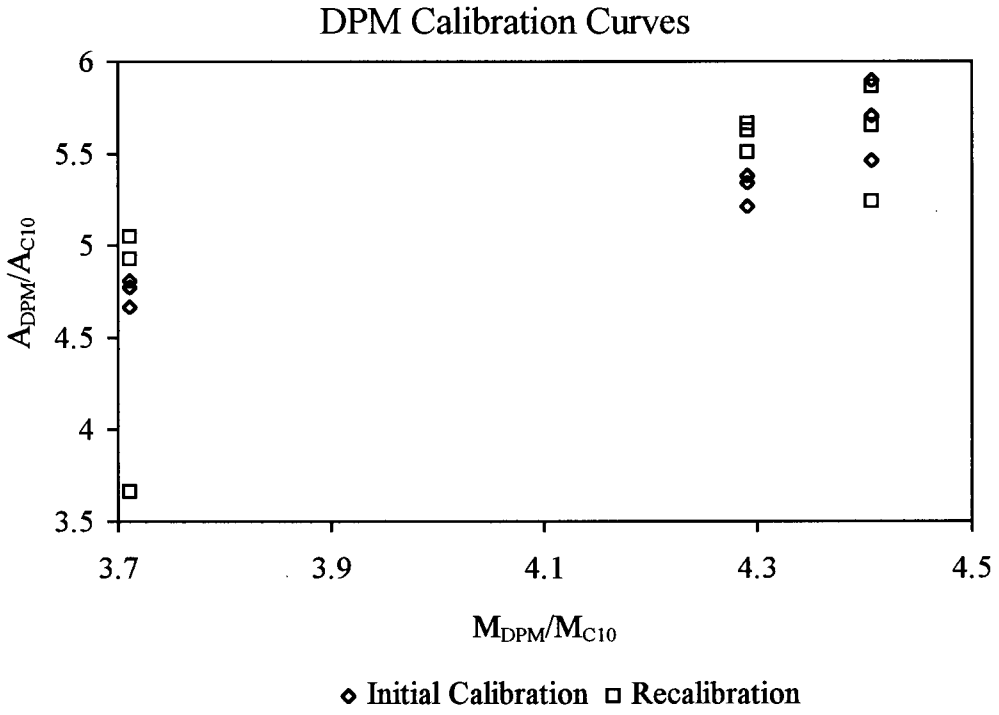
DPM Calibration Curves
6
5.5
5
4.5
4
3.5
A_{DPM}/A_{C10}
3.7
3.9
4.1
4.3
4.5
M_{DPM}/M_{C10}
◇ Initial Calibration □ Recalibration

Appendix 1.7 : Equations for the calculation of conversion

$$\% \text{ Conversion (based on Benzene)} = \frac{\#\text{ moles of Benzene in Reactor Product}}{\#\text{ moles of DPM in Reactor Feed}} \cdot 100$$

$$\% \text{ Conversion (based on Toluene)} = \frac{\#\text{ moles of Toluene in Reactor Product}}{\#\text{ moles of DPM in Reactor Feed}} \cdot 100$$

$$\% \text{ Conversion (based on DPM)} = \frac{\#\text{ moles of DPM in Feed} - \#\text{ moles of DPM in Product}}{\#\text{ moles of DPM in Reactor Feed}} \cdot 100$$

Appendix 2

2.1 TEM Photographs of reduced Co and Fe colloids

2.2 EDX of reduced Co and Fe colloids

2.3 EDX spectrum of Ni sulfide prepared using DMDS

2.4 Synthesis of metal sulfide colloids in the water/PE4LE/hexane microemulsion using 5% H_2S in H_2

2.5 TEM Photographs of metal sulfide colloids synthesized using 5% H_2S in H_2

2.6 Explanation of terms used in Table 4.6

2.7 Standard binding energies of various Ni, Co and Fe species

2.8 BET surface area calculations

Appendix 2.1 TEM photographs of reduced Co and Fe colloids

Photograph #925 : Reduced Co colloids at 100 000* magnification
(1 mm = 4nm)

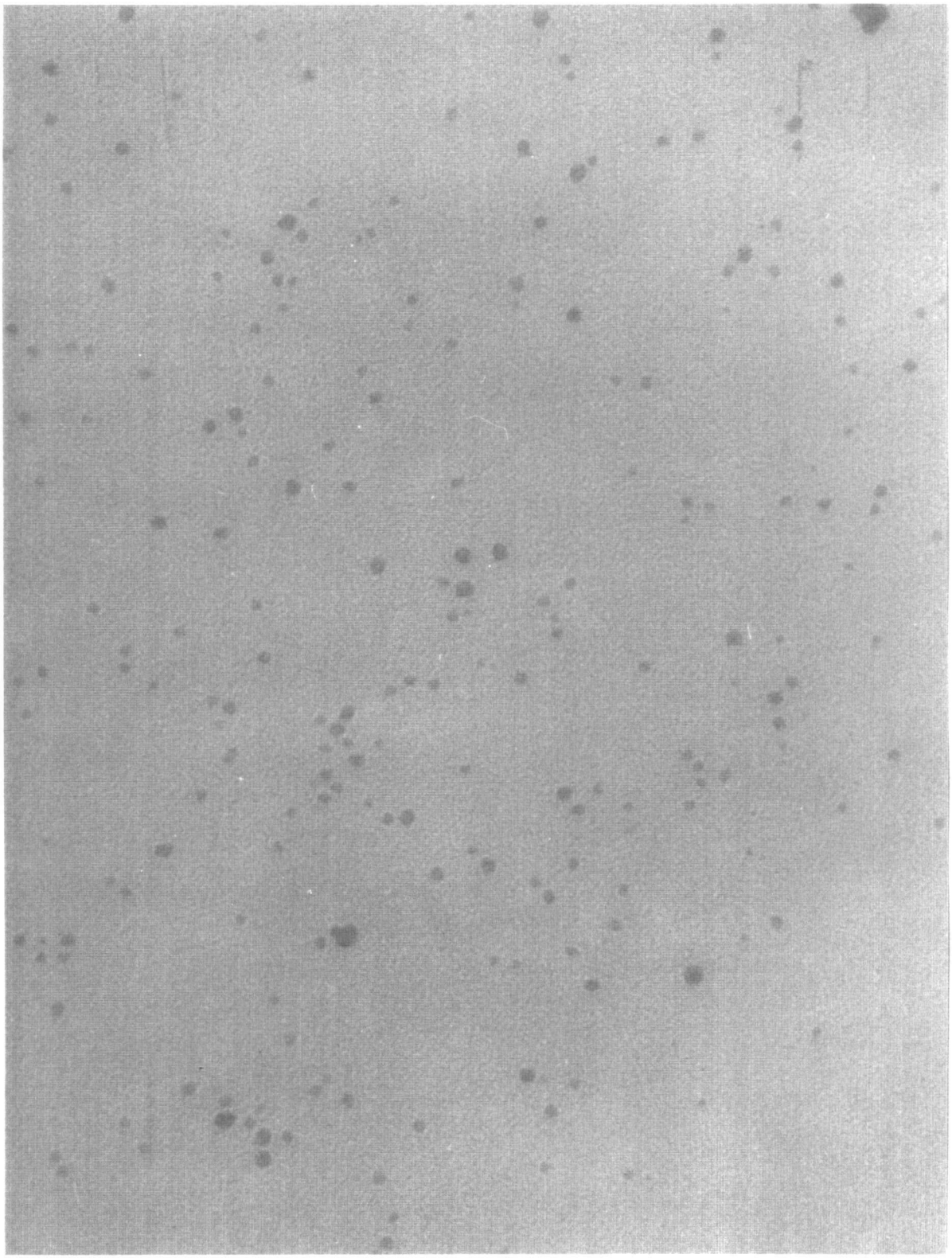

Photograph #926 : Reduced Co colloids at 100 000* magnification
(1 mm = 4 nm)

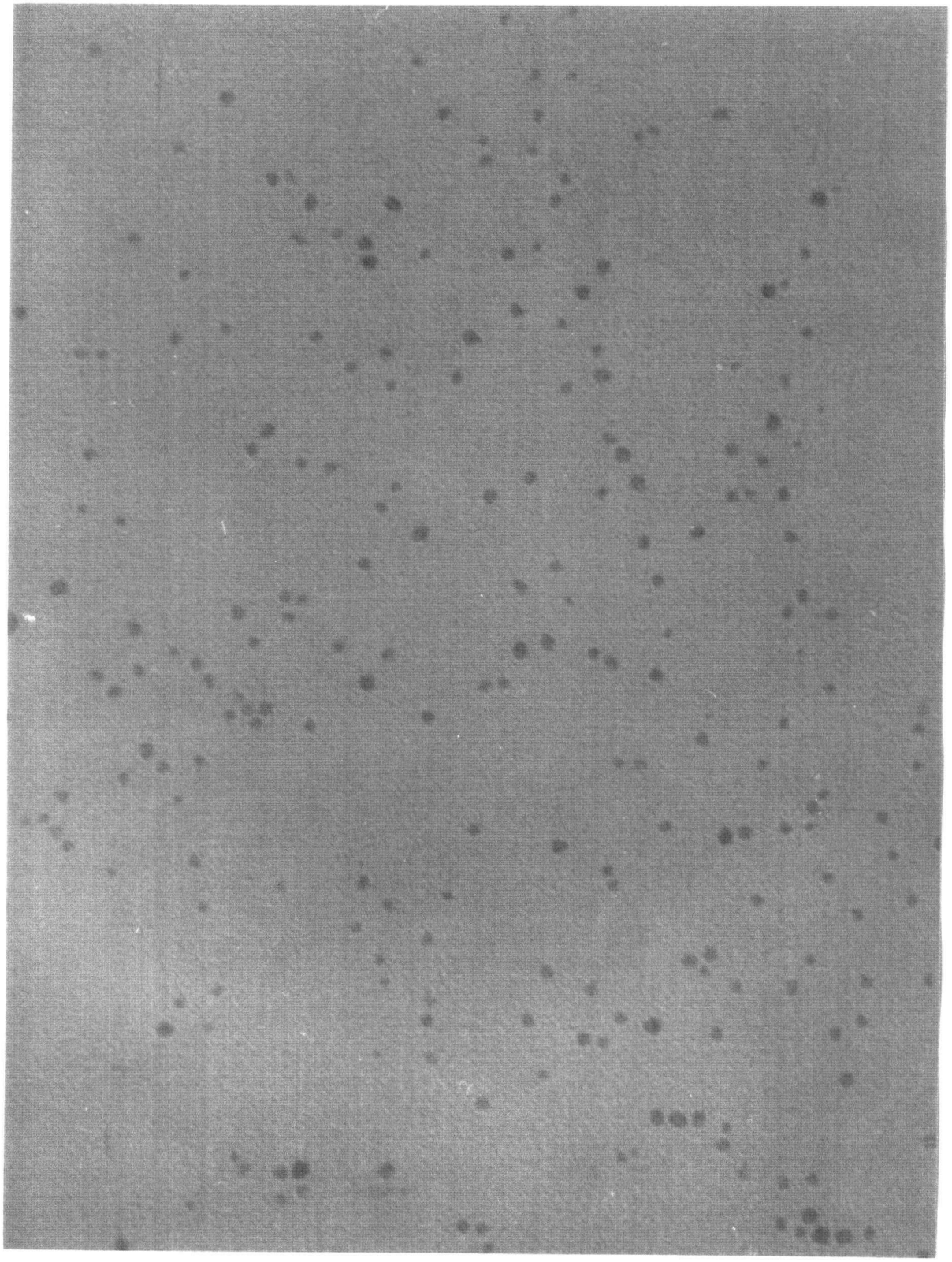

Photograph #928 : **Reduced Fe colloids at 50 000* magnification**
(1 mm = 8 nm)

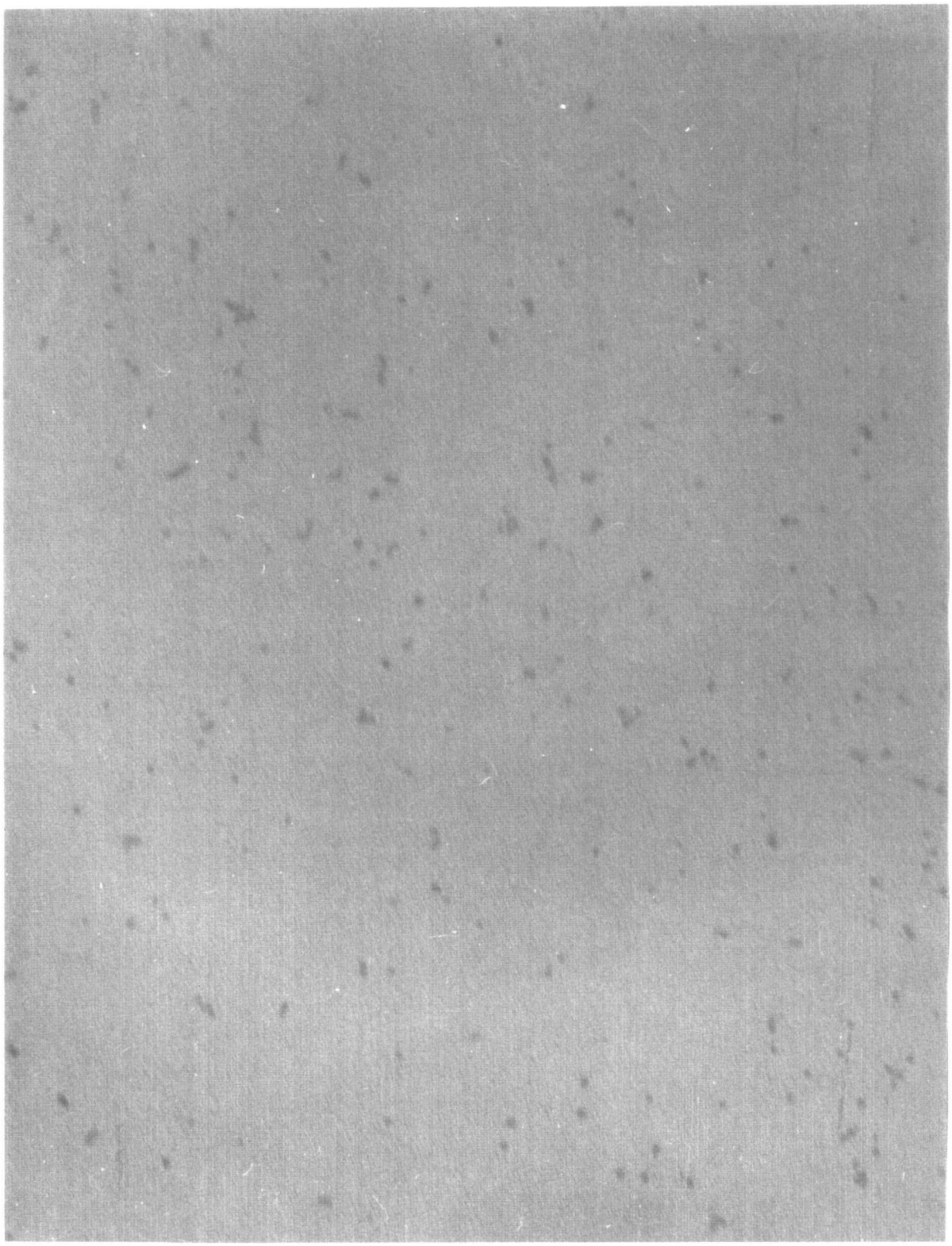

Photograph #929 : **Reduced Fe colloids at 100 000* magnification**
(1 mm = 4 nm)

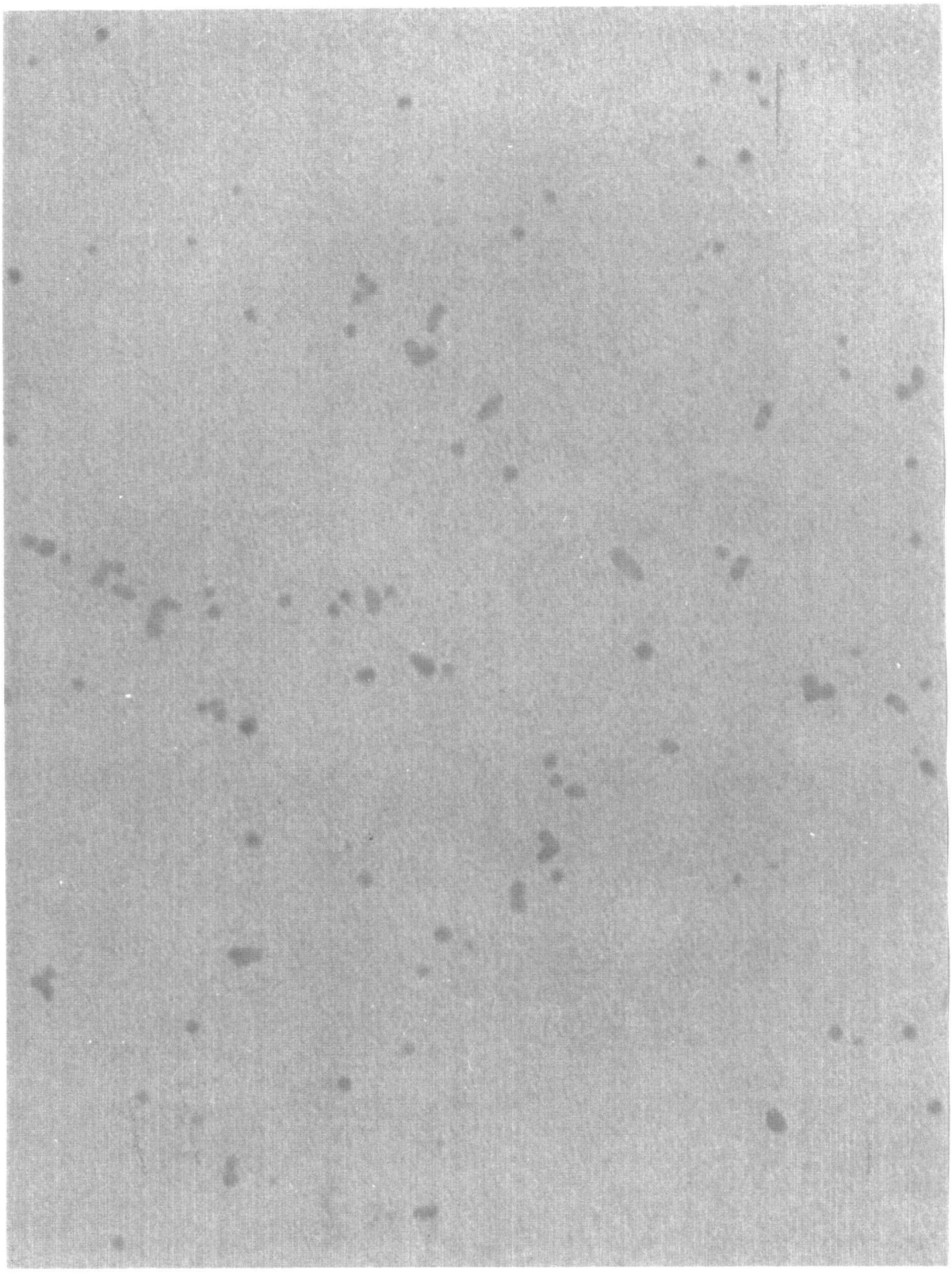

Appendix 2.2 : EDX spectra of reduced Co and Fe colloids

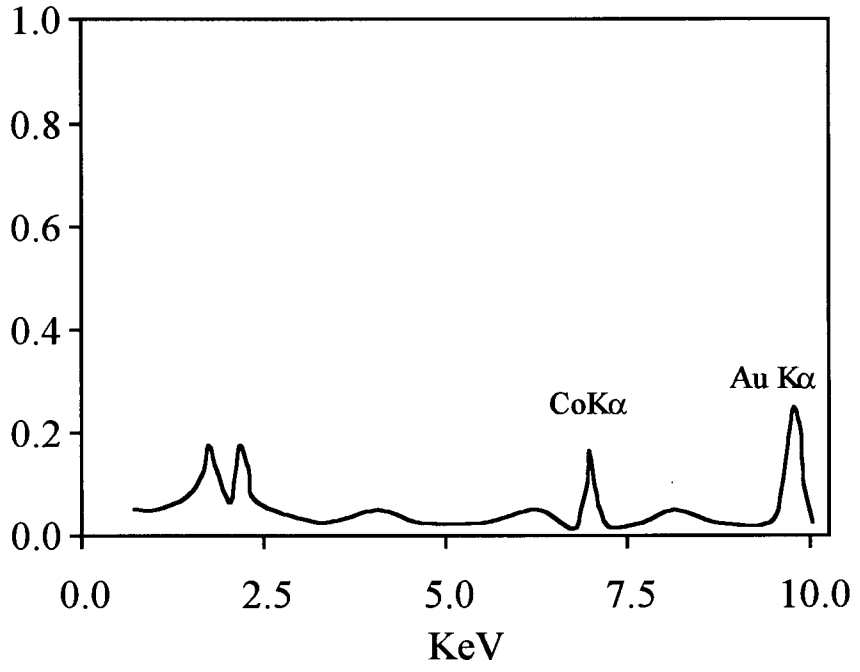

EDX Spectrum of a typical reduced Co colloid

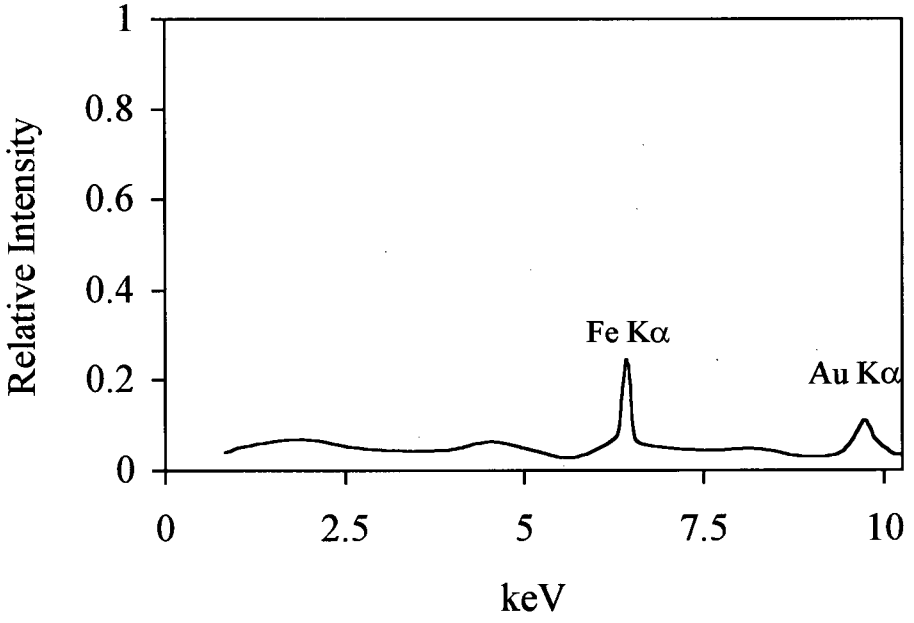

EDX Spectrum of a typical reduced Fe colloid

Appendix 2.3 : EDX spectrum of Ni sulfide prepared using DMDS

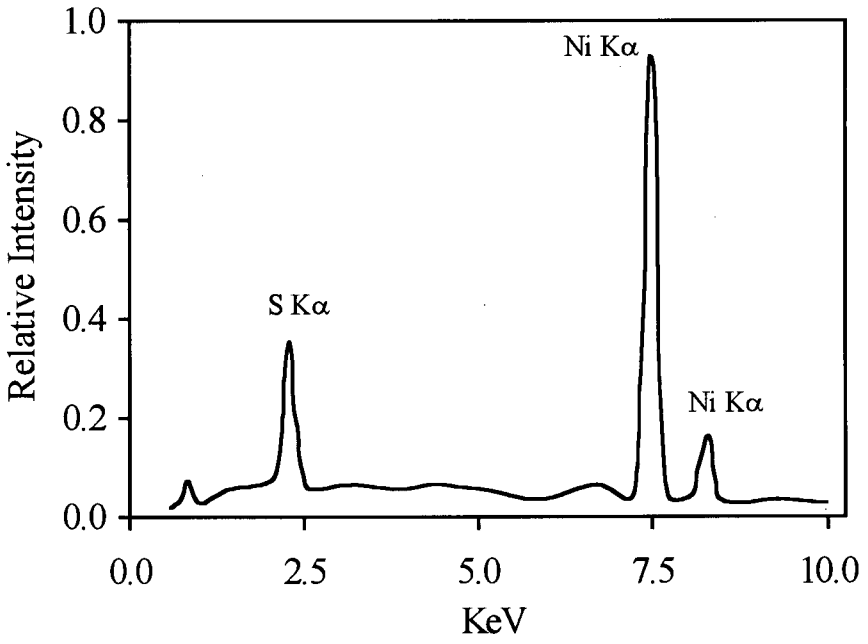

Appendix 2.4 : Synthesis of metal sulfide colloids in the water/PE4LE/hexane microemulsion using 5% H_2S in H_2.

(T = 22 °C, ω=0.066, $[Ni^{2+}]$ in water pool = 3 mol/L, $[Co^{2+}]$ = 3 mol/L, $[Fe^{3+}]$ = 2.75 mol/L)

Exp. #	Metal / Microemulsion #	Pressure (MPa)	Time (hours)	Particle Size by TEM	Elements by EDX	Surface species by XPS
26	Ni (Batch #1)	7	6	No	Yes	Yes
27	Co (Batch #2)	7	6	No	Yes	Yes
28	Fe (Batch #3)	7	2	No	Yes	Yes
29	Fe (Batch #3)	7	6	No	Yes	Yes
30	Ni (Batch #1)	7	6	Yes	Yes	No
31	Co (Batch #2)	7	6	Yes	Yes	No
32	Fe (Batch #3)	7	6	No	Yes	No

Appendix 2.5 : TEM photographs of metal sulfide colloids synthesized using 5% H_2S in H_2

Photograph #127 : Ni sulfide colloids at 20 000* magnification (1mm = 20 nm)

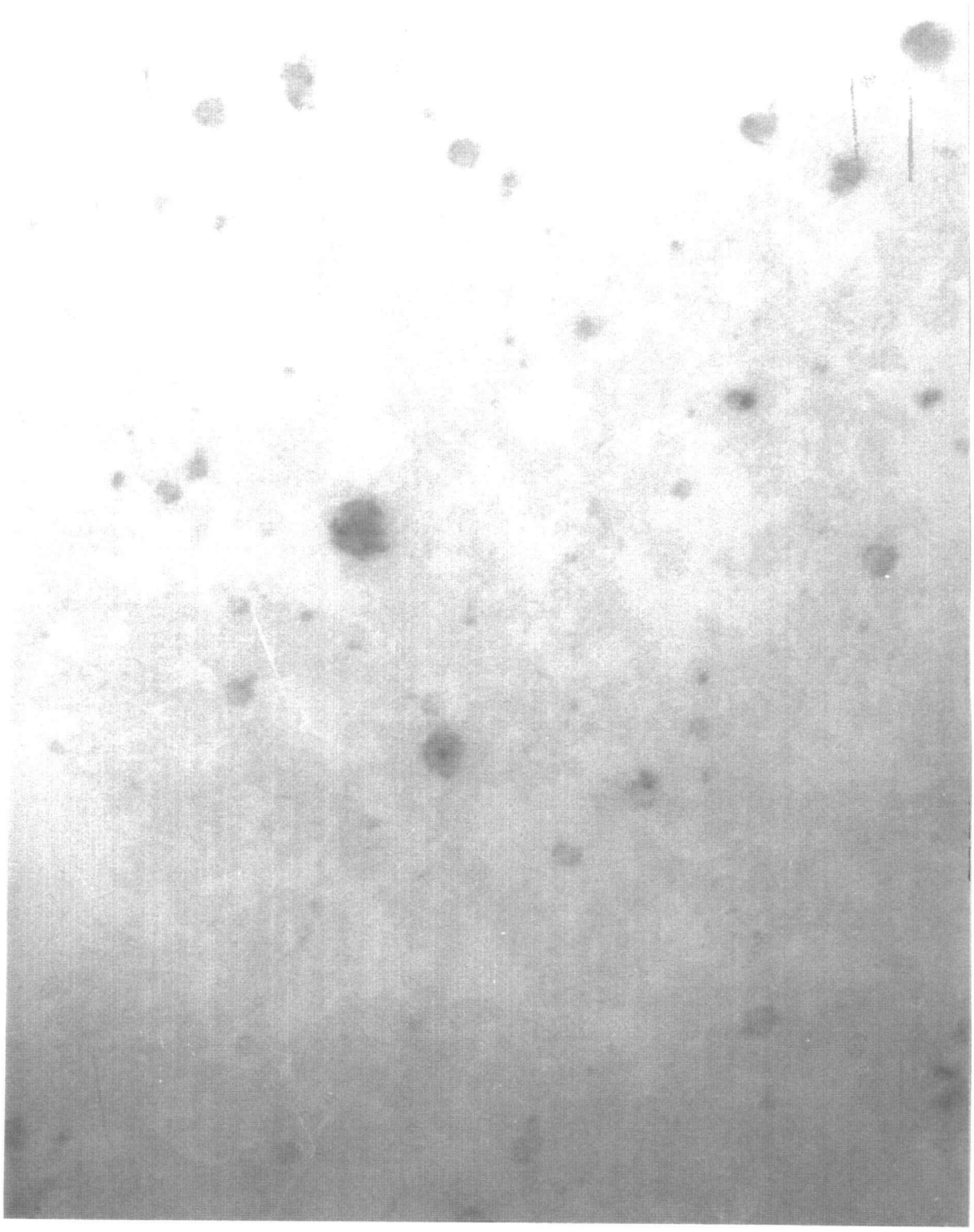

Photograph #130 : Ni sulfide colloids at 20 000* magnification (1mm = 20 nm)

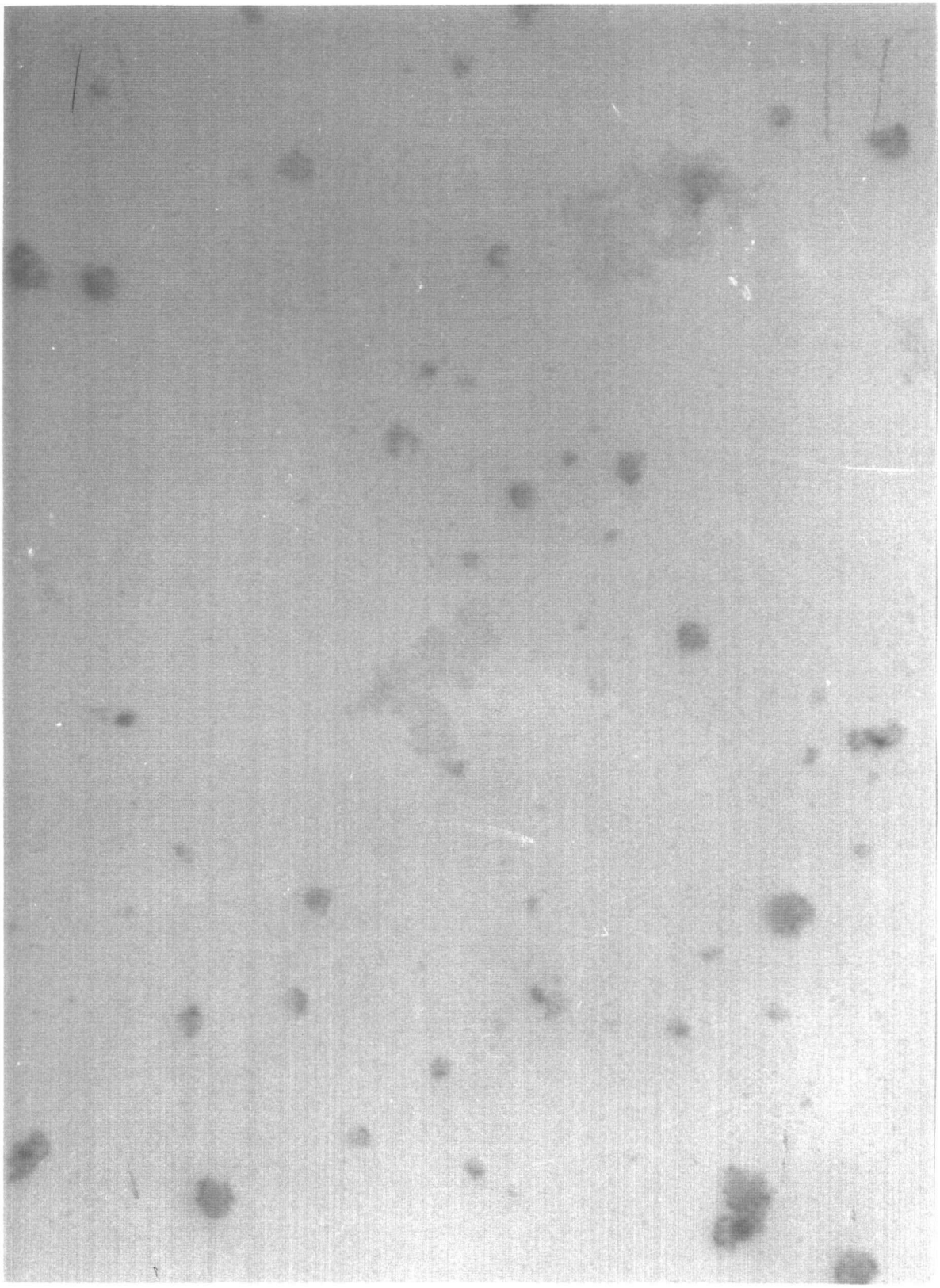

Photograph #131 : Ni sulfide colloids at 100 000* magnification (1mm = 4 nm)

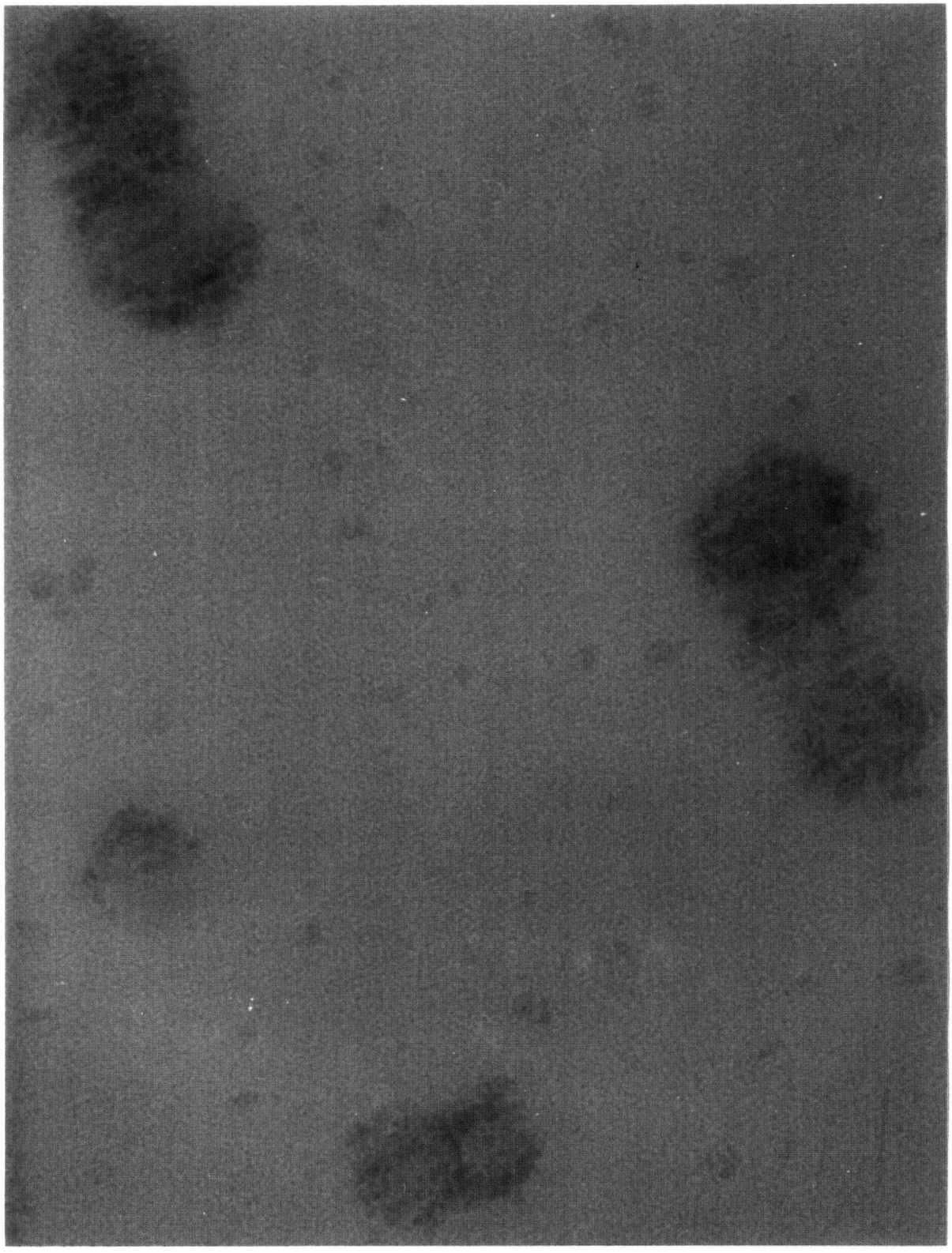

Photograph #132 : Ni sulfide colloids at 20 000* magnification (1mm = 20 nm)

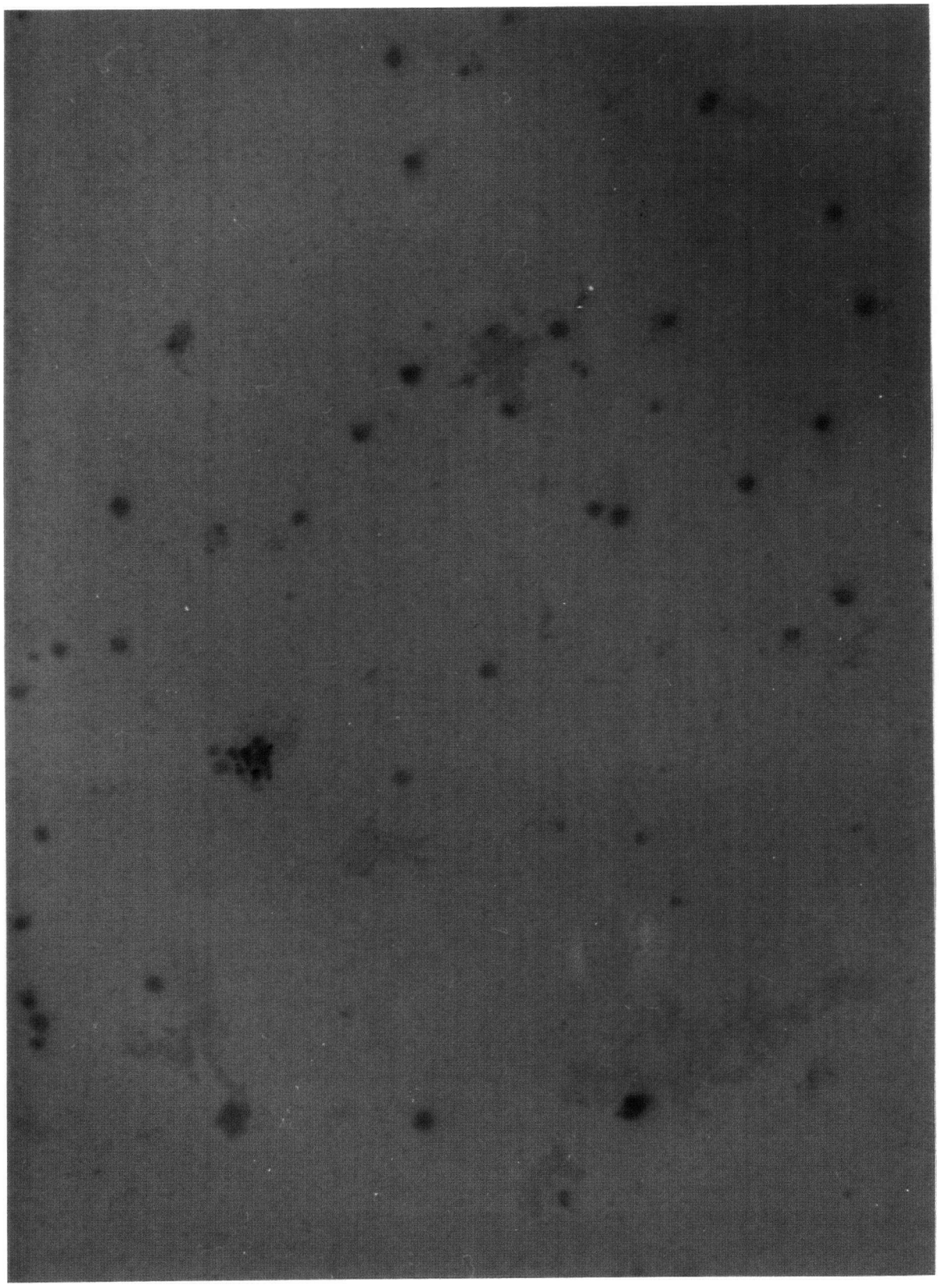

Photograph #134 : Ni sulfide colloids at 30 000* magnification (1mm = 13 nm)

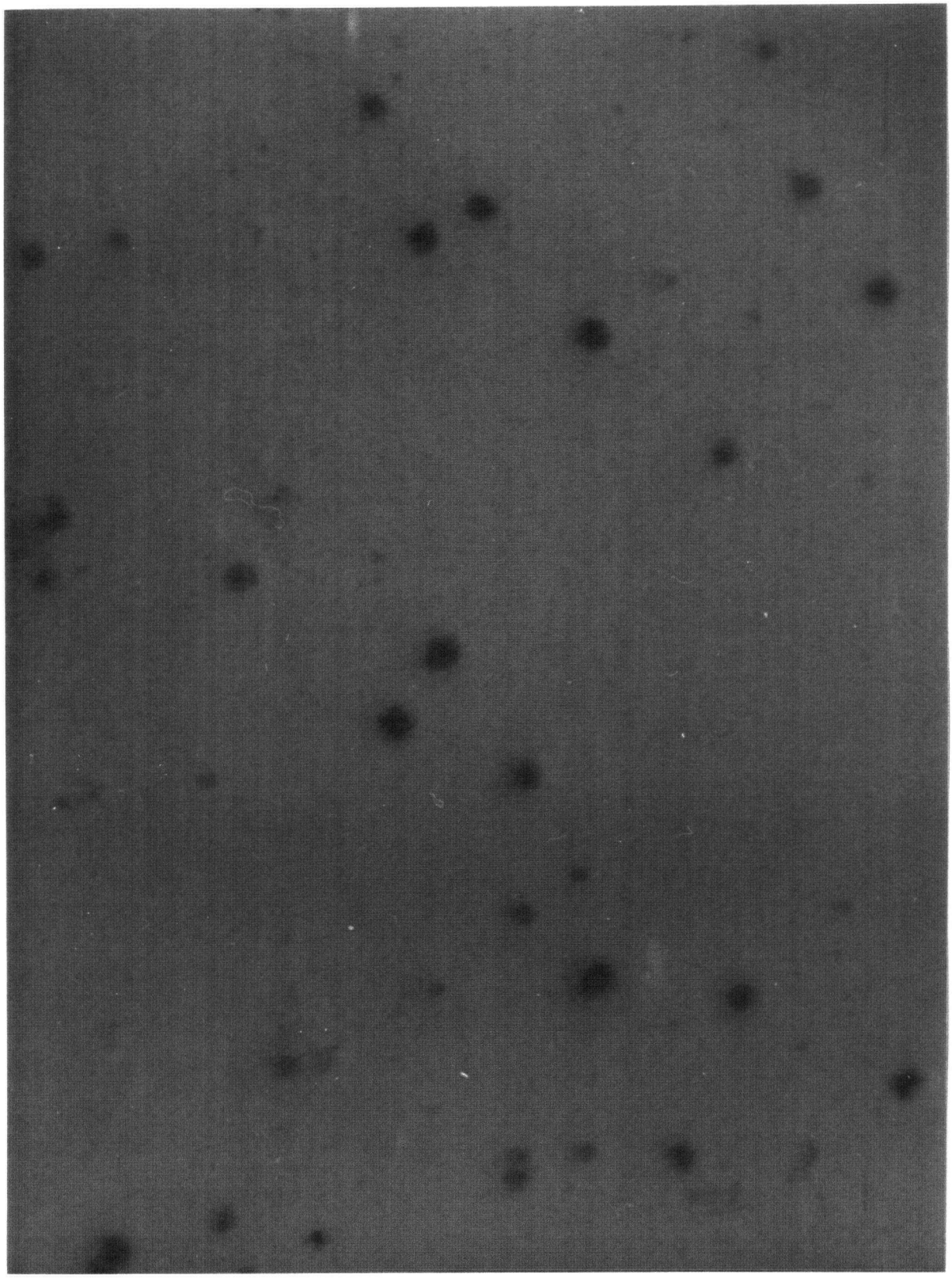

Photograph #138 : Co sulfide colloids at 20 000* magnification (1mm = 20 nm)

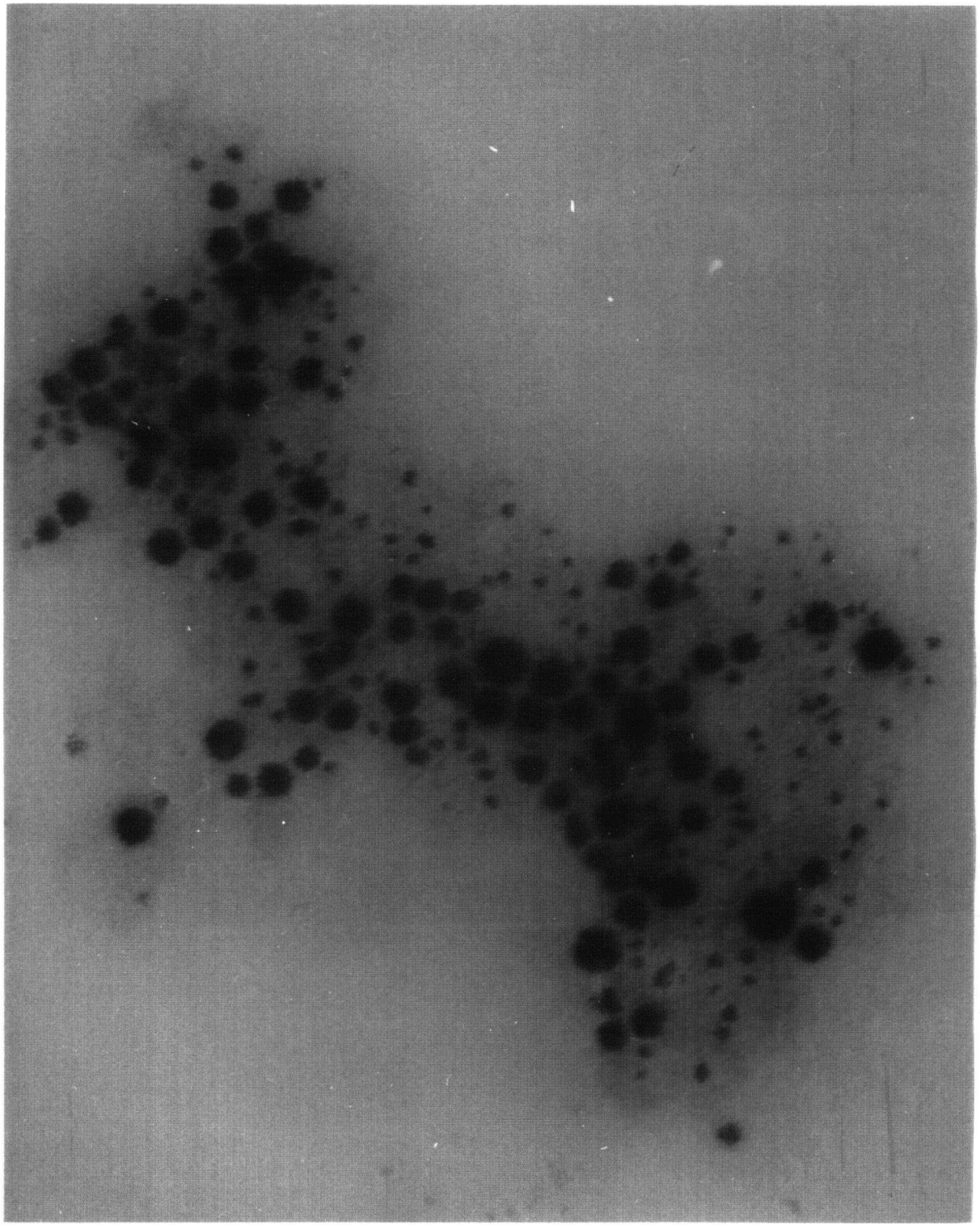

Photograph #139 : Co sulfide colloids at 20 000* magnification (1mm = 20 nm)

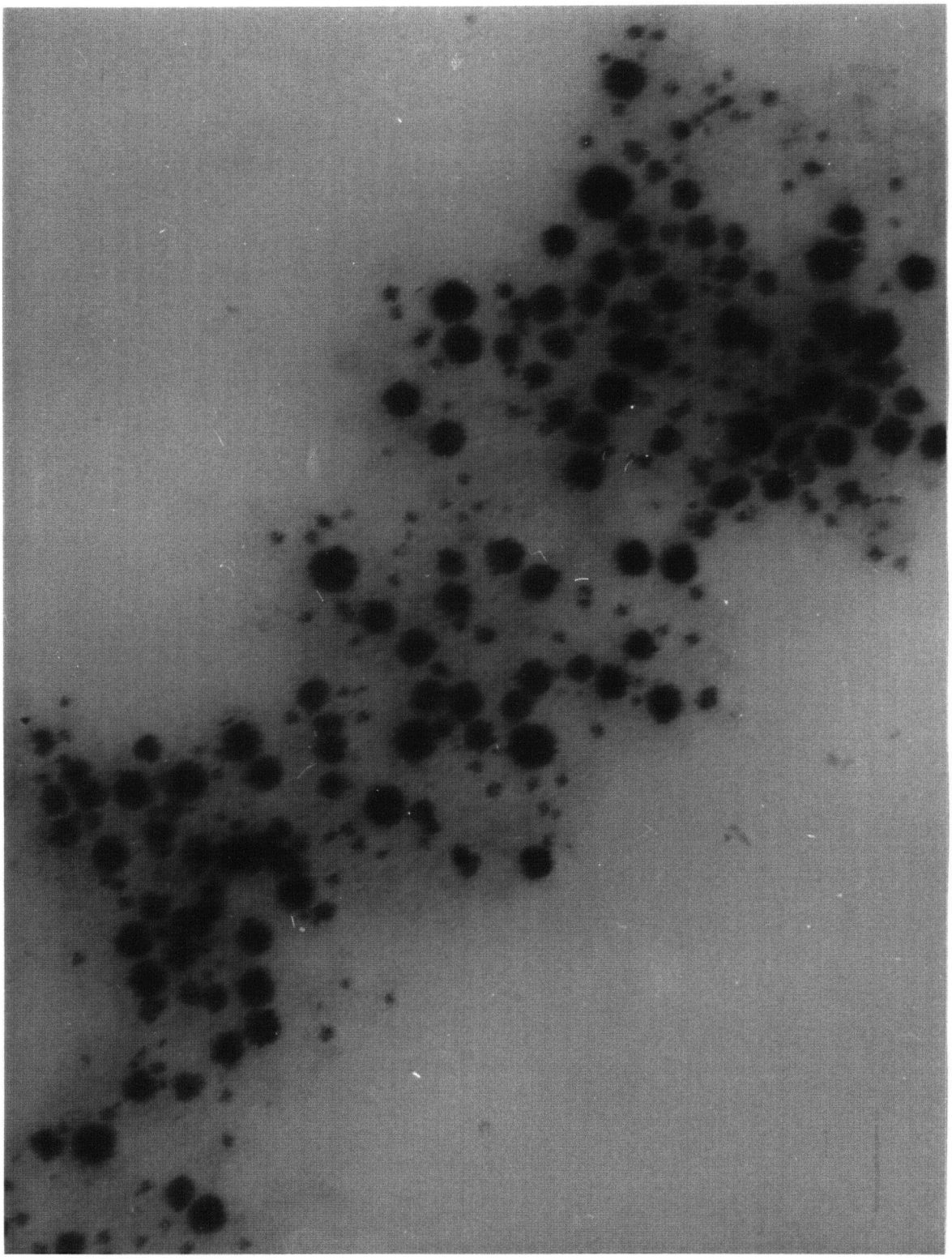

Photograph #141 : Co sulfide colloids at 20 000* magnification (1mm = 20 nm)

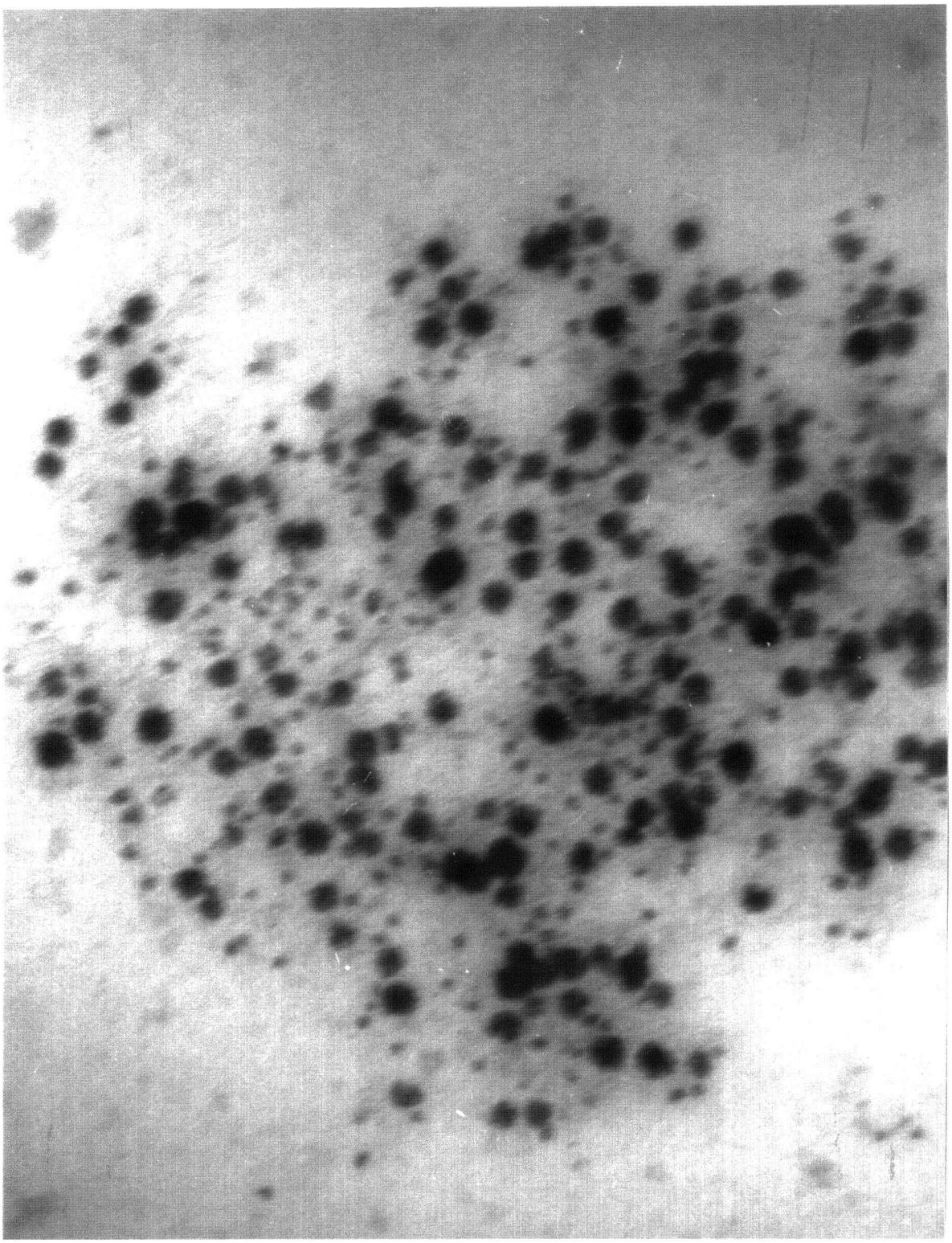

Photograph #142 : Co sulfide colloids at 20 000* magnification (1mm = 20 nm)

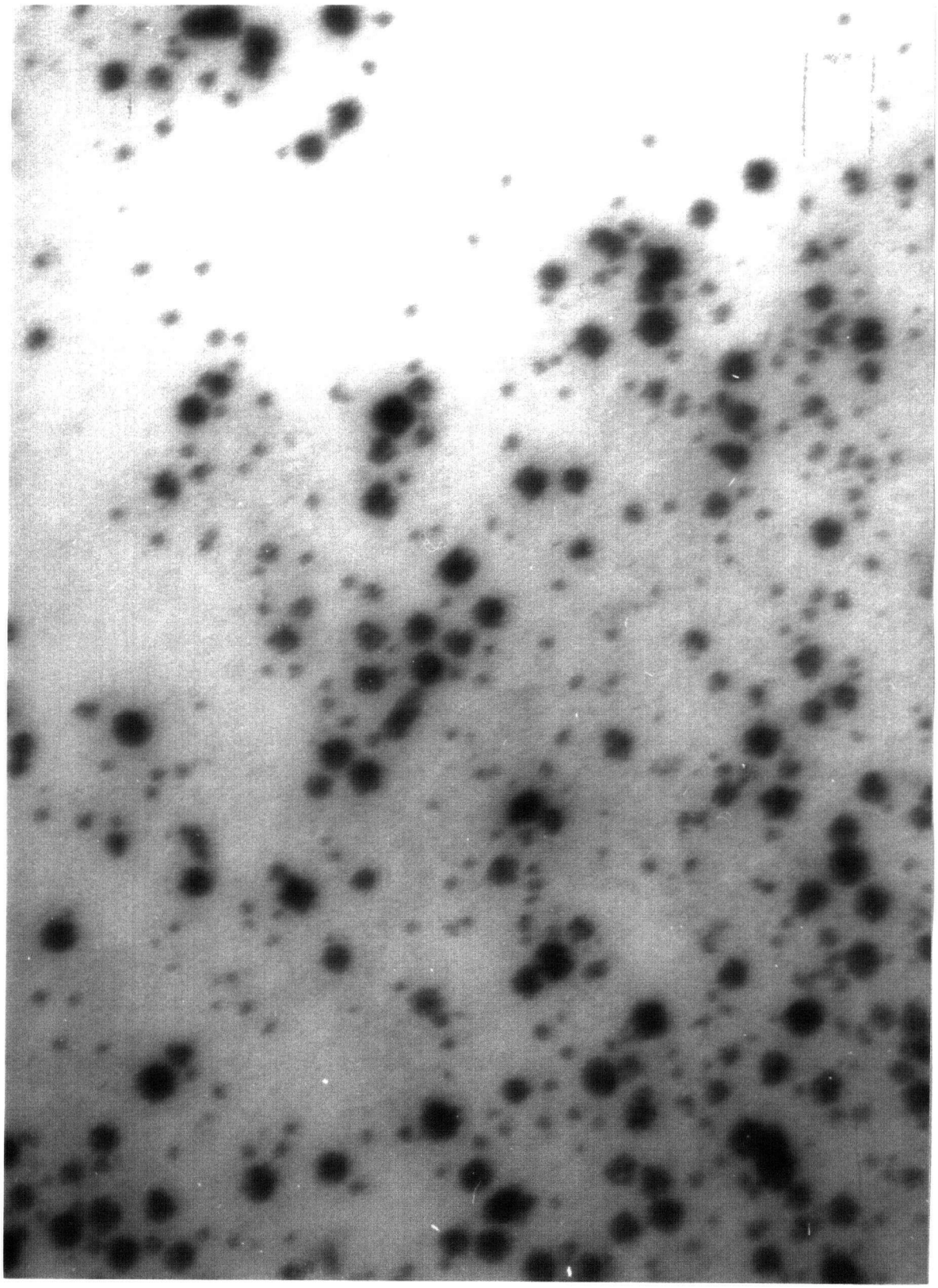

Appendix 2.6 : Explanation of terms used in Table 4.6

The number average particle size $\bar{d}_n$ was calculated as follows:

$$\bar{d}_n = \frac{\Sigma d_i}{n}$$

Where, d_i = diameter of particle i
n = number of particles

The number standard deviation δ_n was calculated as follows:

$$\delta_n = \sqrt{\frac{\Sigma(d_i - \bar{d}_n)^2}{n-1}}$$

The surface areas of the metal sulfide colloids in the photographs were calculated (assuming spherical particles) and the average surface area $\overline{SA}$ was calculated as follows:

$$\overline{SA} = \frac{\Sigma SA_i}{n}$$

Where, SA_i = surface area of particle i

The surface area average particle size $\bar{d}_{SA}$ was calculated from $\overline{SA}$ as follows:

$$\bar{d}_{SA} = \sqrt{\frac{\overline{SA}}{\pi}}$$

Appendix 2.7 : Standard binding energies of various Ni, Co and Fe species

Compound	Metal $2p_{3/2}$	S 2p
ZnS	-	161.7
S_2O_3	-	162.5
Na_2SO_4	-	169.1
FeS	706.7	162.7
FeO	709.6	
Fe_2O_3	710.9	
CoS_2	778.1	162.8
CoO	780.4	
$Co(OH)_2$	781.3	
NiS	853	162.3
NiO	855.9, 861.4	
Ni_2O_3	856	
$NiSO_4$	857.0	169.4

Appendix 2.8 : BET surface area calculations

1. Calculation of Specific Surface Area

Mass of Sample = 0.053 g

Surface Area (adsorption) = 1.33 m^2

Surface Area (desorption) = 1.33 m^2

$\therefore$ Specific Surface Area = 1.33/0.053

= 25 m^2/g

2. Calculation of mean particle size

For Spherical non-porous particles,

$$r \text{ (particle radius)} = \frac{3}{(\text{Specific Surface Area} * \rho)}$$

Assuming spherical non-porous particles of CoS_2 present,

$\rho = 4.26*10^6$ g/m^3

$$\therefore r = \frac{3}{4.26*10^6 \cdot 25}$$

= 28.2 nm

$\therefore$ d = 56.4 nm

Appendix 3

3.1 ASPEN simulation of the reaction system

3.2 Sample calculation of rate constant for activity measurements

3.3 Data for the preliminary activity measurements

3.4 Data for activity measurements with recovered colloids

3.5 GC traces of experiment #19 and decomposition of Co naphthenate

3.6 XRD spectra of the spent catalysts from the second set of activity measurements

Appendix 3.1 : ASPEN simulation of the reaction system

1. Determination of the number of moles of each component at the initial conditions (22 °C, 314 psi):

The system was modeled as a simple mixer, as follows:

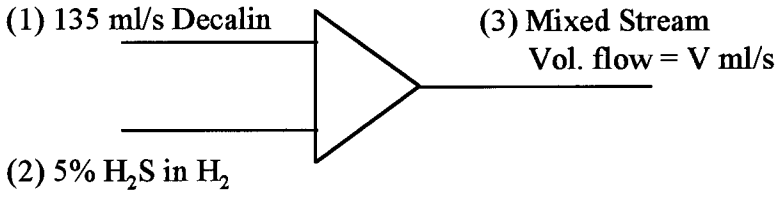

∴ The DESIGN SPEC block of ASPEN was used to adjust the flowrate of stream (2) such that V = 300 ml/s.

∴ The reaction system was : 2.7 kmol/h Decalin

0.54 kmol/h H_2

0.03 kmol/h H_2S

2. The reaction system determined in part 1. above was entered into the FLASH CURVE option of ASPEN at the final reaction temperature T (varied from 390 °C to 410 °C) . The V/L distribution was then determined for a range of pressures. The particular pressure P which resulted in V= 300 ml/s defined the system at temperature T.

Appendix 3.2 : Sample calculation of rate constant for activity measurements

Rate equation for batch reactor:

$$1-x = \exp(-k.\tau)$$

Where, x = Conversion

k = Rate Constant ($cm^3/g/h$)

τ = Space time

$$= \frac{w.t}{v}$$

w = Mass of catalyst (g)

t = Reaction time (h)

v = Liquid volume (cm^3)

$\therefore$ For experiment #8 (Table 5.2),

$v = 135\ cm^3$

$w = 0.076\ g$

$t = 2\ h$

$x = 0.05$ (conversion w.r.t. benzene or toluene)

$$\therefore k = \frac{-\ln(1-0.05)}{\frac{0.076*2}{135}}$$

$$= 49\ cm^3/g/h$$

Appendix 3.3 : Data for preliminary activity measurements

Experiment #8

Summary:	Co Microemulsion cracking of DPM	
	Sulphiding Time @ 1000 psig	2 h
	Reaction Time	2 h
	Reaction Temperature	430 °C
	Total Volume	135 ml

1. Reactor Charge :	120 ml	Unreduced Co/PELE/Decalin.
	15 ml	Diphenylmethane
	300 psig IP	5% H_2S in H_2

2. Reactor Preparation:
2.1. Reactor and internals cleaned with soap and water, rinsed with water
2.2. Reactor and internals scoured with 'Brasso'
2.3. Reactor rinsed with hexane (2 hours with stirring)

3. Nitrogen Purging: Reactor purged with N_2 before and after run.

4. Catalyst Synthesis: Reactor charge including DPM presulphided in 5% H_2S/H_2 for 2 hours. (with stirring)

5. Reaction Profiles:

Time to reach 430 °C	90.5 min
Air cooling time 430 °C to 250 °C	24 min
Water cooling Time 250 °C to 15 °C	- min
Total Reaction Time	- min

Time (min)	Temp. (°C)	Furnace Temp	Pressure (psig)	Stirring (rpm)
0	18	18	300	996
11	79	99	400	1000
20	124	148	450	996
30	174	193	460	991
40	225	240	500	993
50	274	288	550	994
60	324	338	650	996
70	373	395	800	996
80	409	454	1180	996
90	428	492	1490	990
90.5	430	493	1500	990
210	430	444	1700	
215	392		1350	
220	345		1150	
225	300		1000	
230	277		900	
234	250			

6. GC Results:

Calibration Curves : # Moles of component i in 1 μl = m*(Area of component i) + c

	m	c
Benzene	2.09E-13	3.23E-9
Toluene	1.99E-13	2.47E-9
DPM	8.91E-14	4.37E-8

Reaction Product

Injection #	Component	Area	Moles in 1 ml
1	Benzene	99697	2.41E-08
	Toluene	158632	3.40E-08
	DPM	6257603	6.01E-07
	Decalin	38845118	
2	Benzene	103546	2.49E-08
	Toluene	165933	3.55E-08
	DPM	6439298	6.17E-07
	Decalin	39988426	
3	Benzene	102189	2.46E-08
	Toluene	164479	3.52E-08
	DPM	6302058	6.05E-07
	Decalin	39258855	

Conversions based on Injections #1, #2 and #3

# moles of DPM before cracking	6.61E-07
Average # moles of DPM after cracking	6.08E-07
Average # moles of Benzene after cracking	2.45E-08
Average # moles of Toluene after cracking	3.49E-08
DPM Conversion based on DPM balance	8
DPM Conversion based on Toluene formed	5.3

Experiment #9

Summary:	Co Microemulsion cracking of DPM	
	Sulphiding Time @ 1000 psig	6 h
	Reaction Time	2 h
	Reaction Temperature	430 °C
	Total Volume	135 ml

1. Reactor Charge :	120 ml	Unreduced Co/PELE/Decalin
	15 ml	Diphenylmethane
	320 psig IP	5% H_2S in H_2

2. Reactor Preparation:
2.1. Reactor and internals cleaned with soap and water, rinsed with water
2.2. Reactor and internals scoured with 'Brasso'
2.3. Reactor rinsed with hexane (2 hours with stirring)

3. Nitrogen Purging: Reactor purged with N_2 before and after run.

4. Catalyst Synthesis: Reactor charge including DPM presulphided in 5% H_2S/H_2 for 6 hours.

5. Reaction Profiles:

Time to reach 430 °C	90 min
Air cooling time 430 °C to 250 °C	25 min
Water cooling Time 250 °C to 15 °C	30 min
Total Reaction Time	265 min

Time (min)	Temp. (°C)	Furnace Temp	Pressure (psig)	rpm Stirring
0	21	22	320	1007
10	76	98	400	1017
20	124	151	450	1011
30	177	197	460	1012
40	226	242	500	1008
50	276	290	550	1007
60	326	340	625	1004
70	375	398	775	1005
80	411	463	1150	1004
90	430	490	1450	1015
210	430	445	1525	1007
215	381		1200	
220	325		960	
225	303		900	
230	272		800	
235	250		750	
240	70		400	
245	37		350	
255	23		340	
265	14		300	

6. GC Results:

Calibration Curves : # Moles of component i in 1 μl = m*(Area of component i) + c

	m	c
Benzene	2.09E-13	3.23E-9
Toluene	1.99E-13	2.47E-9
DPM	8.91E-14	4.37E-8

Reaction Product

Injection #	Component	Area	Moles in 1 ml
1	Benzene	105059	2.52E-08
	Toluene	169433	3.62E-08
	DPM	6403035	6.14E-07
	Decalin	39772695	
2	Benzene	105670	2.53E-08
	Toluene	169502	3.62E-08
	DPM	6370335	6.11E-07
	Decalin	39441154	
3	Benzene	105224	2.52E-08
	Toluene	168940	3.61E-08
	DPM	6311489	6.06E-07
	Decalin	38906733	

Conversions based on Injections #1, #2 and #3

# moles of DPM before cracking	6.61E-07
Average # moles of DPM after cracking	6.11E-07
Average # moles of Benzene after cracking	2.52E-08
Average # moles of Toluene after cracking	3.62E-08
DPM Conversion based on DPM balance	7.7
DPM Conversion based on Toluene formed	5.5

Experiment #11

Summary:	Thermal Cracking with Blank Microemulsion	
	Sulphiding Time @ 1000 psig	2 h
	Reaction Time	2 h
	Reaction Temperature	430 °C
	Total Volume	135 ml

1. Reactor Charge :	120 ml	Water/PELE/Decalin
	15.015 g	DPM
	335 psig IP	5% H_2S in H_2

2. Reactor Preparation:
2.1. Reactor and internals cleaned with soap and water, rinsed with water
2.2. Reactor and internals scoured with 'Brasso'
2.3. Reactor rinsed with hexane (2 hours with stirring)

3. Nitrogen Purging: Reactor purged with N_2 before and after run.

4. A311Presulphiding: Reactor charge including DPM presulphided in 5% H_2S/H_2 for 2 hours

5. Reaction Profiles:

Time to reach 430 °C	91.5 min
Air cooling time 430 °C to 250 °C	20 min
Water cooling Time 250 °C to 15 °C	8 min
Total Reaction Time	- min

Time (min)	Temp. (°C)	Furnace Temp	Pressure (psig)	rpm Stirring
0	24	24	335	1004
10	75	95	400	1010
21.5	132	156	460	1009
30	175	195	500	1010
40	225	242	510	1008
50	275	288	600	1004
60	325	337	700	1003
70	374	393	870	1000
80	410	460	1300	997
90	426	488	1600	999
91.5	430	490	1640	993
160	430	443	1550	1019
211.5	430	449	1550	995
221.5	326		1040	
226.5	291		920	
231.5	262		850	
233.5	250		840	
236.5	110		530	
238.5	51		450	
241.5	30		410	
End	20		400	

6. GC Results:

Calibration Curves : # Moles of component i in 1 μl = m*(Area of component i) + c

	m	c
Benzene	2.09E-13	3.23E-9
Toluene	1.99E-13	2.47E-9
DPM	8.91E-14	4.37E-8

Reactor Feed

Injection #	Component	Retention Time	Area	Moles in 1 ml
1	Decalin	5.323	41520945	
	Surfactant	7.291	90352	
	DPM	8.07	6593892	6.31E-07
2	Decalin	5.312	40063288	
	Surfactant	7.325	76382	
	DPM	8.057	6340212	6.09E-07
3	Decalin	5.337	43820740	
	Surfactant	7.317	92634	
	DPM	8.084	7047160	6.72E-07

Reaction Product

Injection #	Component	Area	Moles in 1 ml
1	Benzene	100391	2.42E-08
	Toluene	154417	3.32E-08
	DPM	5882786	5.68E-07
	Decalin	36157816	
2	Benzene	109730	2.62E-08
	Toluene	169529	3.62E-08
	DPM	6467442	6.20E-07
	Decalin	39582279	
3	Benzene	96909	2.35E-08
	Toluene	149876	3.23E-08
	DPM	5737077	5.55E-07
	Decalin	35757466	

Conversions based on Injections #1and #3

# moles of DPM before cracking (from GC)	6.37E-07
Average # moles of DPM after cracking	5.61E-07
Average # moles of Benzene after cracking	2.39E-08
Average # moles of Toluene after cracking	3.28E-08
DPM Conversion based on GC results	11.9
DPM Conversion based on Toluene formed	5.1

Experiment #13

Summary:	Fe Microemulsion cracking of DPM	
	Sulphiding Time	6 h
	Reaction Time	2 h
	Reaction Temperature	430 °C
	Total Volume	135 ml

1. Reactor Charge :	120 ml	Unreduced Fe/PELE/Decalin
	15.015 g	DPM
	300 psig IP	5% H_2S in H_2

2. Reactor Preparation:
2.1. Reactor and internals cleaned with soap and water, rinsed with water
2.2. Reactor and internals scoured with 'Brasso'
2.3. Reactor rinsed with hexane (2 hours with stirring)

3. Nitrogen Purging: Reactor purged with N_2 before and after run.

4. Catalyst Synthesis: Reactor charge including DPM presulphided in 5% H_2S/H_2 for 6 hours (with stirring)

5. Reaction Profiles:

Time to reach 430 °C	90 min
Air cooling time 430 °C to 250 °C	20 min
Water cooling Time 250 °C to 15 °C	min
Total Reaction Time	- min

Time (min)	Temp. (°C)	Furnace Temp	Pressure (psig)	rpm Stirring
0	21	22	300	1005
10	77	101	400	1005
20	133	165	450	
30	183	207	480	
40	234	255	510	
50	283	299	590	
60	333	349	690	
70	382	410	890	
80	412	466	1300	
90	430	487	1600	
102	431	461	1660	
135	430	457	1700	
150	430	457	1700	
180	430	458	1710	
210	430	458	1750	
215	377		1300	
220	344		1150	
225	297		1010	
230	263		950	
235	90		500	

6. GC Results:

Calibration Curves : # Moles of component i in 1 μl = m*(Area of component i) + c

	m	c
Benzene	2.09E-13	3.23E-9
Toluene	1.99E-13	2.47E-9
DPM	8.91E-14	4.37E-8

Reaction Product

Injection #	Component	Area	Moles in 1 ml
1	Benzene	61035	1.60E-08
	Toluene	121334	2.66E-08
	DPM	5992375	5.78E-07
	Decalin	37445883	
2	Benzene	57518	1.53E-08
	Toluene	117148	2.58E-08
	DPM	5754914	5.57E-07
	Decalin	36228767	
3	Benzene	60292	1.58E-08
	Toluene	122260	2.68E-08
	DPM	6020792	5.80E-07
	Decalin	37672308	

Conversions based on Injections #1and #3

# moles of DPM before cracking (from mass)	6.61E-07
Average # moles of DPM after cracking	5.79E-07
Average # moles of Benzene after cracking	1.59E-08
Average # moles of Toluene after cracking	2.67E-08
DPM Conversion based on DPM balance	12.4
DPM Conversion based on Toluene formed	4

Experiment #14

Summary: Fe Microemulsion cracking of DPM with extra Sulphur added

Sulphiding Time	6 h
Reaction Time	2 h
Reaction Temperature	430 °C
Total Volume	135 ml

1. Reactor Charge :

120 ml	Unreduced Fe/PELE/Decalin
15.015 g	DPM
300 psig IP	5% H_2S in H_2
0.173 g	Elemental Sulphur (4:1 molar ratio S:Fe)

2. Reactor Preparation:
2.1. Reactor and internals cleaned with soap and water, rinsed with water
2.2. Reactor and internals scoured with 'Brasso'
2.3. Reactor rinsed with hexane (2 hours with stirring)

3. Nitrogen Purging: Reactor purged with N_2 before and after run.

4. Catalyst Synthesis: Reactor charge including DPM presulphided in 5% H_2S/H_2 for 6 hours (with stirring)

5. Reaction Profiles:

Time to reach 430 °C	91 min
Air cooling time 430 °C to 250 °C	24 min
Water cooling Time 250 °C to 15 °C	15 min
Total Reaction Time	- min

Time (min)	Temp. (°C)	Furnace Temp	Pressure (psig)	rpm Stirring
0	25	25	300	1005
10	79	100	350	
20	129	151	400	
30	179	196	440	
40	229	242	480	
50	279	288	510	
60	329	338	600	
70	378	393	800	
80	411	455	1200	
90	425	478	1450	
91	430	478	1450	
211	430	451	1650	
220	339		1100	
225	301		1000	
230	272		900	
235	250		850	
240	72		450	
245	37		400	
250	25		380	

6. GC Results:

Calibration Curves : # Moles of component i in 1 μl = m*(Area of component i) + c

	m	c
Benzene	2.09E-13	3.23E-9
Toluene	1.99E-13	2.47E-9
DPM	8.91E-14	4.37E-8

Reaction Product

Injection #	Component	Area	Moles in 1 ml
1	Benzene	82239	2.04E-08
	Toluene	135553	2.95E-08
	DPM	6363651	6.11E-07
	Decalin	39000863	
2	Benzene	74722	1.89E-08
	Toluene	121175	2.66E-08
	DPM	5735454	5.55E-07
	Decalin	35766537	
3	Benzene	80570	2.01E-08
	Toluene	129503	2.82E-08
	DPM	6176983	5.94E-07
	Decalin	38077492	

Conversions based on Injections #1and #3

# moles of DPM before cracking (from mass)	6.61E-07
Average # moles of DPM after cracking	6.02E-07
Average # moles of Benzene after cracking	2.02E-08
Average # moles of Toluene after cracking	2.88E-08
DPM Conversion based on DPM balance	8.9
DPM Conversion based on Toluene formed	4.4

Appendix 3.4 : Data from activity measurements with recovered colloids

Experiment #15

Summary:	Thermal Cracking	
	Sulphiding Time	0 h
	Reaction Time	3 h
	Reaction Temperature	400 °C
	Total Volume	135 ml

1. Reactor Charge :	130 ml	Reactant Mixture	(120 ml Decalin, 15.015g DPM)
	340 psig IP	5% H_2S in H_2	

2. Reactor Preparation:
2.1. Reactor /internals cleaned with soap and water, then rinsed
2.2. Reactor and internals scoured with 'Brasso'
2.3. Reactor rinsed with hexane (2 hours with stirring)

3. Nitrogen Purging: Reactor purged with N_2 before and after run.

4. Pressure Testing: Reactor pressure tested @ 1000 psig for 30 min
No obvoius leaks / pressure decrease

5. Reaction Profiles:

Time to reach 400 °C	77 min
Air cooling time 400 °C to 250 °C	20 min
Water cooling Time 250 °C to 15 °C	31 min
Total Reaction Time	180 min
Pressure Rise @ 400 °C	50 psi
Overall Pressure Rise	0 psi

Time (min)	Temp. (°C)	Pressure (psig)	rpm Stirring	Notes
0	22	340	700	
10	80	390	712	
25	147	450	698	
35	194	500	693	
45	250	540	700	
55	295	600	710	
75	390	850	700	
77	400	910	701	Reaction Temp.
90	400	940	708	
257	400	960	710	Air Cooling Started
267	315	725	720	
277	250	600	723	Water Cooling Started
282	71	400	718	
387	37	360	719	
308	18	340	-	Water Cooling Stopped

6. GC Results:

Reactor Feed Sample:

	1	2	3	Average
C10	985545	1019525	1024387	1009819
Decalin	36119681	36550496	36510708	36393628
DPM	5415974	5391745	5418128	5408616
A_{DPM}/A_{C10}	5.495	5.288	5.289	5.358
$A_{DECALIN}/A_{C10}$	36.649	35.851	35.642	36.047

Reaction Product:

	1	2	3	Average
Benzene	14254	13508	13130	13631
Toluene	19028	17916	18073	18339
C10	965336	915797	917725	932953
Decalin	35393582	34246205	34236266	34625351
DPM	5392734	5176039	5189307	5252693
$A_{BENZENE}/A_{C10}$	0.015	0.015	0.014	0.015
$A_{TOLUENE}/A_{C10}$	0.02	0.02	0.02	0.02
A_{DPM}/A_{C10}	5.586	5.652	5.655	5.631
$A_{DECALIN}/A_{C10}$	36.665	37.395	37.306	37.122

7. GC Analysis:

Calibration Curves: $Mi/MC10 = (1/m)*Ai/AC10 - c/m$

	m	c
Benzene	0.5931	-0.0032
Toulene	0.6971	-0.0057
DPM	1.4872	-0.8807

	Feed Sample	Reactor Feed	Reactor Product
Vol. C10 (ml)	0.139		3.611
Moles C10	0.00071		0.01853
Moles Benzene			0.00056
Moles Toulene			0.00067
Moles DPM by GC	0.00299	0.08626	0.08112
Theoretical Moles DPM	0.00331	0.08595	
% Conversion (Benz. ref.)	0.6		
% Conversion (Tol. ref.)	0.8		
% Conversion (DPM ref.)	6		

Experiment #16

Summary: $Fe(CO)_5$ Cracking @ 1000 ppm Fe

Sulphiding Time @ 1000 psig	2 h
Reaction Time	3 h
Reaction Temperature	400 °C
Total Volume	135 ml

1. Reactor Charge :

130 ml	Reactant Mixture	(120 ml Decalin, 15.015g DPM)
325 psig IP	5% H_2S in H_2	
254 µl	$Fe(CO)_5$	

2. Reactor Preparation:
2.1. Reactor /internals cleaned with soap and water, then rinsed
2.2. Reactor and internals scoured with 'Brasso'
2.3. Reactor rinsed with hexane (2 hours with stirring)

3. Nitrogen Purging: Reactor purged with N_2 before and after run.

4. Pressure Testing: Reactor pressure tested @ 1000 psig for 2 h during Sulphiding
Small pressure decrease (1000 - 975 psig)

5. Reaction Profiles:

Time to reach 400 °C	78 min
Air cooling time 400 °C to 250 °C	17 min
Water cooling Time 250 °C to 15 °C	20 min
Total Reaction Time	180 min
Pressure Rise @ 400 °C	50 psi
Overall Pressure Rise	25 psi

Time (min)	Temp. (°C)	Pressure (psig)	rpm Stirring	Notes
0	23	325	721	
10	68	360	723	
21	122	426	718	
30	163	460	714	
40	213	500	714	
50	263	540	711	
60	314	650	715	
70	364	790	709	
78	400	950	712	Reaction Temp.
258	400	1000	715	Air Cooling Started
263	339	800	722	
268	293	700	726	
273	262	650	727	
275	250	640	726	Water Cooling Started
295	18	350	-	Water Cooling Stopped

6. GC Results:

Reactor Feed Sample:

	1	2	3	Average
C10	1038115	1074322	1049790	1054076
Decalin	39492939	39276443	38779450	39182944
DPM	5690263	5677645	5642867	5670258
A_{DPM}/A_{C10}	5.481	5.285	5.375	5.38
$A_{DECALIN}/A_{C10}$	38.043	36.559	36.94	37.181

Reaction Product:

	1	2	3	Average
Benzene	14311	13998	13909	14073
Toluene	16159	18386	17164	17236
C10	1039945	1021124	1014252	1025107
Decalin	38299378	38203249	37893746	38132124
DPM	5593604	5663763	5681375	5646247
$A_{BENZENE}/A_{C10}$	0.014	0.014	0.014	0.014
$A_{TOLUENE}/A_{C10}$	0.016	0.018	0.017	0.017
A_{DPM}/A_{C10}	5.379	5.547	5.602	5.509
$A_{DECALIN}/A_{C10}$	36.828	37.413	37.361	37.201

7. GC Analysis:

Calibration Curves: $Mi/MC10 = (1/m)*Ai/AC10 - c/m$

	m	c
Benzene	0.5931	-0.0032
Toulene	0.6971	-0.0057
DPM	1.4872	-0.8807

	Feed Sample	Reactor Feed	Reactor Product
Vol. C10 (ml)	0.139		3.661
Moles C10	0.00071		0.01878
Moles Benzene			0.00054
Moles Toulene			0.00061
Moles DPM by GC	0.003	0.08625	0.0807
Theoretical Moles DPM	0.00331	0.08595	
% Conversion (Benz. ref.)	0.6		
% Conversion (Tol. ref.)	0.7		
% Conversion (DPM ref.)	6.4		

Experiment #17

Summary:	Recovered NiS Cracking @ 655 ppm Ni	
	Sulphiding Time @ 1000 psig	2 h
	Reaction Time	3 h
	Reaction Temperature	400 °C
	Total Volume	135 ml

1. Reactor Charge :	130 ml	Reactant Mixture	(120 ml Decalin, 15.015g DPM)
	300 psig IP	5% H_2S in H_2	
	0.3481 g	Recovered NiS	

2. Reactor Preparation:
2.1. Reactor /internals cleaned with soap and water, then rinsed
2.2. Reactor and internals scoured with 'Brasso'
2.3. Reactor rinsed with hexane (2 hours with stirring)

3. Nitrogen Purging: Reactor purged with N_2 before and after run.

4. Pressure Testing: Reactor pressure tested @ 1000 psig for 2 h during Sulphiding
No pressure decrease observed

5. Reaction Profiles:

Time to reach 400 °C	77 min
Air cooling time 400 °C to 250 °C	20 min
Water cooling Time 250 °C to 15 °C	13 min
Total Reaction Time	180 min
Pressure Rise @ 400 °C	40 psi
Overall Pressure Rise	40 psi

Time (min)	Temp. (°C)	Pressure (psig)	rpm Stirring	Notes
0	22	300	722	
10	68	350	721	
20	117	400	722	
32	180	450	723	
40	218	490	721	
50	265	540	721	
60	315	600	721	
70	365	740	720	
77	400	920	718	Reaction Temp.
257	400	960	723	Air Cooling Started
262	356	800	731	
267	312	700	735	
272	275	640	737	
277	250	600	735	Water Cooling Started
290	32	340	-	Water Cooling Stopped

6. GC Results:

Reactor Feed Sample:

	1	2	3	Average
C10	1056615	1046479	1098626	1067240
Decalin	37247151	37233793	38357069	37612671
DPM	5596447	5705342	5803819	5701869
A_{DPM}/A_{C10}	5.297	5.452	5.283	5.344
$A_{DECALIN}/A_{C10}$	35.251	35.58	34.914	35.248

Reaction Product:

	1	2	3	Average
Benzene	8400	8856	8071	8442
Toluene	13413	14400	13481	13765
C10	946416	979846	1041281	989181
Decalin	34550790	35024041	36344210	35306347
DPM	5202088	5259779	5622184	5361350
$A_{BENZENE}/A_{C10}$	0.009	0.009	0.008	0.009
$A_{TOLUENE}/A_{C10}$	0.014	0.015	0.013	0.014
A_{DPM}/A_{C10}	5.497	5.368	5.399	5.421
$A_{DECALIN}/A_{C10}$	36.507	35.744	34.903	35.718

7. GC Analysis:

Calibration Curves: $Mi/MC10 = (1/m)*Ai/AC10 - c/m$

	m	c
Benzene	0.5931	-0.0032
Toulene	0.6971	-0.0057
DPM	1.4872	-0.8807

	Feed Sample	Reactor Feed	Reactor Product
Vol. C10 (ml)	0.139		3.611
Moles C10	0.00071		0.01853
Moles Benzene			0.00037
Moles Toulene			0.00052
Moles DPM by GC	0.00298	0.08627	0.07851
Theoretical Moles DPM	0.00331	0.08595	
% Conversion (Benz. ref.)	0.4		
% Conversion (Tol. ref.)	0.6		
% Conversion (DPM ref.)	9		

Experiment #18

Summary: $Fe(CO)_5$ @ 1000 ppm Fe (Repeat of Experiment #16)

Sulphiding Time @ 1000 psig	2 h
Reaction Time	3 h
Reaction Temperature	400 °C
Total Volume	135 ml

1. Reactor Charge :

130 ml	Reactant Mixture	(120 ml Decalin, 15.015g DPM)
340 psig IP	5% H_2S in H_2	
275 µl	$Fe(CO)_5$	

2. Reactor Preparation:
   2.1. Reactor /internals cleaned with soap and water, then rinsed
   2.2. Reactor and internals scoured with 'Brasso'
   2.3. Reactor rinsed with hexane (2 hours with stirring)

3. Nitrogen Purging: Reactor purged with N_2 before and after run.

4. Pressure Testing: Pressure tested @ 1000 psig for during sulphiding
   No pressure decrease observed

5. Reaction Profiles:

Time to reach 400 °C	77 min
Air cooling time 400 °C to 250 °C	17 min
Water cooling Time 250 °C to 15 °C	18 min
Total Reaction Time	180 min
Pressure Rise @ 400 °C	50 psi
Overall Pressure Rise	0 psi

Time (min)	Temp. (°C)	Pressure (psig)	rpm Stirring	Notes
0	20	340	709	
10	69	400	702	
20	116	450	701	
30	165	490	700	
40	216	550	701	
50	266	600	700	
60	315	690	697	
70	365	810	699	
77	400	990	699	Reaction Temp.
257	400	1040	702	Air Cooling Started
262	339	850	711	
267	297	760	711	
272	262	600	710	
274	250			Water Cooling Started
277	125	500	707	
282	60	430	707	
292	20	340	-	Water Cooling Stopped

6. GC Results:

Reactor Feed Sample:

	1	2	3	Average
C10	739232	895610	815900	816914
Decalin	33073940	38068173	34572937	35238350
DPM	4982167	5768849	5056495	5269170
A_{DPM}/A_{C10}	6.74	6.441	6.197	6.459
$A_{DECALIN}/A_{C10}$	44.741	42.505	42.374	43.207

Reaction Product:

	1	2	3	Average
Benzene	19598	18400	17520	18506
Toluene	21797	20671	21289	21252
C10	788787	758817	713411	753672
Decalin	28017178	27054419	25764932	26945510
DPM	4580654	4297111	4118708	4332158
$A_{BENZENE}/A_{C10}$	0.025	0.024	0.025	0.025
$A_{TOLUENE}/A_{C10}$	0.028	0.027	0.03	0.028
A_{DPM}/A_{C10}	5.807	5.663	5.773	5.748
$A_{DECALIN}/A_{C10}$	35.519	35.653	36.115	35.763

7. GC Analysis:

Calibration Curves: $Mi/MC10 = (1/m)*Ai/AC10 - c/m$

	m	c
Benzene	0.5931	-0.0032
Toulene	0.6971	-0.0057
DPM	1.4872	-0.8807

	Feed Sample	Reactor Feed	Reactor Product
Vol. C10 (ml)	0.139		3.611
Moles C10	0.00071		0.01853
Moles Benzene			0.00087
Moles Toulene			0.0009
Moles DPM by GC	0.00352	0.08573	0.08258
Theoretical Moles DPM	0.00331	0.08595	
% Conversion (Benz. ref.)	1		
% Conversion (Tol. ref.)	1.1		
% Conversion (DPM ref.)	3.7		

Experiment #19

Summary:	Cobalt Naphthenate @1000ppm Co	
	Sulphiding Time @ 1000 psig	2 h
	Reaction Time	3 h
	Reaction Temperature	400 °C
	Total Volume	135 ml

1. Reactor Charge :	130 ml	Reactant Mixture	(120 ml Decalin, 15.015g DPM)
	340 psig IP	5% H_2S in H_2	
	1.475 g	Cobalt Naphthenate (8% Co)	

2. Reactor Preparation:
2.1. Reactor /internals cleaned with soap and water, then rinsed
2.2. Reactor and internals scoured with 'Brasso'
2.3. Reactor rinsed with hexane (2 hours with stirring)

3. Nitrogen Purging: Reactor purged with N_2 before and after run.

4. Pressure Testing: Reactor pressure tested @ 1000 psig for 2 h during Sulphiding
No pressure decrease observed

5. Reaction Profiles:

Time to reach 400 °C	77 min
Air cooling time 400 °C to 250 °C	18 min
Water cooling Time 250 °C to 15 °C	17 min
Total Reaction Time	180 min
Pressure Rise @ 400 °C	150 psi
Overall Pressure Rise	50 psi

Time (min)	Temp. (C)	Pressure (psig)	rpm Stirring	Notes
0	20	340	716	
10	68	390	713	
20	113	440	709	
30	164	460	706	
40	214	500	719	
50	265	550	719	
60	314	640	719	
70	364	790	716	
77	400	950	719	Reaction Temp.
257	400	1100	721	Air Cooling Started
262	344	900	724	
267	298	800	724	
272	267	740	725	
275	250	700	724	Water Cooling Started
277	131	500	728	
292	18	390	728	Water Cooling Stopped

6. GC Results:

Reactor Feed Sample:

	1	2	3	Average
C10	868359	863831	840645	857612
Decalin	37992928	38119872	37226146	37779649
DPM	5782060	5864828	5725924	5790937
A_{DPM}/A_{C10}	6.659	6.789	6.811	6.753
$A_{DECALIN}/A_{C10}$	43.753	44.129	44.283	44.055

Reaction Product:

	1	2	3	Average
Benzene	308662	315151	297559	307124
Toluene	358091	365047	342429	355189
C10	778496	793545	750393	774145
Decalin	28290020	28735905	27415395	28147107
DPM	3883433	3941921	3759559	3861638
$A_{BENZENE}/A_{C10}$	0.396	0.397	0.397	0.397
$A_{TOLUENE}/A_{C10}$	0.46	0.46	0.456	0.459
A_{DPM}/A_{C10}	4.988	4.967	5.01	4.989
$A_{DECALIN}/A_{C10}$	36.339	36.212	36.535	36.362

7. GC Analysis:

Calibration Curves: Mi/MC10 = (1/m)*Ai/AC10 - c/m

	m	c
Benzene	0.5931	-0.0032
Toulene	0.6971	-0.0057
DPM	1.4872	-0.8807

	Feed Sample	Reactor Feed	Reactor Product
Vol. C10 (ml)	0.139		3.611
Moles C10	0.00071		0.01853
Moles Benzene			0.01249
Moles Toulene			0.01234
Moles DPM by GC	0.00366	0.08559	0.07312
Theoretical Moles DPM	0.00331	0.08595	
% Conversion (Benz. ref.)	14.6		
% Conversion (Tol. ref.)	14.4		
% Conversion (DPM ref.)	14.6		

Experiment #20

Summary:	Recovered CoS_2 @ 1000 ppm Co	
	Sulphiding Time @ 1000 psig	2 h
	Reaction Time	3 h
	Reaction Temperature	400 °C
	Total Volume	135 ml

1. Reactor Charge :	130 ml	Reactant Mixture	(120 ml Decalin, 15.015g DPM)
	360 psig IP	5% H_2S in H_2	
	0.523 g	Recovered CoS_2	

2. Reactor Preparation:
2.1. Reactor /internals cleaned with soap and water, then rinsed
2.2. Reactor and internals scoured with 'Brasso'
2.3. Reactor rinsed with hexane (2 hours with stirring)

3. Nitrogen Purging: Reactor purged with N_2 before and after run.

4. Pressure Testing: Reactor pressure tested @ 1000 psig for 2 h during Sulphiding
No pressure decrease observed

5. Reaction Profiles:

Time to reach 400 °C	77 min
Air cooling time 400 °C to 250 °C	18 min
Water cooling Time 250 °C to 15 °C	17 min
Total Reaction Time	180 min
Pressure Rise @ 400 °C	100 psi
Overall Pressure Rise	0 psi

Time (min)	Temp. (°C)	Pressure (psig)	rpm Stirring	Notes
0	18	360	715	
10	70	440	718	
20	120	490	715	
30	170	510	714	
40	220	560	714	
50	270	640	714	
60	320	740	711	
70	369	860	713	
77	400	1000	716	Reaction Temp.
257	400	1100	718	Air Cooling Started
262	342	900	726	
267	306	800	726	
272	267	750	726	
275	250	700	728	Water Cooling Started
277	129	500	728	
292	19	360	729	Water Cooling Stopped

6. GC Results:

Reactor Feed Sample:

	1	2	3	Average
C10	853651	879035	848613	860433
Decalin	37347250	38699657	37153824	37733577
DPM	5693173	5965816	5653750	5770913
A_{DPM}/A_{C10}	6.669	6.787	6.662	6.706
$A_{DECALIN}/A_{C10}$	43.75	44.025	43.782	43.852

Reaction Product:

	1	2	3	Average
Benzene	50483	53714	52201	52133
Toluene	58562	62974	61311	60949
C10	779895	830132	800811	803613
Decalin	28758832	30338733	29283992	29460519
DPM	4517299	4894702	4659430	4690477
$A_{BENZENE}/A_{C10}$	0.065	0.065	0.065	0.065
$A_{TOLUENE}/A_{C10}$	0.075	0.076	0.077	0.076
A_{DPM}/A_{C10}	5.792	5.896	5.818	5.836
$A_{DECALIN}/A_{C10}$	36.875	36.547	36.568	36.663

7. GC Analysis:

Calibration Curves: $Mi/MC10 = (1/m)*Ai/AC10 - c/m$

	m	c
Benzene	0.5931	-0.0032
Toulene	0.6971	-0.0057
DPM	1.4872	-0.8807

	Feed Sample	Reactor Feed	Reactor Product
Vol. C10 (ml)	0.139		3.611
Moles C10	0.00071		0.01853
Moles Benzene			0.00213
Moles Toulene			0.00217
Moles DPM by GC	0.00364	0.08561	0.08367
Theoretical Moles DPM	0.00331	0.08595	
% Conversion (Benz. ref.)	2.5		
% Conversion (Tol. ref.)	2.5		
% Conversion (DPM ref.)	2.3		

Experiment #21

Summary:	Co Naphthenate @ 1000 ppm Co, No DPM	
	Sulphiding Time @ 1000 psig	2 h
	Reaction Time	3 h
	Reaction Temperature	400 °C
	Total Volume	135 ml

1. Reactor Charge :	120 ml	Decalin
	340 psig IP	5% H_2S in H_2
	1.475 g	Cobalt Naphthenate (8% Co)

2. Reactor Preparation:
2.1. Reactor /internals cleaned with soap and water, then rinsed
2.2. Reactor and internals scoured with 'Brasso'
2.3. Reactor rinsed with hexane (2 hours with stirring)

3. Nitrogen Purging: Reactor purged with N_2 before and after run.

4. Pressure Testing: Reactor pressure tested @ 1000 psig for 2 h during Sulphiding
40 psi pressure decrease observed (leak in thermocouple well)

5. Reaction Profiles:

Time to reach 400 °C	75 min
Air cooling time 400 °C to 250 °C	min
Water cooling Time 250 °C to 15 °C	min
Total Reaction Time	180 min
Pressure Rise @ 400 °C	250 psi
Overall Pressure Rise	100 psi

Time (min)	Temp. (°C)	Pressure (psig)	rpm Stirring	Notes
0	22	340	708	
11	83	420	710	
31	183	500	719	
41	233	540	716	
51	284	600	717	
61	333	700	713	
71	381	890	709	
75	400	990	717	Reaction Temp.
255	400	1240	724	Air Cooling Started
-	20	440	-	

6. GC Results:

Negligible Benzene/Toluene in reactor product
Therefore B/T products in Experiment #19 due to catalytic cracking of DPM with sulphided Co catalyst

Experiment #22

Summary:

Co Microemulsion cracking of DPM	
Sulphiding Time @ 1000 psig	6 h
Reaction Time	3 h
Reaction Temperature	400 °C
Total Volume	135 ml

1. Reactor Charge :

120 ml	Unreduced Co/PELE/Decalin
15 ml	Diphenylmethane
360 psig IP	5% H_2S in H_2

2. Reactor Preparation:

2.1. Reactor /internals cleaned with soap and water, then rinsed
2.2. Reactor and internals scoured with 'Brasso'
2.3. Reactor rinsed with hexane (2 hours with stirring)

3. Nitrogen Purging: Reactor purged with N_2 before and after run.

4. Pressure Testing: Reactor pressure tested @ 1000 psig for 6 h during Sulphiding
50 psi pressure decrease observed

5. Reaction Profiles:

Time to reach 400 °C	75 min
Air cooling time 400 °C to 250 °C	- min
Water cooling Time 250 °C to 15 °C	- min
Total Reaction Time	180 min
Pressure Rise @ 400 °C	160 psi
Overall Pressure Rise	-60 psi

Time (min)	Temp. (°C)	Pressure (psig)	rpm Stirring	Notes
0	18	360	660	
10	76	400	711	
20	130	450	710	
32	189	490	702	
40	228	540	769	
50	278	590	767	
60	328	660	768	
70	378	790	769	
75	400	890	775	Reaction Temp.
255	400	1050	779	Air Cooling Started
-	17	300	-	

6. GC Results:

Reactor Feed Sample: No GC analysis possible due to Co in Microemulsion

Reaction Product:

	1	2	3	Average
Benzene	14005	16921	13434	14787
Toluene	24269	30230	24178	26226
C10	1296257	1611836	1262819	1390304
Decalin	44285884	51866371	41777247	45976501
DPM	5618212	6921936	5357194	5965781
$A_{BENZENE}/A_{C10}$	0.011	0.010	0.011	0.011
$A_{TOLUENE}/A_{C10}$	0.019	0.019	0.019	0.019
A_{DPM}/A_{C10}	4.334	4.294	4.242	4.290
$A_{DECALIN}/A_{C10}$	34.164	32.178	33.083	33.142

7. GC Analysis:

Calibration Curves: Mi/MC10 = (1/m)*Ai/AC10 - c/m

	m	c
Benzene	0.5931	-0.0032
Toulene	0.6971	-0.0057
DPM	1.4872	-0.8807

	Feed Sample	Reactor Feed	Reactor Product
Vol. C10 (ml)	-		3.611
Moles C10	-		0.01853
Moles Benzene	-		0.00043
Moles Toulene	-		0.00065
Moles DPM by GC	-	-	0.06442
Theoretical Moles DPM	-	0.08925	
% Conversion (Benz. ref.)	0.5		
% Conversion (Tol. ref.)	0.7		
% Conversion (DPM ref.)	27.8		

Experiment #23

Summary:	Recovered CoS_2 @ 2000 ppm Co	
	Sulphiding Time @ 1000 psig	2 h
	Reaction Time	3 h
	Reaction Temperature	400 °C
	Total Volume	135 ml

1. Reactor Charge :	130 ml	Reactant Mixture	(120 ml Decalin, 15.015g DPM)
	350 psig IP	5% H_2S in H_2	
	0.4017 g	Recovered CoS_2	

2. Reactor Preparation:
2.1. Reactor /internals cleaned with soap and water, then rinsed
2.2. Reactor and internals scoured with 'Brasso'
2.3. Reactor rinsed with hexane (2 hours with stirring)

3. Nitrogen Purging: Reactor purged with N_2 before and after run.

4. Pressure Testing: Reactor pressure tested @ 1000 psig for 2 h during Sulphiding
No pressure decrease observed

5. Reaction Profiles:

Time to reach 400 °C	75 min
Air cooling time 400 °C to 250 °C	17 min
Water cooling Time 250 °C to 15 °C	23 min
Total Reaction Time	180 min
Pressure Rise @ 400 °C	50 psi
Overall Pressure Rise	n.a. psi

Time (min)	Temp. (°C)	Pressure (psig)	rpm Stirring	Notes
0	19	n.a. (est. 350)	728	Pressure gague not
10	75	n.a.	739	Working
20	124	n.a.	742	
30	174	n.a.	741	
40	224	n.a.	740	
50	274	n.a.	739	
60	324	n.a.	737	
70	374	n.a.	736	
75	400	925	741	Reaction Temp.
255	400	975	752	Air Cooling Started
260	342	975	758	
265	299	970	758	
270	261	950	760	
272	250	950		Water Cooling Started
275	101	650		
295	17	400		Water Cooling Stopped

6. GC Results:

Reactor Feed Sample:

	1	2	3	Average
C10	944192	949507	965048	952916
Decalin	45083965	44402572	45260195	44915577
DPM	4280117	4423399	4517067	4406861
A_{DPM}/A_{C10}	4.533	4.659	4.681	4.624
$A_{DECALIN}/A_{C10}$	47.749	46.764	46.899	47.137

Reaction Product:

	1	2	3	Average
Benzene	22228	21217	20300	21248
Toluene	28745	27768	26968	27827
C10	1040431	993293	949890	994538
Decalin	44058125	42510483	41006977	42525195
DPM	4598841	4396039	4215317	4403399
$A_{BENZENE}/A_{C10}$	0.021	0.021	0.021	0.021
$A_{TOLUENE}/A_{C10}$	0.028	0.028	0.028	0.028
A_{DPM}/A_{C10}	4.420	4.426	4.438	4.428
$A_{DECALIN}/A_{C10}$	42.346	42.798	43.170	42.771

7. GC Analysis:

Calibration Curves: $Mi/MC10 = (1/m)*Ai/AC10 - c/m$

	m	c
Benzene	0.5931	-0.0032
Toulene	0.6971	-0.0057
DPM	1.4872	-0.8807

	Feed Sample	Reactor Feed	Reactor Product
Vol. C10 (ml)	0.139		3.611
Moles C10	0.00071		0.01853
Moles Benzene			0.00077
Moles Toulene			0.00090
Moles DPM by GC	0.00264	0.08661	
Theoretical Moles DPM	0.00331	0.08595	
% Conversion (Benz. ref.)	0.9		
% Conversion (Tol. ref.)	1.0		
% Conversion (DPM ref.)	4.2		

Appendix 3.5 : GC traces of experiment #19 and decomposition of Co naphthenate

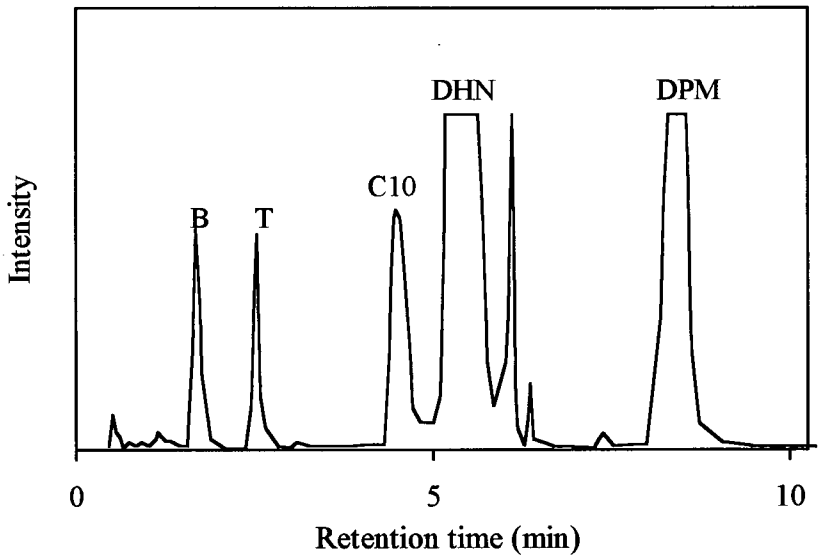

GC trace of Experiment #19 : Reaction product of activity test using Co Naphthenate (C10 is the n-decane GC internal standard).

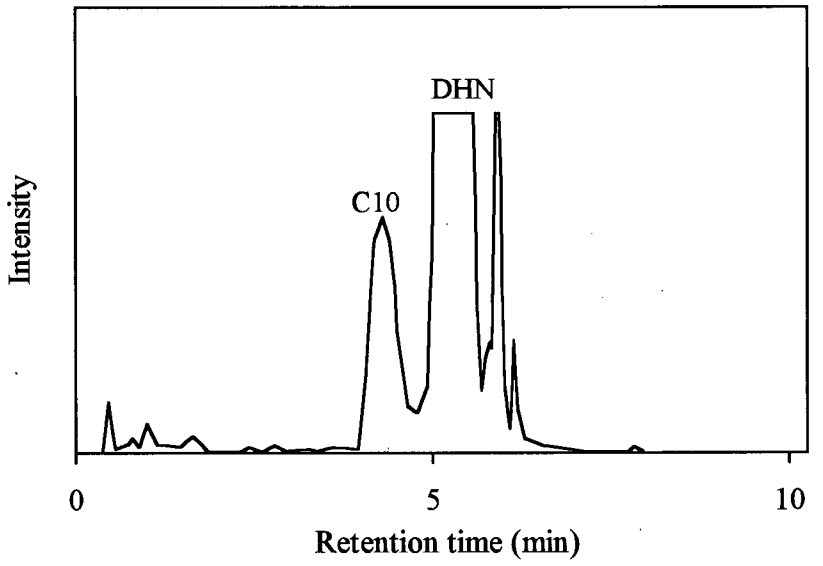

GC trace of the product of the decomposition of Co Naphthenate in decalin at 400 °C (IP 5 % H_2S in H_2 = 300 psig, reaction time = 3 hours).

Appendix 3.6 : XRD spectra of the spent catalysts from the second set of activity measurements.

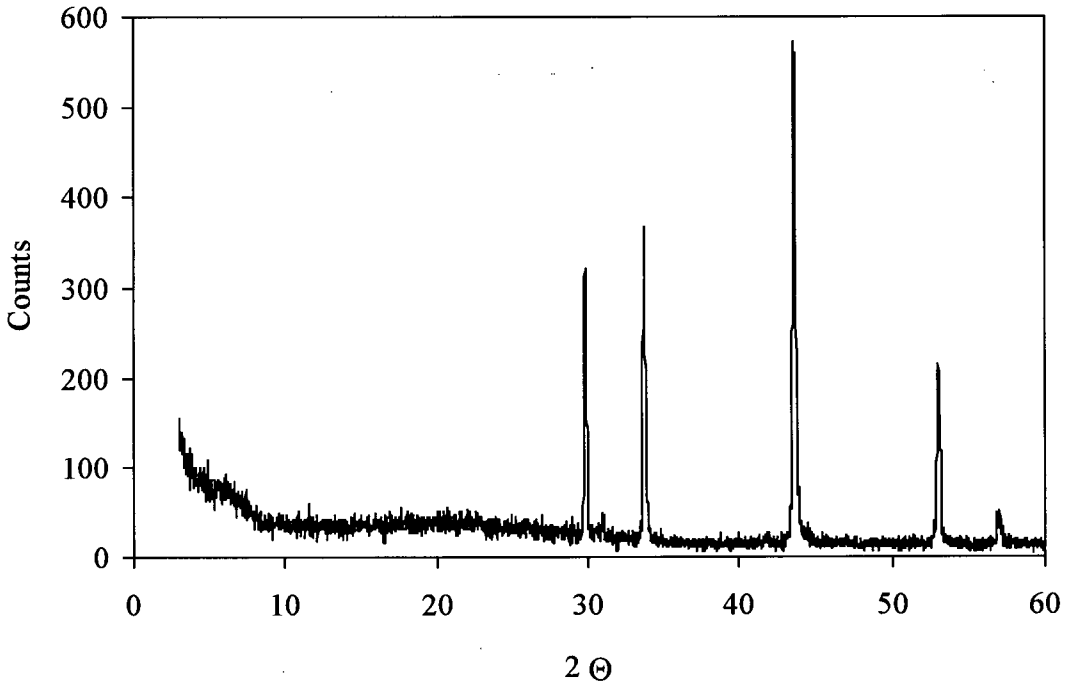

XRD spectrum of spent catalyst from experiment #18 ($Fe(CO)_5$ precursor).

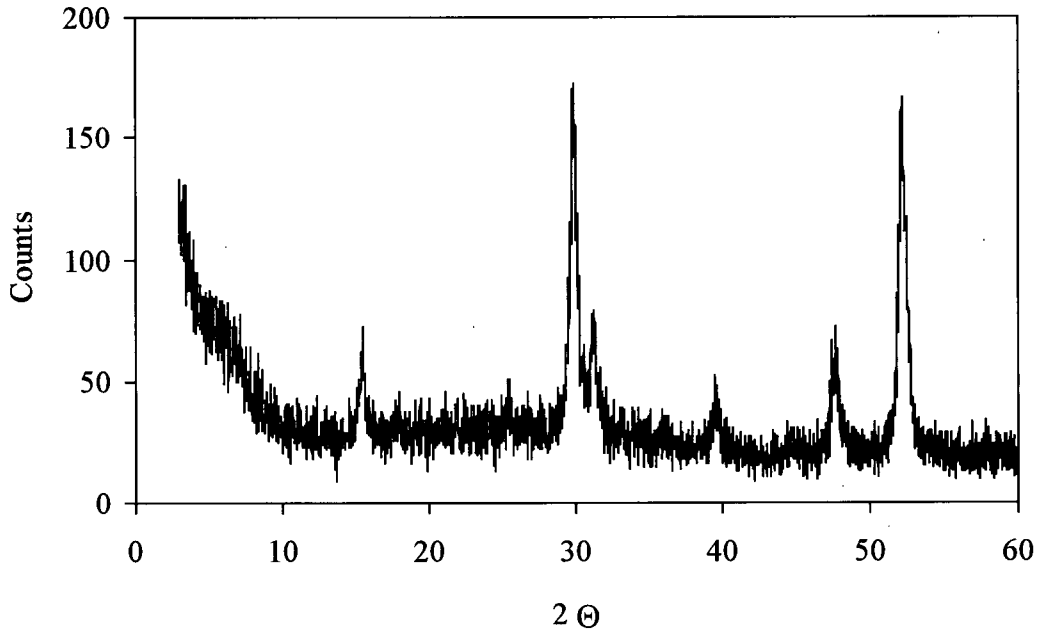

XRD spectrum of spent catalyst from experiment #19 (Co Naphthenate precursor).

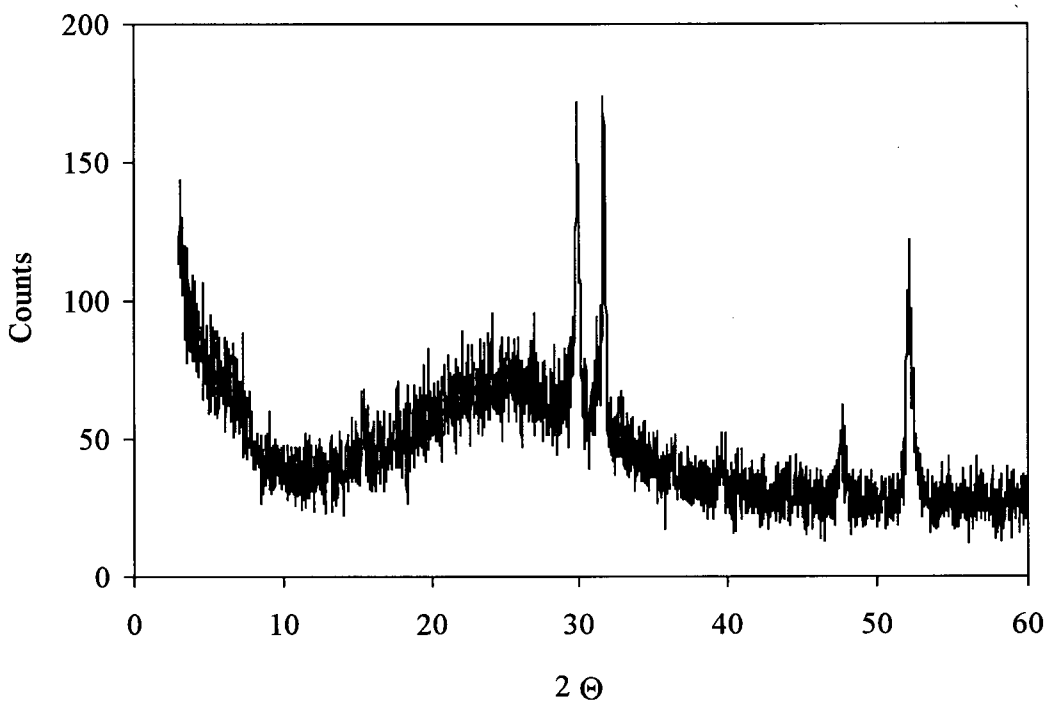

XRD spectrum of spent catalyst from experiment #20 (raw data).

XRD spectrum of spent catalyst from experiment #20 (baseline sutracted).

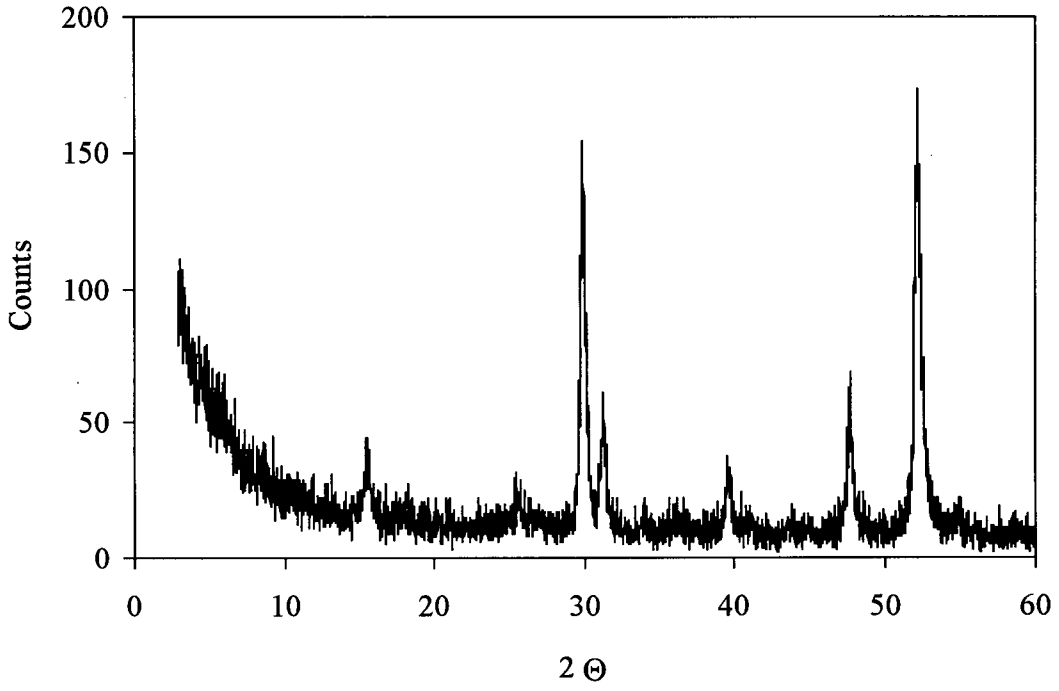

XRD spectrum of spent catalyst from experiment #23.

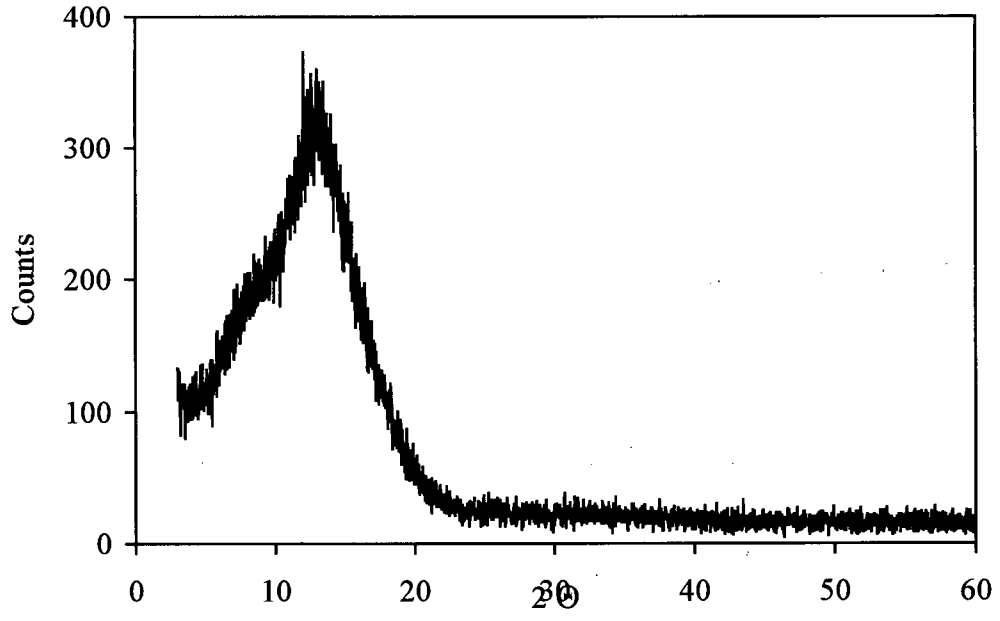

XRD spectrum of fresh catalyst for experiment #23 (recovered from microemulsion with THF).